UNIVERSITY OF SOUTHAMPTON

FATIGUE OF WELDED ALUMINIUM STRUCTURES IN HIGH SPEED MARINE VESSELS

John Peter Kecsmar

Thesis submitted for the degree of
Master of Philosophy

SCHOOL OF ENGINEERING SCIENCES
FACULTY OF ENGINEERING AND APPLIED SCIENCE

April 2003

UNIVERSITY OF SOUTHAMPTON

ABSTRACT

FACULTY OF ENGINEERING AND APPLIED SCIENCE

SCHOOL OF ENGINEERING SCIENCES

Master of Philosophy

FATIGUE OF WELDED ALUMINIUM STRUCTURES IN HIGH SPEED MARINE VESSELS

by John Peter Kecsmar

This thesis seeks to explore important issues underpinning the fatigue design of high speed marine vessels made from aluminium. Understanding of fatigue mechanisms requires a study of the microstructure of the material to include slip planes and systems and the manner in which these form cracks. Such cracks in a material or a structure lead to stress concentrations, which can be modelled using fracture mechanics concepts.

The principal characteristics of both the principal grades of aluminium used in shipbuilding, namely the 5000 and 6000 series, are discussed. The critical influence of sea water and welding on the mechanical properties of the alloys, particularly on the fatigue behaviour, is highlighted. The effects of various other forming, shaping and joining operations in a shipyard are also explored.

The thesis addresses the manner in which choice of design details, such as shapes of cutouts, affects both the mechanical performance and the production costs. The proper use of finite element analysis to model stress concentration factors of shipyard joints and around cutouts is discussed in depth.

Finally, the fatigue design concepts are applied to assess the efficacy of structure in the water jet ducting system of a high speed Tricat vessel made from aluminium alloys.

CONTENTS

Dedicated to my father,
a consummate engineer

Nomenclature

a	crack Length
a	Width of Circular Aperture
A	Cross Sectional Area of Structural Member
$a_{1,2}$	Depth of Flaw in Weld
AA	Aluminium Association
a_i	Initial Crack Length
AW	Aluminium Wrought
b	Distance of a Single Dislocation
b	Weld Width
b	Depth (height) of Circular Aperture
BCC	Body Centred Cubic
BS	British Standards
BSEN	British Standards European Number
C	Constant, Function Crack Geometry
C	Material Constant
COD	Crack Opening Displacement
CPH	Close Packed Hexagonal
CSSC	Cyclic Stress Strain Curve
CTOD	Crack TIP Opening Displacement
Cu	Copper
da/dN	Crack Growth Rate
DNV	Det Norske Veritas
E	Youngs Modulus
e	Linear Misalignment
ECA	Engineering Critical Assessment
EN	European Normative
EPFM	Elastic Plastic Fracture Mechanics
F	As Fabricated
F	Axial Force

FCC	Face Centred Cubic
FE	Finite Element
FEA	Finite Element Analysis
FEM	Finite Elemenet Model
G	Shear Modulus
G_{IC}	Energy Realise Rate
H	Strain Hardening Designation
h	Weld Bead height
h	Element Size in Mesh
HAZ	Heat Affect Zone
I	Moment of Inertia
IMO HSC	International Maritime Organisation High Speed Craft Code
K	Stress Concentration Factor
K	Stress Intensity Factor
K_C	Critical Stress Intensity factor
K_C	Critical Stress Intensity Factor, Under Plane Stress
K_{CW}	Stress Concentration Width factor
K_f	Fatigue Styrength Reduction Factor
K_{IC}	Critical Stress Intensity Factor, Under Plane Strain
K_{Id}	Critical Stress Intensity Factor, Under Plane Stress & Dynamic Loading
K_m	Stress Magnification factor
K_{max}	Stress Intensity at Maximum Load
K_{min}	Stress Intensity at Minimum Load
K_R	Crack Growth Resistance, at Instability
K_s, K_{SO}	Structural Stress Concentration Factor
K_{SL}	Stress Concentration factor Lower Profile
K_{SU}	Stress Concentration factor Upper Profile
K_t	Theoretical Stress Concentration factor
K_t	Theoretical Notch Factor
K_t	Stress Concentration Factor

kW	Kilo-Watts
LOF	Lack of Fusion
LOP	Lack of Penetration
m	Material Constant
Mg	Magnesium
MIG	Metal Inert Gas
Mn	Manganese
MPa	Mega Pascal's
N	Number of Cycles to Failure
NDT	Non-Destructive Testing
N_I	Load Cycles
N_P	Total Life for Crack Propagation
N_T	Number of Cycles to Failure
O	Annealed Condition
PSB	Persistent Slip Bands
q	Notch Sensitivity Factor
QA	Quality Assurance
QC	Quality Control
r	Radius of Weld Toe
r_P	Radius at Crack Tip, Under Plan Stress
RPM	Revolutions per Minute
s	Arc Length
S	Stress
SCC	Stress Corrosion Cracking
SCF	Stress Concentration Factor
SEM	Scanning Electron Microscope
Si	Silicon
SN	Stress v Number of Cycles
S_Y	Yield Stress
T	Traction Vector

T	Solution Heat Treatable, Stable
t	Plate Thickness
TIG	Tungsten Inert Gas
U	Displacement Vector
UTS	Ultimate Tensile Strength
w	Width of Atomic Diameters
W	Strain Energy Density
W	Solution Heat Treatable, Unstable
Y	Geometric Factor of Crack
Y	Distance of Centroid to Considered Point on Structural Member
Zn	Zinc
°C	Degrees Centigrade
α	Weld Toe Angle
γ	Fatigue Strength Reduction Factor
δ_C	Fracture Toughness Parameter
Δa	Increase in Crack Length
ΔN	Increment of Cycles
$\Delta \varepsilon$	Strain Rate
ΔK	Stress Intensity Factor Range
ΔK_T	Stress Intensity Factor Threshold Range
ΔK_I	Stress Intensity Factor Range in Mode I Loading
ΔK_{eff}	Change in Effective Value of ΔK_I
$\Delta a/\Delta N$	Crack Growth Rate
ν	Poisson's Ratio
σ	Yield Stress
σ_b	Shell Bending Stress
σ_{hs}	Hot Spot Stress
σ_m	Membrane Stress
σ_{max}	Maximum Stress
σ_n	Nominal Stress

σ_{no}	Nominal Surface Stress
σ_{nlp}	Nonlinear Peak Stress
σ_{nom}	Nominal Stress
σ_{ll}	Stress in Weld Bead, Parallel to Loading
$\sigma_{\perp}$	Stress in Weld Bead, Perpendicular to Loading
σ_x	Stress in X Axis/Direction
σ_y	Stress in Y Axis/Direction
τ_o	Peierls-Nabarro Stress

Acknowledgements

I would like to thank FBM Babcock Marine for funding this thesis, and the information used for the basis of the structural appraisal. Jon Story of CENIT, for providing the COSMOS/M pdf files of figures. My thanks to Professor Ajit Shenoi, for his guidance throughout the research and his understanding of my delayed deadlines, owing to studying whilst working full-time. To Pechiney, France, for their endless openness with their research and findings of new alloy's. Finally, I would like to thank Nigel Warren, without whom, most of this would not be possible. His never ending generosity, guidance and inspiration in all matters has and, remains always, a source of both professional and personal enlightenment and friendship.

1. Introduction

The thesis is a study into the fatigue design of structures of high speed marine vessels [1.1]. The high speed craft market began in the 1950s. During the boom of the late 1970s and 1980s [1.2] with the aluminium catamaran, it grew to the industry it is today. The focus of this thesis is on high speed passenger ferries. The definition of high speed is laid down in the IMO HSC Code [1.3]. The code defines the relationship between speed and displacement. One consequence of the high speed requirement is the structure of the craft needing to be as light as possible [1.4]. The material used for construction is predominately aluminium, since it offers weight advantages over steel [1.5]. Additionally the installed power must be high to achieve the desired power to weight ratio to satisfy the IMO criterion. A catamaran hull form has an installed power saving of 50% [1.6] when compared to a monohull. It is this reason that the catamaran is the preferred hull configuration choice for a high speed ferry.

If a lightweight structure is required, other materials are available to the designer. Composites are an ideal choice. Where aluminium is one third the weight of steel, composite is approximately half the weight of aluminium [1.17]. A composite structure can be optimised to an even greater degree than an aluminium one. This leads to an even greater saving in weight. In the pleasure boat market, composites are extensively used with great success despite the high tooling costs [1.18]. The problem for the designer using composites as structural material on high speed ferries, is legislation [1.3][1.19]. The code permits any type of structural material to be used so long as it is non-combustible. This is defined as [1.3] a material which neither burns nor gives off flammable vapours in sufficient quantity for self-ignition when heated to approximately 750°C. Safety on a passenger vessel is paramount. Therefore, it is essential that in the event of a major fire structural integrity be maintained. Clearly a composite material is unable to satisfy this criterion.

Correct sizing of structural components is an essential pre-requisite in overall vessel design [1.7]. Early designs underestimated the stresses within the hull structure. Slimming down the scantlings and plate thickness gave rise to fatigue cracking in way of weld seams. The fatigue properties of aluminium coupled with poor detail design were found to be the cause for these structural failures. Reducing the scantlings and plate thickness leaves little margin for error. The transom of KaMeWa waterjets, for instance, required the transom area of some hull designs to be increased in thickness by a factor of two. One of the key issues for the underwriter of these vessels is the lack of skilled fabricators and welders of aluminium. The lack of convenient skills and resources increases the prospect that the cost of repair can exceed the insured value of the vessel [1.2] [1.7].

In [1.8] Lloyd's Register addressed some of the issues that were raised by these structural failures. The work points to a lack of corroborative service experience for large aluminium catamarans. It also notes the lack of fatigue related analysis for these vessels within their own rules. In the absence of detailed methods for analysing structure for fatigue, the endurance of structural details subjected to high stress concentration and cyclic loading, would need to be addressed by other means. In the early 1990s Det Norske Vertias (DNV) demonstrated its methodology of structural analysis for high speed vessels [1.9]. It is interesting to note that DNV emphasised the importance of stress concentrations and structural continuity as well as deflections checks by the designer. However, unlike in [1.8], DNV made no reference to fatigue or design for fatigue in their rules for guidance to the designer.

There are many factors that affect fatigue [1.10]. These range from: detail design, fatigue assessment, control of production, material properties and operation of the vessel. The influence of operational limits on a vessel and its effect on the global response is addressed in [1.11] and questions standard frame analysis. The use of finite element (FE) modelling for global and local structure analysis is discussed in [1.10]. Using the results from the FE analysis, a more detailed analysis of structural configurations allows for an evaluation of stress concentrations. The calculation of stress concentration enables the designer to evaluate and assess the fatigue life of the joint [1.4].

The local hot spot stress is obtained by a local nominal stress multiplied by a stress concentration factor, K. In detailed analysis, e.g. a stiffener girder connection, the total stress concentration factor is dependent on the weld toe radius and almost independent of the weld toe angle [1.12]. The determination of the stress concentration factor for a structural joint is required for the designer to understand the fatigue life of that joint.

In [1.13] DNV demonstrate their experience, design philosophy and publish examples of fatigue failure on high speed craft using their rules. Typical lifetimes of structural joints are presented as well as typical locations of structural failure through fatigue. The work identifies four important factors for the control of fatigue of high speed crafts:

- Stress range
- Detail design
- Workmanship
- Corrosion control

This thesis seeks to concentrate on two of these issues, namely detail design and workmanship, since it is these two factors that are most overlooked. The rules for High Speed craft by DNV [1.14] now include fatigue by the definition of the general stress level. Basic guidelines are given but there is little guidance on the analysis of detailed joints. The designer must determine the stress concentration factor by means other than Classification rules. With workmanship being identified as an important factor in the fatigue life of a welded joint, the guidelines for the designer and the shipyard are minimal. The quality of workmanship in fabricating these structural joints requires as much detailed analysis as the mathematical modelling. Good understanding of the pre-fabrication and post-fabrication of a structure is required.

To address the problem of structural failure from fatigue, Lloyds Register published a manual for ship designers [1.15]. This manual is aimed at large Bulk Carriers and Tankers. However, the chapter *Guidance for Designers* is applicable to any vessel that is subjected to fatigue. The manual gives guidance on the production design of structural joints to improve fatigue strength, which includes fabrication procedure and the shape of joints. Construction tolerances, notable in the early stages of construction, are reviewed. Guidance on everyday shipyard processes like grinding is shown to have advantages as well as disadvantages. Geometrical stress concentrations and their effects are given.

The rules only give notice to the designer regarding reduction of hot spot stresses, rather than prescriptive rules for determination. Considerable discussion on welding and weld beads is given. Highlighting the attention that is required to reduce hot spot stresses due to the fabrication of the joint; owing to poor access by the design, including the stress within the weld itself. The designer requires an understanding of the long chain of events that occur in pre and post fabrication for fatigue to take place. It is these factors that this thesis will draw to the attention of the working designer; to educate and inform how basic production methods and detail design can affect the fatigue life of a structure.

Therefore, the purpose of this thesis is to review the issue of fatigue design in high speed craft shipbuilding. Using current design guidelines, such as British Standards [1.16], fatigue is addressed in a generic nature rather than a practical step-by-step guide for the shipyard designer. This is also noted in [1.12]. The British Standard only addresses uniaxial loading for two-dimensional structure unlike an actual complex three-dimensional structure. Therefore, there is a need for the designer to understand the mechanisms and the events leading up to a structural failure from fatigue which is beyond the scope of the British Standards. A review of the mechanics of fatigue is necessary to fully understand the phenomenon. The choice of material, in this case aluminium, will be investigated to ascertain the mechanical properties in the unwelded and welded condition and how this effects the fatigue life. The method of manufacturing and fabrication of aluminium into ship structures is discussed.

Common shipyard joints are reviewed and how detail design influences the stress concentrations of typical complex structural joints. Comparisons of various geometric joints are given for guidance to establish how minor changes can affect the stress concentration. Mathematical modelling for analysing complex ship structures using finite element modelling is investigated. The application of using finite element analysis is reviewed with regard to ship structures to establish general guidelines for the designer. A worked example of a typical structural configuration that is in a fatigue environment is shown. The guidelines used in the worked example are in a format that can be reproduced within the time frame required by a working shipyard designer.

2 The Mechanics of Fatigue

This chapter discusses the phenomenon of fatigue. The physical science at the metallurgical level is discussed, giving an insight to the molecular behaviour that culminates in the onset of crack initiation, along with methods of predicting its behaviour and the effect of microscopic cracks. Crack growth and laws defining the path of such growth, are also investigated and how the geometry of a crack can be defined in terms of stress intensity. Fracture mechanics and how the application of crack geometry affects crack growth are reviewed.

2.1 Definition

Fatigue can be described as a failure of a metal under repeated or otherwise varying load which never reaches a level sufficient to cause failure in a single application [2.1]

The basis for understanding the influences of fatigue strength is the crystalline structure of the material. Every material is made up of molecules, which in turn form a crystalline structure. This crystalline structure can be represented in the shape of a cube. Defining the shape of a cube and how the molecules of the material are arranged in this cubic system establish how the material will behave when subjected to a cyclic load, or fatigue. The principal systems are known as: Body Centred Cubic (BCC), Face Centred Cubic (FCC) and Close Packed Hexagonal (CPH).

2.2 Fatigue of materials with a Single Crystal or Polycrystal structure

Face-centred cubic (FCC) materials, such as copper fig 2.1, have been used for the study of fatigue due to the fact that they were thought to be well behaved materials [2.2]. Pure FCC metals and many of their alloys, deform by dislocation motion on very well defined slip planes and directions, which simplifies the study of deformation and dislocation structure.

It has been found that in some cases, the cyclic response is almost identical when the proper normalisation of the stress and strain is carried out; copper and nickel are examples of this. When a copper single crystal or polycrystal is tested, under plastic strain control for example, which has not been mechanically treated, it hardens under the cyclic load until it reaches saturation state [2.3]. A typical plot of the hardening of a polycrystal tested under plastic strain control is shown in fig. 2.2, where neither the load nor the total strain changes.

When a sample has previous plastic deformation, cyclic loading below the last level of stress applied, will produce cyclic softening until saturation is reached. This behaviour shows that within a certain range of loads and plastic deformation, the saturation state of samples with identical microstructural or crystallographic features, depends only on the plastic strain amplitude applied. This means that two identical samples tested under plastic strain control at the same amplitude, will have the same saturation stress, regardless of the previous mechanical treatment of each sample. Furthermore single crystal orientation for single slip, hardens to the same saturation stress as far as the resolved shear stress and shear strain on the primary slip system is concerned. This behaviour is present in what is called the Cyclic Stress-Strain Curve or CSSC, as shown in fig.2.3 [2.4]. The stable loops are commonly termed hysteresis loops.

An example of a typical CSSC for copper single crystals tested under plastic strain control is shown in fig.2.4. The CSSC is constructed by taking the average stress amplitude and the average plastic strain at saturation. The CSSC shown in fig 2.4 shows a very important characteristic of the cyclic behaviour of single crystals of copper and other FCC metals. The CSSC has a plateau or region where deformation takes place at an approximately constant value of stress. Plateaus in single crystals are associated with localisation of deformation in slip bands, steps or planes that have distinct dislocation structures. Fatigue crack initiation in Cu single crystals and many FCC materials, is closely related to the development of surface roughness. This results from the onset and growth of zones of localised strain [2.5]. As the dislocation structure keeps evolving, the plastic strain increases.

The structure consists of bands one or two microns wide, where the plastic deformation is heavily localised. These are called persistent slip bands (PSB), see 2.6, and are the main reason for the presence of plateaus. The plateau starts when the first PSB is nucleated and further increases on the plastic deformation beyond what that band can carry. The plateau ends when the volume fraction of PSBs is 100%.

2.3 Slip Planes and Directions.

Consider fig 2.5, which shows a crystal loaded as in a tensile test. The applied tensile force can be resolved into components normal and parallel to any plane, such as XX, in the specimen [2.6]. This is shown in fig 2.5b, where the applied force, P, is resolved into a normal, tensile component P_T and parallel component P_S (i.e. a shear force) on the plane XX'. This means that a simple tensile force produces shear forces, and hence shear stresses, in a test sample. The value of the shear stress varies with the orientation of the plane and its maximum for the planes at 45° to the tensile axis. If a single crystal is deformed plastically, that is, increasing the tensile force until there is a permanent shape change, the result, looking under a microscope, is a series of parallel black lines as shown in fig.2.6.

These lines are small steps on the surface of the crystal, called slip lines or slip steps. On increasing the tensile force still further, so causing more plastic strain, the number and/or height of the slip lines increase. It is as if whole blocks of the crystal are slipping over one another under the action of the resolved shear stresses, as shown in fig. 2.5c. The fact that the slip lines are parallel and that they do not necessarily correspond to slip along the planes of maximum shear, indicates that the slip process is closely connected with the crystallography of the crystal, and is shown in fig.2.5d. Slip only occurs on preferred crystallographic planes, the slip planes, and in certain directions, the slip directions. The two constitute a slip system. The orientation of a surface or a crystal plane may be defined by considering how a plane intersects the main crystallographic axes of the solid.

This is by the use of the Miller Indices. This is a set of integers, {1,1,1}, which quantify the intercepts and thus may be used to uniquely identify the plane [2.7]. The uses of round brackets ( ) describe a single plane and curly brackets { } describe a family of planes.

2.4 Slip Systems

As it can be shown in the following slip systems, the slip direction is usually the direction in which the atoms are most closely packed. The slip plane is the most densely packed plane containing that direction [2.8].

(i) FCC the {110} directions are the closest packed directions in the face-centred cubic structure and are, therefore, the slip directions. The {110} directions lie in the most densely packed planes, which are the close-packed {111} planes, fig.2.7. Thus the four {111} planes are the slip planes and, as each plane contains three {110} directions, there are altogether 3 x 4 = 12 slip systems.

(ii) Close-Packed Hexagonal, (CPH). The slip directions are the closest packed directions. Three such directions lie in the close-packed basal plane, giving only 3 x 1 = 3 slip systems. These are shown in fig.2.8.

(iii) Body-Centred Cubic, (BCC), fig.2.9. The most closely packed directions in the BCC structure are the {111}. Therefore, the slip directions, but do not have close packed planes like the FCC and the CPH. There are six {110} planes with two {111} directions, each giving 6 x 2 = 12 slip systems. There are also twelve systems of the type {112} and {111}.

2.5 The Propagation of Dislocations

Dislocations play an important role in crack initiation. They can be seen as the result of part of a crystal, slipping over another. If the slip plane does not extend through the crystal, the boundary is a dislocation. The magnitude and direction of the slip resulting from the motion of a single dislocation, is called the *Burgers vector.* Dislocations can be classified by the angle between the propagation direction and the Burgers vector. The special cases of 90° and 0° angles are known as *edge* and *screw* dislocations [2.9]. It can be shown that for an edge dislocation, the Burgers vector is perpendicular to the line of a dislocation fig.2.10a. When the vector is parallel to the dislocation, this is called a screw dislocation and is shown in fig.2.10b. As for an edge dislocation, under the influence of a shear stress, the screw dislocation moves in the slip plane. This time the direction of motion of the dislocation is perpendicular to the Burgers vector and is, hence, a mixed dislocation as shown in fig.2.10c.

All dislocations are line defects and, therefore, only measure a few atomic diameters at right angles to their length. The width, w, can be defined as the distance over which the displacements of atoms is greater than b/4. Where b, is the distance of a single dislocation in a crystal, as shown in fig.2.11. When w, is one or two atomic spacings, the dislocation is said to be narrow. On the other hand, a wide dislocation has a width of several atomic spacings, which is typical of most metals.

It follows that the minimum stress for the type of motion shown in fig.2.10, is the stress to move a dislocation in an otherwise perfect crystal. This intrinsic lattice friction stress is known as the *Peierls-Nabarro* stress [2.10]. The significance of the width of a dislocation is that it determines the magnitude of the Peierls-Nabarro stress, τ_O, as can be seen in the following equation:

$$\tau_o = \frac{2G}{(1-\upsilon)} . e^{\frac{-2\pi w}{b(1-\upsilon)}} \qquad \text{.....(2.1)}$$

Where G = shear modulus, ν = Poisson's ratio, τ_o is very sensitive to w. The wider the dislocation, the lower τ_o is and the easier it is to move the dislocation. It can also be seen that a small Burgers vector, b, leads to a low τ_o value. This is one of the reasons why the dislocations responsible for plastic deformation often have the smallest b, compatible with the crystal structure. In terms of macroscopic slip, why the slip direction is generally the closest packed direction.

It is worth noting that although edge dislocations cannot avoid obstacles by cross-slip; they can avoid them by moving normal to their slip planes, by the process of climb. This process can be repeated many times, so the edge dislocation can climb a number of atomic spacings.

2.6 How a Slip Plane Becomes a Crack

Examination of fracture surfaces can tell a lot about the mechanism by which a crack advances, very near the crack nucleus [2.11]. While the crack length is still small, conditions of plane strain hold at the crack tip. The fracture surface is macroscopically flat and orientated perpendicular to the tensile axis. As the crack grows in length, a shear lip begins to develop where the fracture surface intersects the specimen surface, fig.2.12.

This reorientation of the fracture surface to a 45° position with respect to the tensile axis, is caused by the plane stress conditions at the crack tip intersecting the surface. As the plastic zone in front of the crack tip increases in dimension, comparable to that of the specimen thickness, plane stress conditions hold at the crack tip. Concentration of plastic strain at the crack tip initiate slip bands to form intrusions and extrusions on the free surface. These extrusions and intrusions [2.12] initiate the first of three stages of what is known as crack growth, fig.2.13. Stage 1 is crack initiation, stage 2, is fatigue crack growth and stage 3 is the final catastrophic fracture. It is worth noting that stage 3 failure is always rapid compared with the preceding stages.

Stage 1

In materials with smooth surfaces, the initiation of the crack involves the localised movement of dislocations on slip planes, as discussed in section 2.4 and 2.6. Cracks forming in slip bands propagate along the active slip planes, which are inclined at ±45° with respect to the tensile stress axis. There is, however, a major difference between the fatigue slip bands and slip lines. On repolishing the surface of a specimen, slip lines are removed, as they are surface steps, whereas slip bands remain. For this reason the fatigue slip bands are know as *persistent slip bands*. These slip bands form extrusions and intrusions on the surface of an otherwise uncracked material, these extrusions or intrusions may be seen by a scanning electron microscope (SEM), fig.2.13.

Stage 2

The crack changes direction and becomes roughly normal to the stress axis. The structure has a series of fine, non-crystallographic ridges known as fatigue striations [2.13]. Each striation is produced by a single stress cycle and there are several modes to account for their formation. These modes are illustrated in fig.2.14 and show that a striation is a consequence of an increment of crack growth and concomitant blunting and resharpening of the crack tip by plastic deformation.

Fig.2.15a, is a zero load condition after a number of cycles: striations 1, 2 and 3 being formed during previous cycles [2.14]. When a tensile load is applied, the crack opens up and shear stresses are set up at the crack tip fig.2.15b. As the applied tensile load increases, plastic deformation occurs due to the shear stresses, which leads to crack extension and blunting, fig.2.15c. Once the compression period of the cycle is entered, the crack begins to close and the shear stresses are reversed, fig.2.15d. Finally at the point of maximum compression, the crack is almost closed and the reverse plastic flow that has taken place during the compression half-cycle has resulted in the formation of a new striation and resharpening of the crack tip.

Crack growth rates can be expressed analytically for different crack lengths and for different loads, and are closely related to the stress situation at the crack tip and directly proportional to the stress intensity factor, K. The correlation of crack growth rates with a crack tip stress intensity factor, provides the key to the study of crack growth mechanisms. See section 2.7, for further information on crack growth and 2.8 for stress intensity.

Stage 3

Occurs when the fatigue crack has grown to such an extent, that the component finally fails in a catastrophic manner. The final fracture mode varies with material and service conditions. It may be a simple ductile over-load failure due to the cross-sectional area of the component having been reduced so much by the fatigue crack, or it may be brittle cleavage failure. Fatigue fracture surfaces are flat and shiny, and very much like brittle fracture. The failure region has characteristic features, called beach marks or clam shell markings [2.15].

Macroscopically there are at least two well defined regions on the fracture surface, left by the crack. The first region corresponds to stage 2 of fatigue crack growth. It is the flat and shiny part, which has been created by the continual rubbing together of the cracked surfaces during the cyclic loading. Which in turn often create the concentric rings mentioned above, as beach marks. These beach markings are usually made visible by corrosion and the significance of the markings is that they focus back to the point of crack initiation. The second region, when the fatigue crack reaches a certain length, has a rougher surface, which may be shiny or dull, depending on the mode of failure, but is generally in a ductile manner.

2.7 Crack Propagation

The increase in crack length, Δa, for an increment of, ΔN, cycles define the growth rate, $\Delta a/\Delta N$ [2.16]. This is a function of both the crack length, a, and the stress or strain amplitude. Observed growth rates may range between 10^{-10} m/cycle at low amplitudes, to about 10^{-3} m/cycle at high amplitudes.

The importance of the growth rate lies in its use to calculate remaining life times, given a certain initial crack length, a_i, after N_I, load cycles. Assuming that, a, is a continuous function of N_T, the total number of cycles to failure, the instantaneous crack growth rate da/dN, can be used to give the total life for a crack propagation, viz:

$$N_p = N_T - N_I = \int_{a_i}^{a_T} \frac{da}{(da/dN)} \quad \text{.....(2.2)}$$

It is desirable to have a theory of fatigue crack growth, yielding universal expressions for da/dN, as a function of its yield stress, σ, crack length, a, or change in strain rate, $\Delta\varepsilon$, and material properties. Clearly, the propagation of a fatigue crack is closely related to the stress field at the crack tip; in stage 2 of crack propagation, as discussed in 2.6. In cyclic loading, K, will vary throughout the cycle and the stress intensity factor range. ΔK is defined as the difference between K at the maximum load (K_{max}) and K, at the minimum load (K_{min}) [2.17]. The stress intensity factor range, ΔK, is a parameter that expresses the effect of load range on the crack. It describes the stress field associated with the cracked body at the crack tip.

That is:

$$\Delta K = K_{max} - K_{min} = Y\Delta\sigma(\pi a)^{1/2} \text{.....(2.3)}$$

If the minimum stress is compressive, then K_{min} is normally taken to be zero. Fig.2.16a shows a $\log_{10}$-$\log_{10}$ plot of the crack growth rate, da/dN against the change in intensity factor ΔK. The lower limit to the curve, ΔK_T, is called the threshold stress intensity factor range for crack growth. At high ΔK values, where K_{max} is approaching the critical stress intensity factor, K_C, crack growth rate is very rapid and the failure modes are characteristic of normal static failures. Experimental correlation in aluminium alloys is shown is fig.2.16b [2.18]. For intermediate values of ΔK, where the plot is linear, for stage 2, the following relationship is derived [2.19]:

$$\frac{da}{dN} = C\left(\Delta K\right)^m \quad \text{.....(2.4)}$$

This equation is know as the *Paris-Erdogan* equation, where C and *m* are constants for a particular material; *m* is usually between 2 and 4 for most ductile metals, see table 2.1 [2.1] for values of m. K, is the stress intensity factor depending upon the instantaneous crack length and overall nominal stress affected by the geometry and loading parameters. The implication of *m* of different alloys of aluminium will be discussed in chapter 3.

2.8 Stress Intensity Factor

The stress intensity factor [2.20] is a measure of the magnitude of the stress field at the crack tip and is computed from the applied stress, $\Delta\sigma$, and the crack length, a. Where, Y, is a geometric factor that accounts for the geometry of a crack, equation 2.3. The calculation of the applied stress is covered in chapter 6 using FEA. The use of stress intensity factors to analyse crack growth data has the advantage that behaviour can be predicted for any cracked body configuration for which a stress intensity factor expression is available.

Crack surfaces are stress-free boundaries adjacent to the crack tip and, therefore, dominate the distribution of stress in that area. Remote boundaries and loading forces affect only the intensity of the stress field at the crack tip. There is a particular type of elastic stress field corresponding to each mode of crack surface displacement. These may be described in terms of the stress intensity factor K, which is a description of the stress at the crack tip. It has the dimensions stress x length$^{1/2}$ and is usually in units of MNm$^{-3/2}$. The stress intensity factor represents the first term in the series expansion for the elastic stress field at a crack tip, and is for many purposes, a sufficiently accurate representation of the elastic stress field.

The elastic stress analysis assumes an ideal elastic material, i.e. a perfectly elastic isotropic material. Provided that yielding is confined to a small region right at the crack tip, the elastic stresses outside this region are only slightly affected and the stress intensity factor still provides a reasonable description of the crack tip stress field. See Appendix A for values of K of standard crack geometry. Since K is directly proportional to the elastics stress field, factors that affect the stress field will have the greatest influence. Stress raisers due to fabrication effects will be covered in chapter 4. Design details that affect local stresses will be discussed in chapter 5. The analysis of stress raising features from fabrication and design details using FEA is reviewed in chapter 6.

2.9 Fracture Mechanics

Fracture mechanics is the science of studying the behaviour of progressive crack extension in structures and is concerned with how cracks behave under load [2.21]. It also accounts for structures which contain discontinuities. Fracture mechanics principles are applicable only to fatigue if a crack or a crack-like flaw is present. Thus, for example they are applicable to:

- Fatigue cracks
- Small inherent crack-like flaws, e.g. at toes of welds
- Planar flaws which may not be cracks, (Porosity in welds, solidification cracking etc)
- Non-planar flaws, e.g. inclusions, can also be considered, treating them like cracks

In the context of fatigue, fracture mechanics is used primarily to describe the rate at which a crack will propagate under repeated loading. It can also be used to determine the extent of fatigue cracking which can be tolerated before facture occurs, i.e. to define the critical crack corresponding to the materials fracture toughness.

The *toughness* of a material is defined as the ability of a smooth, unnotched member to absorb energy. *Notch toughness*, is defined as the ability of a material to absorb energy in the presence of a flaw. In the context of aluminium structures, it is worth noting that unlike steel, the toughness of aluminium is unaffected by temperature, fig.2.17. There are three primary factors in fracture mechanics that control the susceptibility of a structure to brittle fracture:

1 Material toughness K_C , K_{IC} , K_{Id}

2 Crack size, a

3 Stress level, σ

1 Material Toughness is the ability to carry load, or deform plastically, in the presence of a notch. It can be described in terms of the critical stress intensity factor under conditions of plane stress K_C or plane strain K_{IC} for slow loading and linear elastic behaviour or K_{Id} under conditions of plane strain and impact or dynamic loading.

2 Crack size or fractures, which originate from discontinuities or flaws. These can vary from extremely small cracks within a weld arc strike, to much larger imperfections such as porosity in welds, lack of fusion and penetration etc, see section 4.7.1. Such discontinuities, though small initially, can grow by fatigue or stress corrosion to a critical size.

3 Stress levels (tensile), nominal, residual or both are necessary for brittle fractures to occur. These are determined by conventional stress analysis techniques for particular structures. Factors such as temperature, loading rate, stress concentrations, residual stresses etc, merely affect the three primary factors listed above.

Material toughness property depends on the particular material, loading rate and constraint: Where:

$$K_C, K_{IC}, K_{Id} = C.\sigma.\sqrt{a} \quad \ldots\ldots\ldots\ldots\ldots\ldots (2.5)$$

C = Constant, function of specimen and crack geometry

σ = Nominal stress

a = Flaw or crack size

K_C critical stress intensity factor for the static loading and plane stress conditions of variable constraints. This value is proportional to specimen thickness and geometry as well as crack size.

K_{IC} critical stress intensity factor for static loading and plane strain conditions of maximum constraint. This is a minimum for thick plates.

K_{Id} critical stress intensity factor for dynamic loading and plane strain conditions of maximum constraint.

The effects of manufacturing, which introduce crack like flaws, will be addressed in chapter 4.

2.9.1 Members with Cracks

Failure of structural members is caused by the propagation of cracks. Hence an understanding of the magnitude and distribution of the stress field, in the vicinity of the crack front, is essential to determine the safety and reliability of the structure. Fracture mechanics can be subdivided into two general categories, namely, linear-elastic and elastic–plastic. It is convenient to define the relative movement of two crack surfaces into three types of displacement [2.22]. Fig.2.18a, which can occur when a cracked structure is loaded, and fig.2.18b, defines the coordinate system and stress components ahead of a crack tip. Mode I is characterised by the displacement of the two fracture surfaces, perpendicular to each other, in opposite directions, i.e. the crack surfaces move directly apart. Mode II, the edge sliding mode, is where the crack surfaces move normal to the crack front and remain in the crack plane. Mode III, the shear mode, is where the crack surfaces move parallel to the crack front and remain in the crack plane. All correspond to respective stress fields in the vicinity of the crack tip.

The stress field at the crack tip can be treated as one, or a combination of the three basic types of stress fields. For practical applications, Mode I is the most important. Since even if a crack starts as a combination of different modes, it is soon transformed and continues its propagation as a critical crack, under Mode I. A crack that has grown entirely in Mode I is not necessarily straight and crack trajectories are difficult to determined. A crack tends to be attracted by the nearest free surface and may follow a curved path even under initially symmetrical loading conditions.

In mixed mode loading, the crack direction normally changes abruptly as growth starts. However, it is usual to consider the two-dimensional case and to assume the initial crack is straight and that crack growth is an extension of the original crack. This can usually be done without significant loss of generality.

2.9.2 Linear Elastic Fracture Mechanics

A linear elastic fracture mechanics (LEFM) approach is based upon an analytical procedure [2.23]. It relates the magnitude and distribution of the stress field in the vicinity of a crack tip to the nominal stress applied to the structure, size, shape and orientation of the crack and to the material properties. The distribution of the elastic stress field, in the vicinity of the crack tip, is invariant in all structural components subjected to this type of deformation. The magnitude of the elastic stress field can be described by a single parameter K, the stress intensity factor. The applied stress, crack shape, size, orientation and the configuration of the structure subjected to this type of deformation affect the value of the stress intensity factor. The stress field distribution is unaltered. The elastic stress field in the vicinity of a crack tip for tensile stresses normal to the plane of the crack, Mode I, can be seen in fig.2.19. Mode I is the predominant stress situation in most practical cases, Mode II and Mode III tend to be less significant and these contributions to fatigue crack growth can often be ignored. The stress intensity factor K, in the case of Mode I loading, can be expressed in the form below. Where σ_{no} is the nominal surface stress, a, is the crack depth and Y accounts for the effects of crack shape and geometry.

$$\Delta K_I = Y \sigma_{no} \sqrt{(\pi a)} \quad \text{.....(2.6)}$$

Provided K is the same for two different cracks, the stress fields near both crack tips will be identical and both cracks should behave similarly. It is for this reason that K can be described as the residual strength of a crack body. When the load is increased on a cracked component, the level of K at which the crack begins to propagate is called the fracture toughness of the material. For relatively thick materials in which conditions of plane strain develop, this critical value of K is considered to be a material property and is designated K_{IC}. For thinner materials where the toughness depends on thickness and developed plasticity, it is denoted K_C. An important limitation of LEFM is that it can only be used to characterise crack growth under conditions of small scale yielding.

2.9.3 Elastic-Plastic Fracture Mechanics

Elastic plastic fracture mechanics (EPFM), is an extension of the LEFM [2.24]. This is where large plastic zones form ahead of the crack tip. For example, where there is insufficient thickness to maintain plane strain conditions under slow loading. Therefore, the linear elastic analysis to calculated K_{IC} is invalid. However, there are three methods of analysing this elastic-plastic region:

- Crack Opening Displacement (COD)
- R – Curve analysis
- J – integral

a) Crack Opening Displacement

The fracture behaviour in the vicinity of a sharp crack can be characterised by the opening of the notch faces, namely the COD. The concept of COD is analogous to the concept of critical crack extension force, and, therefore, COD values can be related to the plane strain fracture toughness K_{IC} [2.25]. COD measurements can be made even when there is considerable plastic flow ahead of the crack tip, and, therefore, it is possible to relate the COD to the applied stress and crack length.

As with the K_I analysis (Mode I), the application of the COD approach to structures requires the measurement of a fracture toughness parameter δ_C. The critical value of the crack tip displacement, is a function of material property, temperature thickness etc.

b) R – Curves

The R–Curve concept, represents threshold behaviour and characterises the resistance to fracture of a material during incremental slow, stable crack extension. It is a plot of crack growth resistance as a function of actual or effective crack extension [2.26] [2.27]. K_R is the crack growth resistance at a particular instability condition, i.e. the limit prior to unstable crack growth, and is in units of MPa$\sqrt{m}$. The shape of the R–curve is assumed to be independent of the initial crack length, a. The specimen is assumed to be initially free from previous residual stresses in the vicinity of the crack tip, such as those resulting from previous fatigue loading.

A Typical R–curve is shown in fig.2.20. Where the solid lines represent the R–curves for different initial crack length, and the dashed lines the variation in K_I with crack length. For different constant loads, P1<P2<P3, each line is a function of the crack length, $K_I = f(P,\sqrt{a})$. The two points of tangency represent points of instability, or the critical plane stress intensity factor $K_C = K_R$, at that crack length. Where K_R is calculated by using the effective crack length a_{eff} and is plotted against the actual crack extension a_{act}. K_{IC} is governed by conditions of plane strain (ε_Z=0) with small scale crack tip plasticity and K_C is governed by conditions of plane stress (σ_Z = 0) with large scale crack tip plasticity. K_C values however, depend on 4 variables, temperature, loading rate, plate thickness and initial crack length.

c) J – Integral

The J-integral is a method of determining the stress strain field at the tip of a crack by an integration path that is taken sufficiently far from the crack tip to be substituted for a path close to the crack tip region [2.28]. For linear elastic behaviour the J-integral is identical to the energy release rate G per unit crack extension.

Therefore, a J-failure criterion for the linear elastic case is identical to the K_{IC} –failure criterion, under linear-elastic strain conditions

$$J_{IC} = G_{IC} = \frac{K_{IC}^2\left(1-\nu^2\right)}{E} \quad \text{.....(2.7)}$$

The energy line integral J is defined for either elastic or elastic-plastic behaviour

$$J = \int_R W.dy - T\frac{\partial U}{\partial x}dx \quad \text{.....(2.8)}$$

Where R = any contour around the crack tip, fig.2.21 shows the crack tip coordinate system and arbitrary integral contour.

2.10 Crack Closure

The assumption that a crack closes when the load falls to zero is a convention that is correct only for the purely elastic case. In practice, because of the crack tip plasticity effects, a crack may close below zero load; as it is propped open by the reversed plastic zone that develops on unloading [2.1]. However, because of the wake of plastically deformed material left by a propagating crack, a crack may close at above the minimum load in the cycle, even when this is above zero. Fig.2.22 [2.1], and is referred to as crack closure. The approximate radius for plane stress conditions r_P, of the plastic zone at a crack tip in a ductile metal, is given by the relationship [2.29] [2.30]:

$$r_p = \frac{1}{2\pi}\left(\frac{K_I}{S_Y}\right)^2 \quad \text{.....(2.10)}$$

Two plasticity effects can have a significant effect on fatigue crack growth behaviour and must be considered in the discussion of fatigue crack growth under non-uniformed conditions. One is caused by the residual compressive stresses due to reverse yielding at the crack tip after unloading; for an initially stress-free crack. This means that a compressive load is required to completely close the crack. Identifying compressive stress in a structure using FEA is addressed in chapter 6. The other is that a propagating fatigue crack leaves behind a wake of plastically deformed material adjacent to the fracture surface, and this phenomenon is responsible for crack closure. This wake may cause the crack to close at above the minimum load in the fatigue cycle, thus reducing the effective value of ΔK_I (ΔK_{eff}) to below the conventionally calculated value, fig.2.23, [2.1].

The concept of crack closure is sometimes used to explain the anomalous growth behaviour of micro structurally short fatigue cracks. Equation 2.6, dictates that for a constant Y, the driving force for crack growth, ΔK, should increase with crack depth. This predicted behaviour is in disagreement with the experimentally observed trends for micro structurally short cracks [2.31], and it is believed that cracks in this size range generate smaller wakes of residual plastic deformation than longer cracks growing under the same range of crack tip stress intensity. This is discussed further in [2.32].

Thus when a crack is very short (in the order of grain size), it remains open for a greater portion of the load cycle. Although it is widely accepted that plastically induced crack closure can influence the fatigue behaviour of cracks growing under conditions of plane stress. However, there is no general agreement that this type of crack closure is possible when there is sufficient material constraint to promote plane strain behaviour.

2.11 Environmental Effects

The environment that any material is subjected to, will have a major affect on the fatigue life of that material. Whether a microscopic flaw is present or not, the effects of inter alia: heat [2.33], atmospheric, acoustic and chemical all contribute.

If these environmental conditions are not fully understood or taken into account, then the failure through fatigue will occur much sooner than predicted. The effects of the environment such as sea water on material properties with regards to influencing fatigue life are address in chapter 3. The effects on the fabrication environment are reviewed in chapter 4.

Joints with high tensile residual stresses and superimposition of the stresses from the applied load in the same direction, largely show endurable stress amplitudes of constant low magnitude in the whole applied mean stress range. A corrosive environment such as sea water can increase the crack growth rate [2.34] and can further reduce the fatigue strength. This is termed Stress Corrosion Cracking [2.35]. This occurs when a metal is subjected to a steady tensile stress, rather than a compressive one, while wetted with a particular corrosive. Like fatigue, it occurs at well below the normal stress range of the metal. See chapter 7 for preventative measures. Salt deposits on stressed parts of standing structure can be the cause of this type of cracking. This acceleration of crack initiation, due to the environment and hence reduction in fatigue life, is beyond the scope of this thesis, but must be recognised and investigated should the material be permanently immersed in a highly corrosive environment.

2.12 Conclusions

The mechanism of fatigue, is well researched and documented, it is an eclectic field. The principal mechanism for fatigue is a constant cyclic load. The magnitude of the load is below that which would cause a failure from a single application. Fatigue cracking is initiated by dislocations within the crystalline structure of a material and forms a microscopic crack. Concentration of plastic strain at the crack tip initiates slip bands to form intrusions and extrusions at the material surface. The stress field in front of and surrounding the crack tip governs the growth rate and the stress intensity factor. The notch toughness of a material influences the rate of crack growth. Fracture mechanics is the science of analysing progressive crack extension. LEFM and EPFM is an analytical procedure to establish the magnitude and distribution of stress fields in a vicinity of a crack tip.

Metallurgical descriptions are concerned with the effect of fatigue loading on the state of the material, whilst mechanical descriptions are concerned with matters such as the number of cycles to failure, or the rate of growth of a fatigue crack. From an engineering viewpoint, the role of stress intensity factors and crack growth rates are important. Since these influence the behaviour of a fatigue crack within a structure, and can be affected and controlled by the designer, once known. It is clear that local stress fields have a significant effect on the stress intensity and hence the crack growth. Therefore the designer must pay particular attention to stress raisers and structural redundancy. Environmental conditions can promote crack initiation and affect crack growth rate. Understanding the nature of these influences is required to obtain repetitive analysis of actual nominal stress adjacent to a crack tip. Calculating the nominal stress and aspects that reduce the nominal stress level, through analysis, is the key to fatigue prediction and prevention.

3. Aluminium in Shipbuilding

In this chapter the merits of aluminium are discussed and comparisons against steel are made. In order to use a material, the designer must first understand its characteristics. Only then can the designer utilise the full benefits of the material. This chapter will investigate the characteristics of aluminium and its alloys so the designer is aware of its limitations as well as its benefits. The annual production of aluminium has steadily grown over several decades, and this trend has also been mirrored in the shipbuilding industry, fig.3.1, [3.1]. It is only by understanding the behaviour and characteristics of aluminium that vessels like that shown in fig.3.2, are able to operate successfully and free from fatigue related problems.

3.1 Atomic and Crystalline Structure of Aluminium.

The analysis of the crystalline structure will highlight any particular irregularities compared with standard crystalline formations, which may then lead to a greater understanding of its behaviour under certain conditions. In section 2.2 and 2.4, the nature of crystalline structure and its effects on fatigue are discussed. Aluminium, chemical symbol Al, has the atomic number 13, and has an FCC crystalline structure [3.2]. The three electrons in the outer orbit give the aluminium atom a valence or chemical combining power of +3. It has a specific gravity of 2.7 compared to steel, which has a specific gravity of 7.8.

As discussed in 2.4, concerning slip systems, the crystalline structure of a material has a direct influence on its fatigue characteristics. It is shown that FCC crystalline structures deform by dislocation motion on very well defined slip planes. When metal changes from the molten to the solid state, it assumes a crystalline structure. The atoms arrange themselves in definite ordered symmetrical patterns that are described as lattice structures. Aluminium, like copper and gold, crystallises with the FCC arrangement of atoms, also fig.3.3, which is common to most ductile metals.

3.2 Mechanical Properties of Aluminium

Aluminium is a versatile metal and has many alloys, see section 3.3. Aluminium has no clearly defined point on the stress-strain curve at which the elastic limit is reached like steel, [3.3] fig 3.4. The convention, for use with aluminium, has been adopted for identifying the stress-strain properties and which is known as the proof stress. Proof Stress is defined as the stress that while the load is still applied, a non-proportional extension equal to a specific percentage of the extensometer gauge length [3.4]. For aluminium this value is 0.2%. This proof stress indicates the onset of plastic movement. From the curve shown in fig.3.4 it can be seen that the strain per unit increase of stress is much higher for aluminium than for steel, as shown by the lines at A and B. Additional properties of aluminium are listed in [3.5].

3.3 Alloy Identification.

Aluminium has many different characteristics and properties when alloyed, and its behaviour and mechanical properties also change depending on the kind of treatment it receives, pre and post alloying, fig.3.5 and table 3.1 [3.6]. The first four digits in the designation indicate the alloy group in terms of the major alloying elements [3.7]. In Group 1XXX, the second digit indicates the modification, if any, in the impurity limits. These can be any number from 0 to 9, where zero indicates that there is no special control of individual impurities. The numbers 1 to 9, inclusive indicate a special control of one or more of the impurities. The last two of the four digits indicate the minimum percentage of aluminium.

For example, 1070 indicates 99.70% purity; the alloy 1100 however, indicates a minimum of 99.00% aluminium, which requires some control of one or more of the impurities. When referring to the alloy series, it is common to use the term thousand as in 6000 (six thousand) or 5000, rather than the official 6XXX where the letter "X" notation for the 'digits' is being used.

For the remaining alloy group, 2000 to 8000 inclusive, the second digit in the 2000 - 8000 alloy serves to indicate the modification. The assigned numbers can be 0 to 9 inclusive, whereas 0 signifies the original alloy and the numbers 1 to 9 indicate alloy modifications. The last two digits only identify the different aluminium alloys within the group. The shipbuilding industry uses only two of the eight alloy groups, the 5000 and 6000 series alloy's [3.8] [3.9]. The HSS Stena vessel did experiment with using the 7000 series alloy, owing to its superior mechanical properties to the 6000 series, [3.10]. However, the 7000 series alloy is prone to corrosion which was not anticipated. It is these two alloy series namely 5000 and 6000 series that this thesis will review. A review of the other alloy groups is beyond the scope of this thesis. There is considerable literature regarding the 5000 and 6000 series alloys. A précis of these two alloy groups and their tempers are given in sections 3.4 - 3.6.

3.4 Temper designations

The temper designation system indicates the strength, hardness and ductility for wrought and cast aluminium alloys, with the exception of ingots. The system is based upon letters that represent the primary temper. Numbers that follow indicate temper subdivisions, see table 3.2, [3.11].

3.5 Non-Heat Treatable Alloys: 5000 Series

The method of hardening the 5000 series alloys is by Strain Hardening and uses the designation of, H, [3.12]. This is where the alloy is rolled or worked by some mechanical means, and uses the slip planes within the alloy to dislocate and move the crystalline structure much closer together, fig.3.6. The dislocations become entangled within the crystal, thereby forming obstacles to further dislocation motion and hence increase in strength, see table 3.4. If the alloy is used at elevated temperatures, work hardened alloys are not recommended. Since the mechanical strain hardened strength will be lost, owing to the aluminium becoming re-annealed, see 3.7.1. The most common tempers are shown in table 3.3, [3.13].

The designations of the tempers are thus:

F	As rolled and implies no guarantee of mechanical characteristics
H111	The Plates are roller levelled after annealing to enhance their dimensional characteristics
H116	This is a special quarter hardness condition with mechanical characteristics close to those of H22 or H32

It is worth noting that the *harder* the temper (highly strain-hardened) the higher the chances of exfoliation, which in turn creates a serious problem with corrosion [3.14]. Exfoliation is a type of corrosion that propagates in a large number of planes running parallel to the direction of rolling, see fig.4.6, such as in the H321. Between these planes there are very thin sheets of sound metal. These sheets are gradually pushed away from the surface by the swelling of corrosion, hence the term exfoliation.

In hot rolled marine grade alloy, the magnesium is distributed evenly throughout the metal in very small quantities. The magnesium reacts with the salt water oxidizing and forming a white hazy coating, which acts to protect the aluminium plate [3.15]. A cold rolled process adopted by some mills, prevents this process from occurring. When using this H321 temper it is important that the alloy has been manufactured under strictly controlled conditions. To overcome this, the free edges must be correctly coated to prevent possible peel.

Table 3.4 shows the change in mechanical properties of strain hardening [3.16], [3.17] using a 5183 filler wire. The as-welded values may vary from source to source. This is owing to the filler wire used for the welding. When using the 5183 filler wire, the as welded strength is in the order 10 MPa higher than would be if using the 5356 filler wire [3.18]; see 4.8 for further discussions on filler wires.

3.6 Heat Treatable Alloys: 6000 Series

The 6000 series aluminium alloys harden and achieve a high strength by heat treatment in a manner different from that of steels [3.19]. The aluminium alloy is first solution heat treated, then quenched and finally age hardened. In contrast to steel, which hardens upon quenching, aluminium alloys becomes soft and ductile. These alloys harden and increase in strength by age hardening (T4 –T6 tempers). The strength of alloy, in this series, is enhanced by the addition of elements such as magnesium and silicon. These elements show increasing solid solubility in aluminium with increasing temperature; thermal treatments impart pronounced strengthening.

The first step called heat treatment or solution heat treatment and is an elevated temperature process designed to place the soluble elements in solid solution [3.20]. Solution treatment involves heating the alloy to a temperature just below the lowest melting point, approx 540° C and holding at this temperature until the base metal dissolves a significant amount of the alloying elements, fig.3.7. The alloy is then rapidly cooled to retain much of the alloying elements in solution as possible, and so produce a supersaturated solid solution.

At elevated temperatures, even at room temperature, the alloys are not stable after quenching, and precipitation of the constituents from the supersaturated solution begins. After a period of several days at room temperature, termed ageing or room-temperature precipitation, the alloy is considerably stronger. Many alloys approach a stable condition at room temperature, but some alloys, particularly those containing magnesium and silicon (6000 series), continue to age harden for long periods at room temperature, such as T4 temper. This ageing process takes place over a matter of days or, at most, a few weeks. After that, the properties will remain stable over decades. However, most alloys are given an additional heat treatment to obtain the highest mechanical properties, table 3.6. This heat treatment consists of holding the material at approximately 205°C for a few hours. During this time, the alloying additions that were dissolved in the prior heat treatment precipitate in a controlled manner, and this strengthens the alloy.

This process is called artificial ageing or precipitation hardening (T6 temper). A combination of solution heat treatment, quenching and artificial ageing, leads to highest strengths being obtained. In the 6000 series there is generally one alloy that is commonly used in shipbuilding, which is 6082, in the T6 temper [3.9]. The alloy 6061 was used for many years, but the high content of copper showed its use, especially under the waterline, to be less than satisfactory owing to its poor corrosion properties [3.21]. Consequently, it has been phased out by the Classification Societies, such as Det Norske Vertias (DNV) and Lloyd's Register (LR). Other 6000 series alloys are being developed and have shown themselves to be as good as 6082, with better extruding characteristics, making them cheaper to produce, 6005A for example [3.22]. However, the higher allowable copper content of the 6005A precludes its use in direct contact with seawater [3.21].

3.7 Effect of Welding on Mechanical Properties

During welding, the heat from the electric arc reduces the alloy strength for distances up to 25mm on either side of the bead, fig.3.8 [3.23]. The reduction in strength depends upon the alloy and its temper, tables 3.4~3.6.

3.7.1 The 5000 Series Alloy

In designing welded structures using non-heat-treatable alloys, it must be noted that the welded and unwelded properties differ for each temper. The heat of welding acts as a local annealing operation, significantly weakening the heat affected zone (HAZ) of the weld, see table 3.4.

If the design is based on the strain-hardened properties, the allowable design stress will be above the yield point of the HAZ. The properties in the HAZ will be those of the O temper annealed material due to the welding operation. Therefore, a design must be based on the annealed properties rather than the strain-hardened properties. In table 3.4, H321 temper as welded is quoted at 125MPa, in [3.17], however it is quoted as 130 MPa.

3.7.2 The 6000 Series Alloy

The situation is different when welding the heat-treatable alloys. The heat-treatment process, which produces the higher strengths, is lost owing to the heat of the arc during welding. The heat from the arc, is above the 540°C used for the precipitation hardening. The welding process will anneal the alloy in way of the HAZ. The reduction in strength of the 6000 series alloy, once welded, is significantly higher that for the 5000 series alloy. The reduction is approx 40-50%, table 3.6. This reduction is reflected in the allowable design stress limits permitted [3.24].

3.8 Fatigue Properties

Structures exposed to fluctuations in load are susceptible to failure by fatigue. In common with other metals, aluminium will fracture when subjected to repeated or variable loads at stress levels considerably lower than would be the case with static loads. The SN curve for aluminium differs from typical curves for mild steel in that in most cases it does not become asymptotic to the N axis, even after the test has been continued well beyond the number of cycles commonly applied, fig.3.9 [3.25]. The fatigue resistance is reduced by local stress raisers, and is discussed further in chapters 4 and 5. The characteristic fatigue behaviour is shown in fig.3.10 [3.1]. It can be seen that the heat treatable alloy, 6000 series, has a lower fatigue limit when compared to the non-heat treatable alloy 5000 series. It can be further noticed that the fatigue strength varies from 25-50% of the static tensile strength. Therefore the designer needs to recognise the differences of fatigue behaviour of these two aluminium alloys to prevent unwanted failures.

3.9 Fatigue Life of Welded Aluminium

The fatigue life of aluminium progressively becomes worse when welded, fig.3.11. This data taken from unpublished US Navy research, shows that in air, the strength of a weld has been reduced by approximately 50%, from the base metal in fig.3.10. The influence of a sea water environment is noticeably damaging.

High speed ferries are in a corrosive environment of sea water [2.35]. Therefore the fatigue strength of aluminium welds in sea water must also be investigated. It can be seen that in seawater the strength reduces significantly to around 10% of its base 0.2% proof stress limit. This is also noted in [3.26]. The fatigue life of welded joints in air is discussed further detail in section 4.7.1. The curves in fig.3.11 demonstrate the deleterious effects that seawater has on the fatigue life of a welded aluminium structure. A designer can accommodate the fatigue strengths of complex welded joints in contact with sea water using large factors of safety coupled with very careful detail design. This however will increase the structural mass of a weight critical vessel [1.4].

Two companies have begun to address the low fatigue life of as welded strength. These new alloys are in the 5000 series. Corus, formerly Hoogovens, Alustar, or 5059 [3.27] as it is designated, and Pechiney's 5383 [3.28]. The two alloys have different chemical compositions noticeably the magnesium and zinc content, yet exhibit similar fatigue characteristics. In fig.3.12 it can be seen that 5383 has improved fatigue strength by 16% compared to the original 5083 alloy. The increase in as welded static strength is also of the same order of magnitude.

3.10 Crack Growth

In section 2.7, crack propagation was discussed and how minor flaws or cracks influence the rate of crack growth. Equation 2.4 and table 2.1 show that the propagation rate of 5000 series alloy is approximately proportional to the cube of the effective stress range. However, when using 6000 series, the propagation rate is to the power 4. This means that when using a 6000 alloy a crack will grow far quicker for the same design detail than in a 5000 series alloy. Hence, for a 5000 series alloy, a doubling of the stress will lead to eight times shorter crack initiation life and eight times faster crack growth. Whereas a 6000 series alloy, will be sixteen times shorter initiation life, and sixteen times faster crack growth. Therefore a designer should avoid using a 6000 series alloy that is in direct contact with sea water and in a high cyclic region if a 5000 series alloy can be used instead.

3.11 Conclusions

Since aluminium is as strong as steel but at a third of its weight, this makes it very attractive for use in high speed vessels of light weight design. The alloys of aluminium are varied in number and behaviour, and range in mechanical strength owing to their differing alloying elements. This influences where the designer can use certain alloys or temper. Once welded, the change in mechanical properties can be significant and should not be overlooked.

The fatigue resistance of aluminium is demonstrated to be poor compared to steel, especially when welded, and in a sea water environment. The fatigue strength of 5000 series alloy is also shown to be higher than 6000 series alloy. Therefore, correct selection by the designer in using the 6000 series alloy is required. However, once the designer understands the limitations of each alloy and its tempers, the benefits can be used with confidence.

4. Manufacturing and its influence on crack initiation

This chapter reviews the manufacturing and production environment and how it influences fatigue life. The designer has little control over the fabrication of a welded vessel. Therefore the designer must specify the choice of material and design controls during the design process. The mechanics and mechanisms involved in the production process promote brittle or ductile fracture.

4.1 The Working Environment

The conditions within a working shipyard for welding are not ideal. For example, the temperature may vary from morning to afternoon, the skill of the welder and his motivation, the condition of the metal prior to welding as well as joint preparation etc. All structural calculations are based upon a prescriptive method, given certain conditions are accepted, and the designer assumes these conditions have been satisfied. The welding procedure in a shipyard environment is different to that in a strictly controlled environment inside a laboratory. The designer must be aware of the difference this has to take into account the environment effects which the joints are prepared and produced. The first link in this long of events begins with the manufacturing process of each temper and alloy.

4.1.1 The Effects of Different Tempers

The first issue is the process involved to manufacture the alloy. The aluminium mill is required to design and control a manufacturing schedule involving the following steps:

Melting $\Rightarrow$ Liquid Treatment $\Rightarrow$ Casting $\Rightarrow$ Heat Treatment $\Rightarrow$ Hot and Cold Rolling $\Rightarrow$ Heat Treating $\Rightarrow$ Finishing

Each of these steps or combinations has a definite influence on the properties and behaviour of the material which satisfies these requirements [3.22]. Two distinct means for optimising the manufacturing and cost requirements for HSLC construction are considered:

- A statistical approach. Based on a large number of design of experiments relating the step parameters to the final properties.
- A physical approach. Which requires the exact description of microstructural parameters and material features relevant to the requirements.

The shipyard and the designer are unable to predict the affects of the processes. The Quality Control, QC, and Quality Assurance, QA, departments within the mill producing the alloy and the shipyard receiving it check the alloy for micro-cracks Such micro cracks can occur during the strain hardening process of 5000 series alloys, see section 3.5, to improve the mechanical properties (slip plane manipulation), as well as the solution treatment process of 6000 series alloys, see 3.5 and 3.6. Tests have shown [4.1] [4.2], that crack initiation is increased at higher temperatures and could arise due to stress corrosion cracking during the quenching phase of the alloy. Despite such tight quality controls, a manufacturing defect can occur. Efforts are made by the mills to prevent this happening. Various methods have been adopted to overcome this rare occurrence [4.3] with limited success.

This is illustrated by the following example. The plating surrounding the region of the inlet duct of a waterjet began to crack in the centre of the plate, after several months in service, see fig.4.1. The plate is subjected to vibration from the waterjet impeller and it appeared that a small micro-crack was present in the plate. This is evidence of failure through ductile transgranular fracture, see 4.2.1, possibly owing to manufacturing of the alloy or the effect of different tempers. This is coincidentally, located in the worse position, i.e. in the centre of a panel. Hence it was subjected to higher displacements owing to the exciting forces. The exciting forces being the vibration of the hull owing to: sea pressure loads, main engine machinery, shafting, jet impellor and hydrodynamic pulses within the jet duct [3.24] [4.4].

4.2 The Alloy's Condition in The Shipyard

Once the alloy arrives in the yard, it must be stored. The most common way to store sheets of aluminium is flat, with wooden blocks between several layers of sheets, or vertically [3.7] [3.13].

Aluminium sheets should never be placed directly on the ground, even if this is cemented, and should be kept away from splash water, condensation and hostile chemical environments. It should be stored, where possible, under cover in a ventilated space. It is worth noting that if a wet, wick-like material (such as wood) is allowed to remain in contact with aluminium for a long period of time, the metal forms a copious amount of a sticky white hydroxide. This is called Poultice corrosion [3.8]. The humidity and temperature must also be monitored, to prevent the ambient environment falling below the dew point of the atmosphere [3.12]. Should the corrosion process begin whilst the alloy is in storage, it will affect the fatigue properties of the alloy. Corrosion in 5000 series alloy for example, will exhibit precipitation of Al_3Mg_2 at the grain boundary. The precipitation will effect the homogenised crystalline structure. This intergranular or exfoliation corrosion is discussed in section 3.5. The intergranular corrosion resistance is improved in the 5383 alloy. This is linked to the improved homogeneous microstructure [4.5].

4.2.1 Intergranular and Transgranular Fracture

The microstructure of engineering alloys is complex, fig.4.2 [4.6]. Examples of transgranular fractures are void coalescence cleavage fracture and fatigue crack initiation and growth. Intergranular fractures include grain-boundary separation with and without void coalescence. Ductile transgranular fractures are caused by void nucleation at second-phase particles or grain boundaries [4.12]. Void coalescence occurs with increasing strain. The two types of types of fracture are classified in table 4.1.

4.3 Dimensional Aspects

There are several important features to be considered when dealing with dimensional aspects [4.7]. Mills control the tolerances with respect to the Classification Society rules [3.17] [3.24]. In the case of plates, shipyards are looking for:

- Wide plates to minimise welding
- Flatness and overall dimensional control to improve workmanship
- Tight tolerances to reduce weight

The availability of wide plates depend upon the rolling line configuration (width of the hot and cold mills) as well as on the alloy type and temper. The width of the product, or sheet, may be limited by the rolling pressure, which is directly related to the work hardening behaviour of the alloy within the roll gap. The work hardening of aluminium alloys increases with the magnesium content during hot or cold working. It is therefore, more difficult to attain large widths with 5456 than for 5083, than for 5754 [3.13] [3.22] [4.8].

Edge cracking during rolling, also increases with the magnesium content [3.13] [3.22]. Strong alloys have a tendency to localised deformation, thus impairing ductility and overall dimensional aspects such as squareness, lateral bow, flatness etc.

4.4 Cutting the Metal

When marking the plate, scribing tools should be avoided, since tracing marks that might be left on the finished part will become sites of crack initiation under high loads. It is advisable to trace using a hard pencil (5H) although shipyards tend to use a permanent marker pen (felt type). Marker pens do not leave carbon deposits on the plate; since carbon is higher on the reactivity series and therefore a potential source of corrosion. Plate or crocodile shears can be used to make straight cuts. The rating of the shear should be more or less the same as for cutting non-alloyed steel with a low carbon content.

For aluminium, in the H116 condition, the use of the shear should be restricted to thinner plate to avoid localised stresses that can lead to stress concentrations. Cutting is a plain-strain process. The chip, the waste material created by the action of cutting, moves along the rake, fig.4.3. There is a distinct transition region in the vicinity of the line AB in the fig.4.3 revealing severe distortion [4.9]. This is termed the primary shear zone. The line AC is the secondary shear zone.

The forces exerted on the chip are shown in fig.4.4. The behaviour of the work material encompasses: finite and localised plastic flow, heat and temperature rise, inhomogeneities and fracture. Fig 4.5 shows a typical temperature distribution in orthogonal machining. It can be seen that regions of greatest gradient in temperature coincide with the primary and secondary shear zone. The shear-plane temperature will affect the mechanical properties of the alloy in the same manner as discussed in section 3.7. Methods for cutting in large quantities are water or fluid jet and plasma. Aluminium can be cut using water jets bearing abrasive particles at high pressures (3000 bars and over). Granules of garnet, corundum or other very hard minerals are used, and can cut aluminium up to 100mm thick. The water jet produces a cut that is straight and clean and accurate to within $\pm$ 0.2mm. There is also no heat affected zone (HAZ) [3.5].

4.5 Bending and Forming

Aluminium does not require any special folding tools. Conventional table folding machines or presses are adequate provided the working parts of the tooling are free from irregularities. It is a good precaution, as in cutting, to remove all score marks from the edges, preventing the formation of cracks at points of deep deformation. Shaping should be performed in the annealed, O and H111 tempers see table 3.3.

The skill of the plater can have a marked effect on the end result of the bending and shaping. An experienced plater can see the line of the rolling on the plate, to work harden the alloy by the mill. The plater will then be able to bend the plate along these lines rather than against it, see fig.4.6 [4.10]. Should the bend be required to be *against the grain*, then the plater's skill will indicate that a larger bend radius is required. This is similar to the bracket failure, discussed in 4.5.1. Therefore the designer must be aware of the implications of the detail design on the manufacturing process. Otherwise small cracks that do not at first appear to the naked eye, will eventually propagate and become visible once the joint has been welded. These surface cracks may go undetected by virtue of the microscopic size. Standards for minimum bend radius assist the plater in preventing crack initiation [3.17] [3.24] [4.11].

Processes described such as rolling, cutting, bending etc will work harden the alloy, see sections 3.4 and 3.5. This reduces its capacity for deformation and its ductility. Reducing a metals ductility and ability to deform affects the behaviour and mechanical properties. This is because the work hardening process can over strain the alloy and promote plastic deformation. A reduction in ductility, as a result of plastic deformation, will lead to ductile fracture, [4.13]. Ductile fracture is normally transgranular.

4.5.1 A Typical Manufacturing Error in Bending

The following example describes an error that is due to the manufacturing procedure of the part. The drawing, and the detail design, was correct; the part did not fail owing to the design. A replacement part was subsequently manufactured correctly and is without a repeat of the failure.

The bracket shown in fig.4.7 is made from steel. The environment that the bracket is in is far from ideal, this being the proximity of the waterjet impeller spinning at 1000 RPM in sea water for 18 hours a day. The bracket is used to act as a spacer between grills in a waterjet inlet grill. The detailed drawing indicated a radius of a certain size. When the bracket was fabricated, it was pressed into shape rather than formed. This resulted in a radius that was too tight on the inner surface of the bracket. Due to the manganese sulphide in the steel, the bonding of the matrix in the voids is weak

As discussed in [4.13], voids can nucleate at low strains, like the tight inner radius of the bracket. This is similar to the process of locally increased strain and plastic deformation of ductile fracture discussed in 4.2.1. However, here the situation is slightly different. The inner radius is constrained; this affects the behaviour and mode of fracture. Fracture is preceded by the formation of large plastic zones ahead of the crack or flaw. This initiated the failure through fatigue. This illustrates the lack of control the designer has on fabrication.

4.5.2 Straightening by Heat

The method of straightening by shrinkage heats is used on alloys without age hardening. For example, alloys in the 5000 series in an annealed, or semi-annealed, metallurgical condition. An appreciable drop in mechanical characteristics, is observed in age-hardened alloys as discussed in 3.7.2, therefore this method should be avoided for the 6000 series grades The reduction in mechanical properties can be as much as 50% in its mechanical properties, as observed in the HAZ [4.14].

4.6 The Welders Skill

This aspect of fabrication is subjective and at times contentious. There is also very little literature on the subject, despite errors that can be seen on the shopfloor of many shipyards. However, the designer needs to be aware that skill is a factor in the weld quality and hence the mechanical property of the weld [4.19]. Owing to a reduction in the position of apprenticeships and day release schemes, the full formal training of skills is lacking. Many shipyard fabricators find it difficult to resource appropriately skilled manpower [4.15]. Many welders have difficulty in demonstrating anything beyond an ability to pass a BS 4872 or BSEN 287 type of welder competency test [4.16]. There is a need to train welders in a wide appreciation of quality acceptance levels, and to recognise that developed skill by means of certification [4.11]. For example, using the dye penetrant test on their own welds, prior to final inspection by the surveyor. This is also recommended procedure for repair of manufacturing errors during construction [4.17].

4.7 Effects of Weld Imperfections

The effect of weld quality has been demonstrated in [4.18] [4.19]. The fatigue life of a weld exhibits different characteristics owing to the quality of the welding by different fabricators, on the same specimens.

This demonstrates the importance of quality control on the welding procedure since the quality effects the anticipated fatigue life of a welded joint. A good quality weld will be indiscernible compared to a poorer quality weld by simple visual inspection.

At any level of examination, all welded structures contain pre existing cracks or crack like flaws. The most significant of these are essentially associated with geometric stress concentrations, for example. Abrupt change in section, weld toes, weld stop/starts, porosity, lack of fusion etc [4.20]. These affects are discussed further in 4.7.1. Welded joints are neither homogenous nor isotropic, and hence the extension of a pre-existing crack will be affected by the properties of the surrounding regions. In particular, crack extension will be affected by variations in fracture initiation and propagation toughness, and variations in yield strength. Because weld metal and HAZ have different yield strengths to the base metals, the welded joint will deform as a composite. Since if one weld region yields, the surrounding regions will experience different stresses or strains and crack driving forces which may be significantly different to those implied by the global stresses on the weldment [4.21].

In terms of geometry, the sites for the onset of ductile and brittle crack extension tend to be the same. Both being associated with stress concentrations and/or pre-existing cracks or crack like flaws. However, the paths of crack propagation may be different, since ductile fractures tend to be dominated by the net section stresses rather more than brittle fractures. Ductile fractures propagate into thinner sections or lower yield strength regions. In contrast with this behaviour, brittle fractures propagate at stresses less than yield and their paths are dominated by brittle regions, residual and/or thermal stresses and reflected stress waves. Additionally, brittle fractures are observed to propagate from thin to thick sections [2.23] [2.24] [2.28] [4.21]

Different weld characteristics, for example internal or external, source of imperfection, or the type of the imperfection can classify weld imperfections, fig.4.8. The implications on fatigue life are investigated in 4.7.1.

4.7.1 Internal Defects

a). Cracks

Cracks usually form as hot cracks in the heat affected zone, or the weld itself, during the cooling period [4.22]. It is a function of the chemical composition. A weld solidifies under the strain imposed on the shrinking metal by its solid surroundings. The larger the difference between the solidus temperature, and that which the solidifying metal first becomes coherent, the larger the strain. Hence the greater tendency to crack. For standard alloys and filler metals, problems arise generally from cracks at end craters only. They can be minimised through joint optimisation, a welding plan and a welding sequence, and a qualified welder. Alloys with higher silicon concentration, may develop cracks in the remelted base material, (liquation cracking, see 4.8.2). This problem depends on the combination filler-base metal and the welding parameters [4.23]. Hot crack sensitivity of aluminium alloys increases with increasing amounts of elements that form eutectics with aluminium, up to a maximum and then decreases see fig.4.9.

b) Porosity

Porosities are the most common defects in welded connections, and are often regarded as an inherent feature of metal inert gas (MIG) welds [4.9] [4.24]. Typical appearance of finely distributed porosity in a weld is shown in fig.4.10. The main cause of porosity is absorption of hydrogen in the weld pool, which forms discrete pores in the solidifying weld metal [4.25]. The most common sources of hydrogen are hydrocarbons and moisture from contaminants on the parent metal and filler wire surfaces, and water vapour from the shielding gas atmosphere, fig.4.11. A gas shield that is unable to protect, owing to lack of shielding from the wind, will also cause porosity. Trace levels of hydrogen may exceed the threshold concentration required to nucleate bubbles in the weld pool. To minimise the risk, rigorous cleaning of the material surface and filler wire should be carried out. This is in evidence in most yards, as the edge to be welded is buffed off with a grinder to expose clean, fresh metal ready to weld [4.11] [4.26].

Up to 35% porosity in welds will reduce the fatigue life of butt welds by a factor of up to 200, once the weld has been ground flush fig.4.12, [2.16]. However, values of up to 15% porosity have been reported as insignificant to the fatigue strength, but much will depend upon the size of the individual pores and their distribution within the weldment. In 5086 alloy, for example, tensile tests [4.27] show that as little as 4% porosity can reduce the tensile ductility by up to 50%. Whereas the yield strength is only slightly reduced.

c) Inclusions, Oxides

Oxides form crack-like imperfections because of their planar character with a thickness of 1 to 10μm and sizes below 0.5mm. Non-metallic inclusions (oxides) in welds are unlikely to originate in the aluminium base metal. As with porosity, it is a function of welding procedure. Internal oxide is usually present only in aluminium powder metallurgy products where internal oxide content greater than 5% severely reduces the apparent fluidity [4.14]. The oxide of aluminium is strong and has a high point of melting, approximately 2050°C. The oxide is heavier than the melting parent metal and can therefore cause inclusions.

Owing to their microscopic size, especially thickness, oxides are difficult to detect by NDT. For aluminium welds the geometry of the weld profile overrides possible notch effects of inclusions, as is often the case with fillet welds. However, it can accelerate the crack initiation and propagation process of a relatively high notch stress [4.28]

d) Lack of Fusion / Penetration

Unfused interfaces between filler metal and base metal or between different layers of the filler material, are characterized as fusion defects, or lack of penetration (LOP) and lack of fusion (LOF). Inadequate penetration means the weld pool does not reach the weld root, therefore a root gap is left [4.29]. Poor alignment can also cause this to occur. LOP and LOF are similar imperfections but they may have different characteristics. However, both will exhibit a detrimental effect on fatigue strength.

The opposite surface of an LOF imperfection will usually be compressed together by residual stresses and this will lead to a higher fatigue life, see effects of compressive loads on crack growth in 2.10. The imperfection may be difficult to detect by means of non-destructive testing. Acceptable imperfection sizes derived from test results are shown in, fig.4.13 [2.16]. For as-welded joints, the LOP size may be between 1 mm and 2 mm and this is compatible with fracture mechanics analysis results. For butt joints with reinforcement removed, this limit value has to be reduced below 0.5 mm for sound welds.

e) Weld Shape

A weld bead across a plate would locally produce a change of shape, and if loaded as shown in the direction shown fig.4.14, a stress concentration is created [4.30]. This concentration occurs at the toes of the weld, and the magnitude of the peak stress will depend upon several factors. If there is a smooth transition between the plate and the weldment, the stress concentration will be low, but if there is an abrupt change of section the stress concentration will be high. The geometry produced by the weld bead is similar to that produced in the transverse butt weld. In general, a transverse fillet weld produces an even greater stress concentration; the change in section is more abrupt. This is explored further in section 6.1.2 in Hot Spot and Notch Stresses. Major parameters of the weld shape are the reinforcement angle and the toe transition radius [2.16] [4.28] [4.30]. The bead height is a secondary parameter. Nevertheless, for butt welds, the bead height, and for fillet welds, the convexity is the standard parameter for characterising the weld profile. On the condition that the weld profile is circular with radius, r, the toe angle, α, is a function of bead height, h, and weld width, b, fig.4.15 & equation 4.1.

$$h=r.(1-\cos\alpha) = b.(1-\cos\alpha) / \sin\alpha \quad \text{.....(4.1)}$$

It is worth noting that the weld itself need not carry, or transmit, the applied load to introduce a stress concentration. Changing the shape of attachments has shown to have about 25% effect on the fatigue strength [4.31]. A weld bead that is either too large for the thickness of plate, or perhaps a slightly cold weld, to the weld that has been dressed (ground flush) can reduce the fatigue life from 25% up to around 60% [3.13]. This is shown in fig.4.16.

f) Arc Strike & Splatter

Arc strikes outside the weld are infrequent in aluminium weldments, but may reduce the fatigue strength of the joint in a way similar to the reduction due to a butt weld. A bead on a plate, parallel or transverse to the plane of loading, $\sigma_{\parallel}$ or $\sigma_{\perp}$ and arc strikes, fig.4.17, can cause a reduction in fatigue strength, γ, in the order γ = 0.6-0.7. Values of γ = 0.9-1.0 can be achieved by grinding flush, as for a butt weld, fig.4.16. It has been reported in early experiments that spot welds only achieve 10-15% of the static strength [4.32]. It is suggested that the low figures are due to a combination of tension and bending stresses. Experiments in steel spot welding have shown this can cause a difference in fatigue crack paths, which in turn creates a change in crack growth rate [4.33], and hence fatigue life. Therefore extra care must be taken to avoid arc strikes and splatter.

g) Geometric Misalignment

The effect of misalignment is to increase the stress experienced by the joint when it is loaded, as a result of the introduction of local secondary bending stress. In the case of stress concentrations due to weld geometry, misalignment is only harmful if it presents a discontinuity to the applied load paths [4.30]. Thus, secondary bending stresses do not arise as a result of misalignment in continuous welds loaded longitudinally. Misalignment has no effect on fatigue strength if the only loading on the joint is bending. The distinction between misalignment and other flaws, already mention in parts a) - f), is that it does not introduce an alternative site for fatigue crack initiation. It enhances the severity of existing stress concentrations, notably the weld toe.

The magnitude of the secondary stress amplitude depends on the overall design of the joint. In the case of linear misalignment of welded plates, the secondary bending stress, σ_M, can be estimated by the simple relation in equation 4.2, fig.4.18, [2.16] [4.30].

$$\sigma_M = \sigma_N .3.e/t. \qquad .....(4.2)$$

With σ_N denoting the axial stress, t, the plate thickness and e, the eccentricity. Thus, the total stress at the weld toe in the plate is:

$$\sigma_N + \sigma_M = \sigma_N \, . \, (1 + 3.e/t) \ldots\ldots\ldots (4.3)$$

The term in brackets is the stress magnification factor, K_m. Thus, for axial misalignment of only 10% of the plate thickness (e/t = 0.1), K_m = 1.3. A similar increase in stress can arise as a result of 1° angular misalignment, while a combination of both these slight imperfections gives K_m = 1 + 0.3 + 0.3 = 1.6. In practice, it is often difficult to avoid such slight misalignment, especially angular distortion, in butt-welded joints. This is also discussed in section 4.9.1.

h) Post Weld Mechanical Imperfections

Post-weld mechanical imperfections reduce the fatigue strength of reinforcement-removed butt welds. Other weld types are not affected by usual mechanical imperfections such as hammer indentations or grinding notches of minor depth. Drilled holes show fatigue behaviour similar to sound as-welded butt welds, if net section stresses are compared. Therefore, improperly drilled holes should not be repaired by filling the hole with weld material. As the result may be LOP and LOF imperfections with consequent lower fatigue strengths. Undercutting the toe of the weld [3.24] [4.28], in regions of high cyclic loading, has a beneficial effect on the fatigue life of the weld, when done deliberately, see section 5.8.1 and fig.5.13. Shot Peening produces work hardening and roughness modifications on the surface and leaves a compressive residual stress field [4.34] [4.35]. As discussed in 2.10, cracks only propagate in regions of tensile loads.

i) Residual Stresses

Manufacturing techniques invariably produce locked-in stresses in the structure. Fabrications by welding also induce stresses of this nature, the existence of which is independent of any external loading. It is a condition that locked-in stresses are balanced within the body of material, which are in equilibrium. This is discussed further in section 4.9.

Residual stresses arise as a consequence of the heating and cooling cycle of welding. The expansion and contraction of material close to the heat source is inhibited by the restraining effect of adjacent material, or structure, at a lower temperature. The structure has to accommodate a new unnatural length by plastic strain and, when cold, is subjected to longitudinal tensile stress. This promotes the onset of ductile fracture owing to the large strains involved.

The magnitude of residual stresses introduced by welding depends upon the tensile strengths of the weld and parent metal. In 5000 series alloy, the two are closely matched, in the 6000 series, the weldment has a lower strength than the parent metal, see section 3.7. Residual stress is altered after the first load, or overload cycle, by local yielding with stress redistribution. This is the reason that in the range of lower cycle fatigue (for $N \leq 10^5$), a difference between the different welded components is difficult to establish. In the high cycle fatigue range, the residual stress state is altered because of cyclic relaxation [4.30]. Stress relieving by heat treatment increases strength significantly under compressive applied stresses. In contrast, deliberately introduced compressive stresses, increase the stress amplitude in the whole applied stress range, see 2.10.

4.8 Solidification and Liquation Cracking

The behavioural characteristic of the weld pool, as it cools and solidifies, also affects the weld quality. This is termed solidification and liquation cracking. The phenomenon of solidification and liquation cracking is controllable. However, the thermal properties affect the rate of cooling. Therefore understanding of the characteristics of the cooling weld pool and its effects requires investigation. This is also discussed in 4.7.1 hot cracks, since the behaviour is ostensibly the same.

4.8.1 Solidification Cracking

Cracking occurs in aluminium alloys because of high stresses generated across the weld. Aluminium has high thermal expansion (twice that of steel) and the substantial contraction on solidification. Solidification cracks form in the centre of the weld, fig.4.19, usually extending along the centreline during solidification.

Cracks can also occur in the weld crater at the end of the welding operation. The main causes of solidification cracks are as follows [4.25]:

- Incorrect filler wire/parent metal combination
- Incorrect weld geometry
- Welding under high restraint conditions

The risk of cracking is reduced, by using non-matching crack-resistant filler (usually from the 4000 and 5000 series alloys). The disadvantage is that the resulting weld metal may have a lower strength than the parent metal and not respond to a subsequent heat treatment, [4.23]. The weld bead is to be thick enough to withstand contraction stresses. The degree of restraint on the weld can be minimised by using correct edge preparation, accurate joint set up and correct weld sequence. Using filler metals relatively high in Si or Mg, the weld composition is less susceptible to cracking. In practise it is preferable to use either 5% Si or 5% Mg filler metals in Tungsten Inert Gas (TIG) and MIG welding of 6000 series alloys, for this very reason. See fig.4.9 and fig.4.20.

4.8.2. Liquation Cracking

Liquation cracking occurs in the HAZ, when low melting point films are formed at the grain boundaries. This promotes intergranular fracture. These films are unable to withstand the contraction stresses generated when the weld metal solidifies and cools. Heat treatable alloys, 6000, 7000 and 8000 series alloys, are more susceptible to this type of cracking [4.23] [4.25] [4.36]. The risk is reduced by using filler metal with a lower melting temperature than the parent metal, for example the 6000 series alloys are welded with a 4000 filler metal (4040A). However, 4000 filler metal should be avoided to weld high magnesium alloys (such as 5083) as excessive magnesium-silicide may form at the fusion boundary. This decreases ductility and increasing crack sensitivity by intergranular crack propagation. This is one of the principal reasons why 5356 and 5183 filler wires are commonly used throughout aluminium shipbuilding. It is high in Mg content to reduce solidification cracking. These filler wires are also beneficial in preventing solidification cracking. Liquation cracking can still occur if little care is taken in preparation and welding.

In the last decade however, it has become more common for shipyards to use 5183 filler wire. The as welded strength is 7% higher than with other wires like 5356 [3.24]. The other benefit is that 5183 is interchangeable between 5000 and 6000 series alloys, unlike 5356, which is only acceptable for 5000-5000 and 5000-6000 alloys. It is unsuitable for the 6000-6000 alloy combination.

4.9 Distortion

Distortion is a complex behaviour and is difficult to predict [4.37]. Identical welded structures will exhibit different distortion characteristics, despite being welded in the same condition, the same welder and same procedure. The understanding of residual stress is important [1.10]. However the designer requires basic knowledge how distortion occurs and the implications. Welding involves localised heating of joint edges to fuse material. This initiates non-uniform stress in the component because of expansion and contraction of the heated material. Initially, compressive stresses are created in the surrounding cold parent metal when the weld pool is formed due to the thermal expansion of the hot metal (HAZ) adjacent to the weld pool. Tensile stresses occur on cooling, as the contraction of the weld metal and the immediate heat affected zone is resisted by the bulk of the cold parent metal. It is during this tensile phase that ductile and brittle fracture crack propagation takes place. If the stresses generated from thermal expansion/contraction exceed the yield strength of the parent metal, localised plastic deformation of the metal occurs. Plastic deformation causes a permanent reduction in the component dimensions and distorts the structure.

4.9.1 The six main types of distortion are:

- Longitudinal shrinkage
- Transverse shrinkage
- Angular distortion
- Bowing and dishing
- Buckling
- Twisting

The principal features of the more common forms of distortion for butt and fillet welds are shown in fig.4.21.

4.10 Conclusions

The designer must take into consideration that the detail design is just one link in a long chain of events that contribute to the fabrication of a welded joint. The process of how the aluminum alloy is made into sheets of plating, prior to being delivered to the shipyard, is the start of this concatenation.

It has been discussed that: welding, poor gas shielding, poor line up or incorrect filler wire for example, contribute to crack initiation. These factors must be taken into account at the early design stage. Poor joint preparation can lead to porosity that can reduce the fatigue life by a factor as much as 200. A misalignment of 10%, which then rotates during welding due to poor constraint, reduces the fatigue life by up 60%. It is clear that weld quality and poor alignment of plating, are contributing factors to the life of a welded joint.

5. The Effects of Detail Design on Local Stress Fields

This chapter considers the role of structural design with respect to stress intensities. That is, designing a structure to be more fatigue resistant. The way a structure is designed can have a major effect on the stress that the structure will experience. For example, is the better connection a sharp square corner or a smooth rounded corner for the joining of frames. This chapter will review and investigate actual structural design for ships. Using stress concentrations the designer is able to compare shapes of cutouts and methods of joining to establish the stress field at a structural discontinuity. Design for production, is a term that is often used without true understanding of the role that production plays, whilst maintaining the design intent. Therefore, an aim of this chapter will be to benefit the designer, who must make choices which affect the cost of production, whilst designing a structure as fatigue resistant as possible.

5.1 The Relationship of Stress Intensity to Design

In chapter 2, the mechanism of fatigue failure is shown to occur at stress levels below the yield stress of the material. This is because of the cyclic environment that the metal is subjected. For a high speed craft (HSC) the exciting forces are the sea loading and local machinery effects [1.11] [3.24] [4.4]. In equation 2.3, the effect of the cyclic loading is calculated. This describes the stress field associated at a crack tip, the stress intensity factor, K. The stress intensity factor is governed by the shape of a crack, and it is also related to the applied stress. It was discussed in chapter 4 that the manufacturing process creates unwanted flaws and cracks into a structural joint with deleterious effects. The behaviour of a crack is analysed with fracture mechanics using LEFM and EPFM, as discussed in section 2.9. The applied stress, in way of a crack tip, is required to calculate the effect on a crack and the influence it has on the fatigue life of a structural joint. The increase in applied stress at a joint is a function of the stress at a nominal distance from the joint being considered. This is called the stress concentration factor, SCF, and is discussed further in 5.2. Therefore structural joints that have high SCFs will increase the stress intensity factor. This reduces the fatigue life of the joint being designed.

5.2 Stress Concentration Factor

In a member under axial loading the stress may be assumed to be uniform over a cross section where the member is long and of constant or gradually changing section. Any abrupt change, for example a notch, groove or hole, causes a local variation in the stress distribution. This is dependent on both the reduction in cross sectional area at the discontinuity and on the shape of the discontinuity. A measure of the severity of a stress concentration is given by the stress concentration factor, K_t, equation 5.1. This is defined as the ratio of the maximum local stress in the region of a discontinuity to the nominal local stress, evaluated by simple theory [5.1] [5.2].

$$K_t = \frac{\sigma_{max}}{\sigma_{nom}} \qquad \text{.....(5.1)}$$

Theoretical stress concentrations factors K_t are dependent solely on the geometry of the specimen concerned. If all materials were uniformly homogenous and free of surface marks or scratches, then K_t would be used for fatigue stress calculations. However, materials are rarely homogenous or free from defects or flaws. This was discussed in chapter 4 with regards to manufacturing. Because of this a value lower than K_t is calculated. A fatigue strength reduction factor K_f, is introduced. It is defined as the ratio of the fatigue strength of a specimen with no stress concentration, to the fatigue strength with stress concentration. A measure of the degree of agreement between K_f and K_t is given by the notch sensitivity factor q [3.11] [5.1]:

$$q = \frac{(K_f - 1)}{(K_t - 1)} \qquad \text{..... (5.2)}$$

The value of q lies between 0 and 1. When $K_f=K_t$, q=1, the material is fully notch sensitive. If K_f = 1 then q = 0, the material is notch sensitive. The value of q depends on the stress concentration, size of specimen and endurance as well as the material. It should be noted that in fig.2.17, that the notch toughness of aluminium is unaffected by temperature.

5.3 Effects of Structural Discontinuity on SCF

Consider the flat plate shown in fig.5.1 [5.2]. Note the stress flow lines are uniformly spaced at each end of the plate. At a notch however, the outer edge stress lines are forced to change direction and are no longer uniformly spaced. Thus, within the vicinity of the notch, lines of stress flow are increased through the unit area. The local stress is thereby increased. It is this increase of stress flow per unit area that creates the stress concentration. As the stress flow lines move away from the notch the stress is reduced to its nominal value.

5.3.1 Stress Concentration in Tension Members

Consider the case of a small elliptical hole in a plate, fig.5.2. The maximum stress σ_{max}, at the ends of the horizontal axis of the hole is given by the equation:

$$\sigma_{\max} = \sigma_{nom}\left(1+2\frac{a}{b}\right) \quad \text{.....(5.3)}$$

Where σ_{nom} is the nominal applied stress at the plate ends and a, and b, are dimensions of the hole in the horizontal and vertical axis respectively [5.3]. In the case of a circle, a and b are constant, the SCF is 3. Therefore the maximum stress is 3 times the nominal stress. In can be seen in equation 5.3, that the stress increases with the ratio of a/b, so that a narrow hole perpendicular to the direction of tension produces a high stress concentration.

This is why cracks which are perpendicular to the direction of an applied force propagate more readily than if the crack is parallel. The propagation can be arrested by drilling holes at the ends of the crack in order to eliminate the sharp corners that produce the high stress concentration. This is the usual way for a shipyard to repair cracks [4.11] [4.17].

5.3.2 Stress Concentration in Combined Tension or Compression

Consider the plate with a circular hole in compression, fig.5.3. At the point a, it has been shown that the magnitude of the stress is 3 x σ_{nom} in tension. Therefore at the point a, there is a compressive stress of $3\sigma_{nom}$ and a tensile stress of σ_{nom} at b. In the case of brittle materials a crack will initiate at point b, [5.3].

In fig.5.4, a circular hole is subjected to tensile stress in 2 directions. The tangential stress at point a, is $3\sigma_y - \sigma_x$ and at point b, the stress is $3\sigma_x - \sigma_y$. In the case of pure shear it is $\sigma_x = -\sigma_y = \sigma_{nom}$ and therefore obtain the stress at point a, as $-4\sigma_{nom}$. At b, the stress becomes $+4\sigma_{nom}$. Thus in this case the maximum stress is four times larger than the stress applied at the plate edges.

5.4 SCF of Complex Joints

The shapes shown in section 5.3 are simple and regular in nature. From these shapes the designer can estimate the SCFs for regular shapes. A variation of simple shapes and thickness' for guidance in determining the SCF is shown in appendix B. The parameters used to calculate the SCFs are only applicable to two dimensional structures and uniaxial loading. This presents a problem to the designer. The designer of a HSC vessel is unable to use these simple shapes with the given geometry for SCF determination, owing to the complexity of ship structures. The complexity of the geometry and the loading conditions of a HSC vessel is considerably different from those presented in SCF of joints from established charts.

5.5 Effect of Ship Structure Joint Configuration on SCF

Studies in Japan [5.4], [5,5] on steel hulled vessels and their joints have produced guidelines and stress concentration factors for various typical shipyard joints. These are applicable to any vessel, which has the frame system designed in the same arrangement since the geometry is identical.

Each joint is characterised by the stress concentration factor, K_s or K_{sO}. The study does point out, however, that the values given should be used with care, in so far as the additional dependence on the dimensional situation is only covered by special cases. In the following sections of this chapter, a review of standardised shipyard configurations, used in the joining of ship structures is shown. These joints behave differently from each other owing to their geometry. The differences affect the SCF, or stress fields, surrounding the area under observation. The stress intensity, K, is a measure of the stress at the crack tip, which is directly proportional to the stress field.

5.5.1 Corner of Double Bottom (Bilge Radius)

The joint in way of a double bottom is similar to that of a standard frame connection joint. The loads to which it is subjected are more than secondary; they can also be global, or primary. This means that as the hull flexes, these joints will also experience these loads. In addition to the impact of localised sea pressure, the joint is subjected to loading from longitudinal axial forces, bending moments and transverse shear force. The standard arrangement for such a joint in this region is characterised in fig.5.5 [5.4].

The stress field can be calculated from the structural K_s or K_{sO}, as shown in the following figures 5.6~5.8. The structural SCF is defined as:

$$K_s=K_{sO}\,K_{cw} \quad \ldots\ldots\ldots\ldots\ldots\ldots\ldots\ldots\ldots\ldots\ldots\ldots (5.4)$$

The K_s is subdivided into the factors K_{sO} for a full load carrying width component and the K_{cw} as a result of the reduced load carrying width of the component. The range of frame spacing to frame web depth of around 0.4~0.6 gives a carrying width component factor K_{CW} = 1.2~1.8. Where K_{CW} is the load carrying width component of stress concentration factor. Therefore a smaller distance between frame webs (i.e. a small frame spacing) is advantageous from the point of view of a stress concentration. From a purely static point of view this also has the benefit of reducing the panel aspect ratio and hence the load on that panel. This in turns reduces the K_s further still, since K_s is proportional to the stress field.

A characteristic of a small frame spacing is that the vessel is labour intensive to fabricate [1.5], owing to the extra cost of additional frames. The weight per square metre is roughly the same for a small or wide spaced frame arrangement. However, for the designer, design is a fine balance of design and implications of cost.

Typical structural arrangements of joints in way of the double bottom, is shown in fig.5.6. It can be seen that the shapes vary and with wide variation in the value of K_s. Crack initiation sites are shown by the arrows, and σ_n as nominal stress. From the basic arrangements shown in fig.5.6 it can be seen that the features which have a favourable effect are:

- Rounded corner with a continuously welded rider bar, i.e. no joint
- Rounded bracket in a right angled corner

5.5.2 Corner of Side with Double Bottom

The corner joint between the side frame and double bottom or tanks, is designed very differently compared to those in fig.5.6. Since these type of joints are often considered free standing. This is where the side frame butts against the tank top at a right angle or obliquely, with the side frame web aligning with the web of the tank frame. From [5.4] [5.5], fig.5.7, a) ~ d) are typical oblique joints, and e) ~ h) are typical right angle joints, with a corresponding structural SCF. Double bottom tanks will become a factor in new build HSC vessels [5.6].

As in fig.5.6, the joint in fig.5.7 that has the lowest K_{sO} is the rounded corner with a rider bar. The joints with brackets extending in line with the web frame, at sharp angles have surprisingly low K_{sO} values. These joints however, will be more expensive to fabricate owing to the addition of two brackets per frame.

5.5.3 Transverse Frame Corner Joints

The corner joint of frames and bar stiffeners of the plates and shells of a ship's hull can be designed in several ways. In each method the structural performance of each joint is required to satisfy two principles of an ideal connection [5.7]:

a) Adequate strength. The connection should be able to resist a movement at least equal to the full plastic moment of the weaker of the two members joined.

b) Adequate elastic stiffness. The connection is defined as ideally rigid when there is no body strain within the joint.

The following joints investigated were subjected to a diagonal tensile force, F, as shown in fig.5.8. [5.4] [5.5].

The reinforcement plate, or rider bar, on the bracket is introduced to reduce the risk of buckling and vibration. As a result of the additional notches, it has an unfavourable effect on the fatigue strength of the joint, hence giving the ends of the bracket a smooth profile is recommended. The joints shown in fig.5.8a)-d) were also investigated in [5.7]. The investigation was for an ideal structural joint rather than a measure of the SCF. However, fig.5.8d was the most efficient in transferring load and rotation whilst 5.8a, and 5.8b, were shown to be the least effective.

5.5.4 Cutouts and Mouse Holes

The shape, design and dimensioning of a cutout is determined on the basis of the stresses at the non-reinforced or reinforced edge, which must remain lower than local strength values. The cutting out of the inner corners of I beams, for example, is from the era of rolled sectional girders made of unkilled steel. In the transition area, from the web to the flange, to remain uninfluenced by welding because of their tendency to crack, fig.5.9 [4.28].

This cutout philosophy is extended into other areas of structural design on similar web-to-flange welded joints/girders. It is to avoid defects caused by bad fitting and welding, as well as unfavourable residual stresses at the inner corner, with the welds crossing. The notch stresses of the transverse weld on the side of the web subjected to transverse force bending of the girder, are also avoided. This is in contradiction to the experiments and recommendations in [5.7].

The notch stress, or stress concentration created by cutouts in shipbuilding can greatly affect the fatigue life of a joint [1.12] [4.30]. In section 3.7, the effects of welding aluminium were shown to be more onerous than steel, since aluminium experiences a loss of mechanical strength when welded. Cutouts that exhibit high stress concentrations with poor mechanical properties can greatly influence crack initiation. Therefore the shape and the location of cutouts, within a structure, must carefully be chosen. Joints which are subjected to biaxial and triaxial stresses, compound the problem and must be avoided. In fig.5.10, typical shipyard cut outs, or scallops, are shown [4.28] with stress concentration factors, K_s, at a nominal bending stress; K_{su} being the upper profile and K_{sl} being the lower profile.

The values of K_s, in fig.5.10, are dependent on the shape of the hole and the ratio of the thickness of the plates. The relatively high K_{sl} values of b) can be explained by the proximity of the weld ends. In the case of intermittent welded web-flange joints in girders without mouse holes, cracks propagate into the web and flange plate. This is classic brittle fracture behaviour as discussed in section 4.7, where a crack propagates from a thin to a thick section. It has been shown that cracks propagate into the flange plate only in the case of a joint with mouse holes. A detailed parametric study of mouse holes used in shipbuilding is investigated in [5.8]. Other design details from shipbuilding are investigated in [5.9].

5.5.5 Cutouts for Longitudinal Stiffening

The dominance of the catamaran for a fast ferry began during the early 1980s [5.10] and is now the predominant choice of hull form for a fast ferry [1.6]. Fast ferries of catamaran hull form are considered as transversely framed. The cutout detail is important with respect to SCF, since the higher nominal stress is in the transverse web [5.11]. The load transfer is affected from the web of the transverse to the longitudinal via the cutouts, which is directly attached to this longitudinal stiffener. Being aluminium compounds the detail design of this cutout. Aluminium exhibiting poor fatigue characteristics compared to steel, as shown in fig.3.9. The transverse web frame is subjected to constant cyclic loading from the global responses of the hull and local plate bending owing to secondary sea loads.

The existence of biaxial stress raisers from the complex geometry and joining of the framing system must be taken into account.

In fig.5.11 are some typical cutout joints, as used in shipbuilding. The type of cut out depends upon the shape of the longitudinal stiffener and the method of production. The cutouts, in fig.5.11a) and c) are traditional cutouts for bulb bar stiffening, whilst d) and e) are more common on Tee bar type stiffening. Fig.5.11 d) using a shear tab connected to the shear web of the stiffener and the web of the transverse frame. Method d) allows for a faster and less accurate build method. The addition of the shear tabs, or fish plates as they are often referred to, can be labour intensive. Fish plates also create a sharp corner weld and a stop-start of the weld. Stop/starts reduce the fatigue life of welded joints, see section 4.7.1.. This may account for the poor experimental results using single fish plates in [5.7], which increased the SCF. The shape of the cutout in e) is smooth and production friendly. However, the flange of the Tee, which is carrying the tensile load, is connected directly to the web of the frame that is carrying the shear load across the rider bar. This places the weldment along the flange, perpendicular to the applied load, into shear. This approach has been demonstrated to be deleterious in [1.8] [4.19] [4.31] [5.12]. Residual stresses in the alloy caused by welding also influences the stress intensity [5.13] [5.14].

All the shapes in fig.5.11 a) to e) have good and bad points for fatigue and production friendliness. The problem the designer must ask, is, which is best. In fig.5.11 b), a new type of pear drop shape slot for the longitudinal has been identified as yielding stress relaxation around the slot [5.15], [5.16]. This slot has also to be investigated for further optimisation [5.17] and guidelines on its use for fatigue. The parameters used in the optimisation of this pear drop shape cut out are shown in fig.5.12. Six different models with chord/height and chord/depth ratios were investigated. The final optimum chord and depth ratios from the study arrived at 0.25 chord/height and 0.35 depth/chord. This resulted in moving the stress concentration away from the weld attachment. The resulting shape, chosen from the study, reduced the stress concentration by a factor of 2. This complex shape of cut out is easy to achieve if the yard has a plasma, or similar type of plate cutter.

5.6 Does One Size Fit All

In section 5.5 typical shipyard details were investigated to aid the designer with values of stress concentrations for joints used throughout the vessel. The designer requires further guidance on these structural members. Stress concentrations at these cutouts maybe obtained either from numerical analyses or from experimental work in a laboratory [5.18]. Once the stress concentration has been obtained, the cutouts can be evaluated as to their effectiveness. This gives the designer important information in being able to choose which type of cutout would be suitable for a given application.

A programme of investigation of such effects requires much planning, time spent analysing in modelling. The problem with many of the models used for fatigue predictions is that they are usually based on one dimensional crack propagation laws and do not address the occurrence of crack paths that differ significantly from co-planar paths. Such branched crack growth is observed in structures containing a high level of residual stress or in details that are biaxially loaded [1.8] [4.19] [4.31] [5.12] [5.13] [5.14]. In some cases the crack will propagate into zones of high or low stress. The crack growth will either be accelerated or it will be retarded, crack arrest may even occur, see section 2.10. The effect of residual stresses, see section 4.9, and biaxial loading along with load shedding needs to be taken into account.

5.7 Design for Production

It can be seen from the various configurations in the fig.'s 5.6~5.12 that geometry plays an important part in the stress concentration of a joint. This corroborates with theory that was discussed in section 5.3 of simple geometric shapes. In fig.5.6 for example, the oblique angled joint 5.6d being constructed using straight lines, has a SCF, K, of 4.6 ~ 4.7. Whereas the same joint, using curved lines, K reduces down to 1.2, an order of magnitude of 4. This trend is also repeated in fig.5.8, corner connections of typical transverse frames. The straight lines joint of fig.5.8a K = 4.2, where as the joint using smoothed curved lines in d) has a K = 1.2.

The use of curved lines for smoothing out the hard spots has a significant effect on the stress concentration of the joint. Whereas there could be a design-based advantage in reducing stresses, the curved geometric configurations have a deleterious affect on the production costs [1.5] [1.15]. The increase in production man-hours of using curved lines increases the production cost Therefore the designer must also be aware of the producibility implications of the joint configurations chosen for a more fatigue resistant structure.

5.8 Post Fabrication Treatment

When the designer has chosen a structural arrangement that has a SCF as low as practicably possible, given production constraints, other aspects become available to the designer in reducing the SCF. For example, the weld geometry may be changed or compressive stresses may be applied to the structure. To influence the SCF after fabrication is a post fabrication treatment. This can be specified by design or production once visual inspection has taken place.

5.8.1 Localised Weld Grinding

This process of post fabrication treatment reduces the local notch effects on the weld bead profile [1.10] [1.12] [1.15] [3.24] [4.28] [4.30], by local grinding of the weld toes (or weld ends) using a grinding burr, fig.5.13. Grinding grooves in the direction of the profile, or grinding disc grinding grooves transverse to the profile. During this procedure the micronotches in the weld metal to parent metal transition area are removed, which prolongs the crack initiation phase [1.10] [4.28] [4.30]. This grinding of toes and end of welds, is recommended in these high cyclic regions by classification societies such as DNV [3.24] and L.R. [3.17].

5.8.2 Shot Peening

Shot peening is performed by one of two types of machines. A machine ejects pellets at a high velocity from a centrifugal wheel and is capable of raining a large volume of shot onto the surface being treated. For volume production, the centrifugal type is preferred.

The other machine uses compressed air to shoot the pellets out at a high velocity. This method is often employed in shot peening difficult areas, such as holes, recesses and so on. Shot peening results in a metal surface finish having a roughness of about 3-8 microns, μm, [5.19], [5.20].

The craters being created push and plastically deform by compression the surface material. This means that any applied load must first overcome the residual compressive stress in the material before it can become a positive load and assist in crack opening and crack growth [2.24] [2.30]. As already discussed in 2.10, crack growth can be arrested during the compressive phase of loading, and it is this mechanism that shot peening utilises. This residual compressive stress is only in the region of the shot peening and extends for several microns into the main body of the material, which is where the highest tensile stress are generated.

It has been pointed out in [5.20] that shoot peening also has beneficial effects on the prevention of stress corrosion cracking [2.35], (SCC), which is not so surprising since the mechanism of SCC and fatigue are near identical. It should also be noted, that in [4.34] that some authors point out that there is some doubt about the effectiveness of shot peening treatments, where a relaxation of the residual stress field during cyclic loading was observed.

5.9 Conclusions

The designer has to satisfy many demands during the design and construction phase of build, for both fatigue life and production costs. The implications of subtle changes, which can be made to the structure, can have a deleterious effect. A smooth transition between structural members, which are at right angles to each other, is shown to be the most beneficial in reducing SCFs. However, other methods of joining which are more production friendly, have been proposed and are shown to provide acceptable solutions. The designer must understand which to use and where to use, without affecting the overall design intent and SCF.

6. Finite Element Modelling of Structural Details.

In the previous chapters, the problem of complex structural analysis in a working shipyard has been discussed. Methods for the analysis of fatigue joints are time consuming and are limited to unidirectional loads [1.16]. This is exacerbated by the fact that a ships' hull is made from a framework of plates, beams and girders, which form a three dimensional structure. There is insufficient guidance for the designer, based upon a three-dimensional structure, suitable for the analysis with loads in three planes of application and which has up to six degrees of freedom. This chapter will guide the designer through the use of finite element analysis software in order to arrive at a meaningful result with confidence, based upon known criteria, and within a time frame suitable to a shipyard designer.

6.1 Stresses in Fatigue Analysis

Stresses used in fatigue analysis are those resulting from dynamic loads, static weights, wind, waves, accelerations, machinery, propeller or waterjet vibrations etc. Secondary stresses, such as bending stresses in rigidly jointed trusses, or fluctuating thermal stresses, must also be included, if relevant. The stresses in fatigue analysis can be broken down into three categories [6.1], namely:

(i) Nominal stress:
(ii) Structural (hot spot) stress:
(ii) Notch stress.

The choice of stress category depends on the method used to express the fatigue strength data, which will be used in the fatigue assessment.

(i) Nominal Stress

In general, nominal stresses are those calculated using simple formulae:

$$\sigma_{nom} = \frac{F}{A} + \frac{M}{I}.y \qquad \ldots\ldots\ldots\ldots \quad (6.1)$$

Where: F is axial force

A is area of cross section

M is the bending moment

I is moment of inertia of the cross section

Y is the distance from centroid to the point considered.

An example of nominal stress in a beam-like component, established according to equation 6.1, is shown in fig.6.1 [6.2] [5.17]. When fatigue at a welded attachment is considered, the nominal stress is calculated in the region containing the weld detail, but excluding any influence of the attachment on the stress distribution. However, in practice it might also be necessary to include in the nominal stress the effects of certain macro-geometric features. As well as stress fields, in the vicinity of concentrated loads and reaction forces.

(ii) Structural Stress

Structural stresses include both nominal stresses and the effects of structural discontinuities; for example, see figs.5.6 ~ 5.8. Structural stress is linearly distributed across the plate thickness and consists of two parts: membrane stress and shell bending stress, fig.6.2. It is usually higher than the nominal stress, although far from discontinuities the structural and nominal stresses are equivalent. In order to avoid confusion with the bending stress in a beam, see eqn.6.1, the bending stress component of the structural stress is called the *shell bending stress*.

(iii) Notch Stress

Local notch stress, σ_{ln}, is the total stress located at the root of a notch, such as a weld toe, see fig.6.3 [6.2] [5.17] [4.28] [4.30]. The nonlinear stress peak, σ_{nlp}, is the maximum stress in the nonlinear part of the stress distribution, usually across the plate thickness caused by a local notch, as shown in fig.6.3. If a refined stress analysis method is used, which yields a nonlinear distribution across the plate thickness, then nonlinear stress peak can be separated from the structural stress as shown in fig.6.3.

First the average stress, which is equal to the membrane stress, σ_m, across the thickness, is calculated. Then the shell bending stress is found by drawing a straight line through the point, O, where the membrane stress intersects the mid-plane of the plate. The gradient of the shell bending stress, σ_b, is chosen (or resolved by calculation) such that the remaining nonlinearly distributed part is in equilibrium. Its value at the surface is the nonlinear stress peak, σ_{nlp}.

6.1.1 Hot Spot Stress

A *hot spot* is the term used to refer to a critical point in a structure, where fatigue cracking can be expected to occur due to a discontinuity and/or a notch [6.3]. Usually, the hot spot is located at a weld toe [1.12] [4.28] [4.30]. Hot spot stress, σ_{hs}, is the value of the structural stress at the hot spot. Although the hot spot is located at a local notch, the hot spot stress does not include the nonlinear stress peak caused by the local notch, as will be evident from a comparison of figs.6.2 and 6.3.

Fig.6.3 represents local notch stress (total stress) at a weld toe, comprising membrane and shell bending stress and a nonlinear stress peak. The hot spot stress approach is used mainly for joints in which the weld toe orientation is transverse to the fluctuating stress component, and the crack is assumed to grow from the weld toe. The approach is unsuitable for joints in which the crack would grow embedded defects or from the root of a fillet weld. Compared with the nominal stress approach, this approach is more suitable for use in the following cases:

1. Difficulty in defining a nominal stress owing to complicated geometric effects:

2. The structural discontinuity is beyond comparison with any classified details included in the design rules, (nominal stress approach);

3. For the above mentioned reasons, the finite element method is in use with shell and/or solid element modelling;

4. Testing of prototype structures is performed using strain gauge measurements.

6.1.2 Effects of Local Notches

Fig.6.4, shows typical local notches found in most welded components, also see section 4.7.1. The main effect of a notch is to produce nonlinearity in the stress distribution, usually in the thickness direction, fig.6.5. The nonlinear stress peak lies within a radius of approximately 0.3t to 0.4t from the notch root, [6.2]. A nonlinear stress peak is one reason why a surface defect, located at a notch, is more dangerous than an embedded defect, which is usually located in an area of lower stress, fig.6.6. Edge notches and small drilled holes cause similar nonlinear stress peaks, but with different orientations.

The notch stress, σ_{ln}, is usually calculated by multiplying the hot spot stress by a stress concentration factor, or, more precisely, the theoretical notch factor, K_t. In many cases the result will exceed the yield strength of the material, thus elastic-plastic behaviour, see 2.9.3, is to be expected, and the calculated stress should be considered as a pseudo-elastic stress. When no solution for K_t is available, finite element analysis (FEA) can be used for the determination of notch stresses. However, because of the small notch root radius and the steep stress gradient in the case of a weld, a fine element mesh is needed. Therefore, to solve notch stresses used for determination of the structural stresses, requires a different finite element model or mesh size.

6.1.3 Stress Concentration Factor, K_t

Low stress brittle fracture occurs in components that are loaded elastically, but contain certain flaws from fabrication, see 4.5.1. The fracture instability must, therefore, be associated in some way with the concentration of stress in the vicinity of the flaw. In engineering design, such stress concentrations are denoted by the term K_t, as discussed in section 5.2

6.2 Using FEA to Model Real Structures

FEA was developed in 1943, by R. Courant [6.4], who utilized the Ritz method of numerical analysis. Using minimization of variational calculus, to obtain approximate solutions, to vibration systems. Shortly thereafter, a paper published in 1956 by M. J. Turner, R. W. Clough, H. C. Martin, and L. J. Topp established a broader definition of numerical analysis [6.5]. In terms of fracture, FEA, most often involves the determination of stress intensity factors, see 2.8, or SCFs see 5.2.

6.2.1 Validation of Model and Elements

The application of finite element analysis should include a validation of the element to be used and its implementation. This can be achieved by a series of simple textbook problems for which authenticated results are available. Having established and understood the behaviour of each element, the analyst will need to gain confidence in the programs ability to produce correct consistent results. For example, means of assessing convergence of displacement type elements for elastic problems in which the shape functions violate continuity [6.9].

In order to achieve this, a *Patch Test* has proven to be a valid convergence test [6.10]. The original test was introduced [6.11] [6.12] [6.13] in a physical way and could be interpreted as a check which ascertained whether a pattern of elements subjected to a constant strain reproduced exactly the constitutive behaviour of material, and resulted in correct stresses when it became infitesimally small. If it did, it could then be argued that the finite element model represented the real material behaviour and, in the limit, as the size of the elements decreased would therefore reproduced exactly the behaviour of the real structure. The NAFEMS [6.14] organisation took steps towards establishing standards for finite element analysis. The analyst should check whether the FE program being used for an analysis conforms to this standard.

6.2.2 Typical Elements Types

There are many different types of elements currently available to the designer, irrespective of the FEA software chosen. However, there are essentially 4 universal element types that are most useful when using FEA for analysis of structures and, in particular, for estimating the SCFs. Also see appendix C.

6.2.3 Beam Elements

Beam elements are mainly used for analysis of nominal stresses in frames and similar structures [6.7] [6.8] [6.15]. A conventional beam element for analysis of 3 dimensional frames has 6 degrees of freedom at each node: three displacements and three rotational. This element can describe the torsional behaviour correctly only in cases in which warping can occur freely and the cross section is unaffected by warping.

6.2.4 Thin Shell Elements

In general, thin shell elements are suitable for solving the elastic structural stresses according to the theory of shells [6.16] [6.17]. The deformation fields are usually formulated as linear, 4 noded, or parabolic 8 noded elements [6.8] [6.15] [6.18]. The mid-plane stress is equal to the membrane stress, and the top and bottom surface stresses are superimposed membrane and shell bending stresses. Thin shell elements can only model the mid-planes of the plates.

6.2.5 Thick Shell Elements

These elements allow transverse shear deformation of the shell in the thickness direction, to be taken into account [6.8] [6.15]. Thick shell elements work better than thin shell elements in details [6.19], for example, where the distance between adjacent shell intersections is small, giving rise to significant shear stresses. It should be noted that these types of elements could be excessively stiff when used in thin shell applications.

6.2.6 Solid Elements

Solid elements [6.8] [6.15] are needed for modelling structures with three dimensional stresses and deformation fields. The two basic types being the 20 noded and the 8 noded 'brick' elements, are most suitable [6.20]. The elements can be modelled as either isotropic, orthotropic or ansiotropic.

6.3 Mesh Density

The most common problem that faces the analyst is choosing the correct mesh density as well as understanding the implications of different mesh density [6.7] [6.8]. A mesh that is too coarse, to save time in modelling, can lead to overestimating the influence and the stress. A mesh that is too fine, to improve accuracy, increases modelling time and can lead to false results. The only requirement is that the selected displacement pattern for the elements is able to produce consistent stress fields inside the elements [6.10] [6.21]. It is recommended that the designer first try to establish the result by beam theory [6.8], since this will give an idea of the stress values that the model should be showing. In the absence of knowing where the high regions of stress will be in the model, it is recommended that a coarse mesh be used. This will give an approximate guide to the size of the mesh density as well as a validation of the model, against the beam theory. The result in the coarse model can be as much as 100-200% different to the beam theory method in complex models, this is to be expected and is common.

Using a coarse mesh will initially identify the regions of higher stress. Therefore, refining the mesh to a much finer density at the higher regions of stress can be performed without having to modify the whole model with a fine mesh [6.22]. Whilst this can be time consuming [6.6], this iterative method of convergence of the model gives confidence to the results [6.23]. However, if a poor deformation pattern is chosen then, although the solutions converge towards a certain value as more and more elements are taken, this value may be in error. There are in fact two criteria that can be of assistance in the choice of displacement function [6.24].

The function chosen should be such that it prevents straining to occur within the element when the nodal displacements are caused by a rigid body movement. In addition, the function chosen should be able to express constant strain conditions within the element when the nodal displacements are compatible with a constant strain condition. If the structure has insufficient constraint to prevent rigid body motion, then an infinite number of solutions to the model (equations) exist [6.6]. Each having the same deformation, but a different location in space.

There will be a desire to make the region of higher stress in the model, from an even finer mesh, since a fine mesh will yield results which approach or duplicate beam theory results. The problem with this is that within this fine mesh region, the elements become too stiff in relation to each other [6.21] due to the restraints that are introduced when selecting the displacement patterns inside the elements. The finer the mesh, the closer the models behaviour will approach infinity at a node. The reason for this is contained in the convergence theorem, which states that convergence to the exact solution will occur $h_{max} \rightarrow 0$, rather than $h \rightarrow 0$, h being the element size. In order to converge to the exact solution, every element must become arbitrarily small. During mesh refinement from a fixed coarse mesh to a fine mesh a finite error will remain in those few elements, which will put a limit on how small an error can be achieved in others [6.6] - regardless how small the elements become. This is also known as a singularity and the function or its derivatives above some order become finite. This is evident at a perfectly sharp vertex, for example, two straight lines meeting at an angle, or any structural discontinuity. This can have a significant effect on the SCF, this is discussed further in 6.4.6.

6.4 FEA Examples

In chapter 5 different types of typical shipyard structures have been strain gauged in order to ascertain the SCFs of each joint. The SCFs have been calculated by: knowing the applied loads, the geometry in terms of beam theory and testing them experimentally to validate the theory and calculate the SCFs. Using these known SCFs for a joint, an FEA can be used to establish guidelines. Using a joint from fig.5.8a, the SCF is known. A unit load may then be applied to the FEA.

The modelling of this structural joint is made significantly easier, since the result is already known. Therefore a methodology of using finite elements can be established for the analyst/designer so that these guidelines can then be used on less orthodox geometry with a degree of confidence. The way in which the FEA is modelled, the type of mesh, the type of elements, the way the loads are applied etc, can be established using a model, with a known result. It is therefore intended that these guidelines on FEA will enable the designer to analysis complex structure with confidence, in the finite time frame that is available to the shipyard designer.

6.4.1 The Coarse Model

In fig.6.7, the first basic FEM is established. This, as shown, is a coarse model. The initial size of these elements can be established from the guidelines of the element from the software program used, or using a maximum aspect ratio of 1:5. For slightly distorted elements, the singular points lie outside the element domain [6.24]. As the distortion increases the singularities move to the element boundary. The distortion can be in the form of the angle between toe corner tangent and chord line of an element, 3 or 4 noded. It is associated with the aspect ratio of the longest side to the shortest side of the element. For both triangular and quadrilateral, a ratio beyond 5 will give rise to a *warning state*. Greater than 15 will be an *error state* [6.25]. If the flat bar rider is 1000mm long and 100mm in width; taking into account the centreline nodes; the element size should not be greater then 50mm by 250mm (50mm x 5). Using a maximum aspect ratio of 1:5.

In order to obtain meaningful results, the correct boundary conditions must be used, so the model behaves in a manner which is expected and reflects reality. In fig.6.8, the red crosses indicate the model is symmetrical about that edge, and the apex corner nodes are simply supported. This allows the model to rotate freely under load. The load is applied at a single node at 45°, as per fig.5.8a in chapter 5, and shown in the centre of the web by the small arrow in fig.6.8. Once the model has been run, the resulting deformed plot will show how the model is behaving and will give an indication to the set boundary conditions.

In fig.6.9 it can be seen that the model does indeed exhibit the correct behaviour, i.e. the corner of the joint is in tension and the frame is being pulled apart in equal and opposite directions.

In fig.6.10, the red areas denote the high stress, and it can be seen that the area of high stress is considerably large, as a percentage of the model size. It covers a large proportion of the flange; which in practice would not be the case. It is, therefore, a reasonable deduction to make, that the model is still too coarse and requires a finer mesh density. As noted in 6.3, the regions of higher stress in the coarse model shown in red, can be modelled with a finer mesh density, whilst the remainder of the model can remain at the coarse mesh size. If the remaining mesh does not encourage a smooth transition, then further mesh refinement maybe necessary, especially at the transition region between the coarse and fine mesh.

6.4.2 Fine Mesh Model

Having established that the coarse model is inadequate, a refined model with a finer mesh density, in way of the higher stress region, can now be modelled, fig.6.11. However, if a smooth transition from coarse to fine mesh is required [6.6] [6.23], selectively using a fine mesh in the vicinity of discontinuities, or an area to be analysed in detail [6.6] [6.7]. This leaves the remainder of the model coarse.

The corresponding stress plot shown in fig.6.12, is also very different from fig.6.10. The region of high stress is now confined to two areas within the model, around the corner joint, as expected, and the centre of the web at the ends. The applied force at the single node has affected the results; this effect can be seen in fig.6.12, by the red areas denoting high stress at the centre of the web ends. The reason for this is that the load being applied, is applied to a single node that has a small area relative to the model. This effect can also be seen in fig.6.10, but is overshadowed by the dominant area of stress, in way of the corner joint. It is clear from fig.6.12 that the finer mesh is yielding the expected results. Therefore this mesh size can be used to investigate and establish the SCF, and see whether it compares favourably with that in fig.5.8a. However, the method of application of the applied load requires a different approach. This is discussed further in sections 6.4.3 and 6.4.4.

The distance between each node, in the mesh shown, is half the thickness of the web. This is in the transverse direction, i.e. across the width of the flange [6.2] [6.26]. In fig.6.13 is a close up view in the corner joint region of the rider bar, with a plot of the membrane stress. The plot of membrane stress follows the classical pattern shown in fig.6.5 relatively well, i.e. a peak stress then falling away to a nominal stress, as outlined in 6.1.2. From the plot of stress versus distance in fig.6.13, and using equation 5.1, an SCF can be calculated. However, in order to calculate the SCF, the shell bending stress, σ_b, also needs to be taken into account, not just the membrane stress, σ_m. As discussed in 6.1 (ii), the structural stress and nominal stress are considered to be equal when measured far from a discontinuity. Establishing the nominal stress is required in order to calculate the SCF.

The region on the inset-plotted graph, in fig.6.13, shows the stress versus distance from the corner joint. Whilst the curve is not entirely asymptotic, it is sufficient to provide a reasonable value for the membrane stress, σ_m, and is estimated at around 2.5 MPa. The maximum stress is shown to be 6.3 MPa. The bending stress, σ_b, can be found by plotting the direct in-plane stress of the top skin, tensile and the bottom skin, compressive.

In fig.6.14 and 6.15, the top and bottom surfaces stresses, of the element respectively, are shown. This result to establish the bending stress. The graph showing the variation of stress from the corner is again plotted. The location of the first node and last node is shown in each figure, and is taken along the centre line of the web junction with the flange.

Fig.6.14 is a plot of the top skin of the flange plate. Whilst the stress plot can be seen to be very different, the values of the stress, as shown in the graph, are identical to the membrane stress. This is unexpected, since the top surface stress should be either higher or lower, depending upon whether the element is in tension or compression. However, in section 6.2.4 it was indicated that thin shell elements can only model mid-plane stresses. Using a shell element is therefore unsuitable for this type of analysis.

Fig.6.15 shows the bottom surface stress plot, i.e. underside of the flange. As in fig.6.14, the graph showing stress versus distance from the corner is again identical. From the theory in 6.1, the net effect between the upper and lower surfaces is zero, hence the SCF becomes 2.5, which is much lower than was obtained by experiment, as noted in fig.5.8a. This again demonstrates the limitation of the thin shell element and is unsuitable for this type of analysis.

6.4.3 Fine Mesh FEA Observations

One of the strangest observations, in fig's 6.14 & 6.15, is the alternating tensile and compressive stress from the left to the right side of the vertical flange; regardless whether the stress plot is top or bottom surface. This is unexpected, since the model is perfectly symmetrical and has no out of plane forces acting upon it. This demonstrates that FEA must be approached with caution, especially when analysing and interpreting the results.

The FEM is showing is that the flange on the right hand side of the web is warping under load and is warping in the opposite direction on the left hand side of the flange. In a complex geometric and multi-loaded structure, such as a ship structure, this may well be the case. However, since the model is a simple Tee joint that is symmetrical, the model should be statically determinate. The result is also expected to be a symmetrical stress plot around the flange.

Therefore, a finer mesh and/or different element types in the model, is worth investigating to eliminate the most common problems in using FEA. That being mesh density and incorrect element types, and even the application of the forces. One final observation in fig.6.12 is the stress distribution in the lower Tee bar. The influence of the applied load on the stress distribution is noticeable, and is markedly different from that on the upper Tee. This requires further investigation and refinement.

In the fine mesh model, fig.6.12, the reddish areas are confined to the nodes where the force is applied and the corner of the joint in question. The red areas, denoting where the force is applied, need to be eliminated in order to obtain any meaningful results, since the purpose of the analysis is to examine and analyse the geometry, not the application and load shedding of the forces [6.27]. Applying the force in a manner that spreads the load evenly within the FEM, without affecting the result is required. This is another example of a singularity within the FEM [6.6]. A linear stress distribution is required as shown in fig.6.1. It is possible that this may explain the warping shown in fig's 6.14 & 6.15.

6.4.4 Extended Fine Mesh Model

The model, in fig.6.16, is lengthened slightly, at the end of each frame, to ensure that the applied force does no interfere with the analysis of the joint. This will prevent localised stress from the application of the loads from interfering unnecessarily with the analysis. It can be seen that the applied load is also spread over a wider area, rather than at a single node. This reduces the force per unit area, and therefore prevents a singularity occurring at the node. As well as the model being extended, a further refinement of the mesh is made to the model. The mesh is finer than recommended in [6.2] & [6.26] in way of the corner joint; so that each node is approximately ¼ of the thickness of the plate apart, i.e. 2.5mm. This is to investigate whether an even finer mesh has an effect on the result, without regard to the modelling time.

The membrane stress plot along the plane of the lower web frame, in the X-axis, shown in fig.6.17, is considerably different to that of the coarse mesh shown in fig.6.10. It can also be seen that the method of applying the loads, in fig.6.16, has removed the higher stress regions from the centre of the web, which is evident in fig.6.12. The forces are acting upon a number of nodes, rather than being concentrated at a single node, which has the desired affect of removing the quasi-singularity. Moving the influence of the applied load away from the joint ensures that the higher stresses in the model are due to the discontinuity of the geometry. Rather than the application of the forces on the model, i.e. decoupling the effects of the loads from the model.

A close up view of the extended and finer mesh model is shown in fig.6.18. The graphical plot of membrane stress, against distance, follows relatively well that shown in fig.6.5, i.e. a peak stress then falling away to a nominal stress. From the plot of stress versus distance in fig.6.18, the SCF can be calculated. The SCF is approximately 2.2, which is lower than for the fine model shown in fig.6.11. Clearly this is incorrect, since the even finer mesh, which is smoothed, should begin to converge with the experimental work. However, looking at the deformed plot shown in fig.6.19, this can be explained.

The refined FEM has an increased number of elements, especially the 3 nodes triangular type and is even finer than the original model shown, in fig.6.7. The result is that element symmetry of the model has been lost. This imbalance is the result of using automatic meshing to smooth out the transitions. More constraints are required, as discussed in section 6.3. The analyst is unable to control the automatic mesh pattern, and hence its symmetry.

6.4.5 Solid Element Model

The method of using the shell element model has been demonstrated and for the purpose of this thesis will not be investigated further. The SCF obtained, so far, is lower than that derived experimentally. The final approach in the FEA will be to use solid elements, using similar techniques to those in the shell element model. Fig.6.20 and fig.6.21 show the FE model with the forces being applied and the final deformed plot under load. In fig.6.22 a similar stress plot, σ_x, is shown to that in fig.6.17, which gives confidence in the model. However, in the model shown in fig.6.21, the forces are balanced, shown by the deformed plot. Being solid element types, each element is like a brick, it has 6 sides and 8 nodes. Therefore, the stress value plotted is the direct, in-plane stress, which is on the face of the brick in the chosen plane. In fig.6.23, it is along the X-axis. (Parallel to the lower Tee member). This should, therefore, be representative in obtaining the SCFs shown experimentally, since the stress calculated is the direct stress at that point. This is irrespective whether the stress is membrane, nominal or otherwise. (It is the force applied over the area of the element face).

A close up of the corner region and the direct stresses is shown in fig.6.23, with the inset graph of stress versus distance from the discontinuity. As before, the SCF can be found. Note the stress plot becomes asymptotic with the X-axis. Using the same method as before in 6.4.2, and equation 5.1, the SCF is now calculated as 4.28 (18.31 ÷ 4.27) or rounding up to 4.3. This value compares well with the published SCF of 4.2. The mesh size in the corner region is ½ t, as recommended in [6.2] [6.26], which validates the recommendation.

The most obvious question to ask, after the result in fig.6.23 is, would a still finer mesh size than the ½ t have an effect on the result. It has already been shown, in fig.6.19, that caution must be exercised when attempting to refine and smooth a mesh further, owing to instability within the model. However, owing to the more regular geometry of a brick element and subsequent modelling using this element, symmetry can be achieved. The manual meshing of the model using solid elements is easier to control with regards to an internal balance check, than by the software's automatic meshing program.

6.4.6 Fine Mesh Solid Model

The methodology for meshing and load application for this finer mesh model, is identical to the first solid element model, in 6.4.5. The mesh is made up of ¼ thickness size elements around the stress concentration region. The results of the finer mesh solid model are shown in fig.6.24. Once again in the close up, a red line identifies the extents of the plotted graph of stress values, also denoted by the *first node* and *last node*, indicating the extremities. Note the absence of warping as experienced by the finer mesh, shell element model in fig.6.14 & 6.15. In fig.6.24, it can be seen that the profile of the curve is the same as the graph in fig.6.23, except that the profile is smoother owing to the increased mesh density.

From the results, the SCF is calculated to be 5.3. Using a significantly finer mesh density has produced a less accurate result. This is discussed in section 6.3 [6.6] [6.21] [6.24] and validates the recommended mesh density of approximately ½ thickness as correct for such FEA models.

6.4.7 Modelling the Welded Joint

One final aspect, which is worth investigating, is to include the weld in the model. Since the frames that were tested to obtain the SCF by experiment, would have been welded together. This may seem obvious, when taking into context the reason for the analysis [6.28], however, the size of the weld compared to the size of the whole model indicates this would require significant mesh refinement and iteration. A substructure [6.6] [6.7] [6.27] [6.29] [6.30] of the weldment may also be performed, but this would increase modelling time further.

To model and investigate the welded joint alone requires a more detailed analysis. This is time consuming to model, since the nodes, which would be common to both models, must exhibit identical displacements and rotations etc. A simpler way would be to include the welded joint in the existing model of fig.6.20. The analyst could investigate whether the SCF is closer to 4.2 as demonstrated experimentally. The model is shown in fig's.6.25 and 6.26.

The model used will be the much finer mesh, which produced SCF result of 4.28, since localised notch effects may influence the result, as discussed in 6.1.2. Whilst this may appear to be contradictory to the discussion in 6.4.6, the logic is sound. On the model with no welded joint, the geometry for both the ½ t mesh and the finer ¼ t mesh is identical. However, with the welded joint, the model geometry has changed. An additional discontinuity has been introduced to the model, and the scale of this discontinuity warrants a finer mesh to prevent that which is outlined in 6.4.6. This enables the model to follow the theory in 6.1.2, by establishing nodes, which lie within the 0.3t to 0.4t radius. It also prevents a quasi-singularity occurring at the structural discontinuity. From the knowledge gained in the use of load application and boundary conditions, resolving the forces into a horizontal and vertical direction prevents the rotation of the model. This is different to the 45° pull on the previous models, since the addition of the weld, element symmetry is lost. Using the 45° pull, created unwanted rotation, as before shown in fig.6.19. The resulting stress plot is shown in fig.6.27.

The result of modelling the joint with a weld can be seen to have little overall effect on the calculated SCF. In this case, the SCF shown in fig.6.27 is calculated to be 4.23, which is closer to the value of 4.2. This is an improvement to that of 4.28 in fig.6.23, of the model without a weld. However, given the increase in time required to model such a joint compared to the fine mesh without a weld model, it can be dismissed as unnecessary. Especially given the accuracy of the former model and the time constraints placed upon the designer to arrive at an answer in time for the drawing office to begin drawing the vessel for production.

6.5 Conclusions

In fig.6.2 the stress distribution through a structure is shown with the corresponding membrane and bending stress, and it has been discussed that establishing these stresses is very difficult and complex in non-standard geometry. Understanding of element types in the analysis for membrane and bending stress when using FEA and the element types chosen in the model can influence the result. Obtaining useful, reliable and consistent results with FEA is to understand the logic and the parameters of the program.

Using too coarse or too fine a mesh is shown to influence the result. The guidelines of using mesh densities of ½ t have demonstrated to be satisfactory and yielding expected results. Element aspect ratio less than or equal to 5:1 provide acceptable solutions. Using finer mesh density is only applicable in way of structural discontinuities, to prevent a singularity, especially if the discontinuity is small in relation to the whole model. Mesh size of ¼ t is shown to be satisfactory for the use of a finer mesh in way of a discontinuity. A mesh that begins coarse and increases to a fine mesh must do so gradually. A mesh that is too fine can cause the non uniform strain conditions within an element, as the element size becomes smaller. The stability within the model is important, as well as the application of the loads into the model. Investigation into sensitivity analysis of these parameters is required to obtain confidence in the model and its behaviour. Rigid body motion must be prevented by the boundary conditions. Once the results have been obtained, the analyst/designer must understand the limitation of the result. If the result is unable to be proved by approximate beam theory or other, than it should be ignored.

7. Redesigning Structure for fatigue

This chapter is a review of the choices that were made during the design process of a high speed aluminium catamaran. The choices concerned the fatigue life of the welded structure, the analysis of the structure using FEA and the changes made from the result of the analysis and its implications on production.

7.1 The Fatigue Design of Waterjet Structures

Fatigue failure of the aluminium structure around the waterjet unit is common [7.1], [7.2], [7.3] and has been outlined in chapter 1. This is surprising in view of the often quoted advantage of the low vibration levels of waterjets [4.4]. However, considering the vibration that the waterjet duct and structure is exposed to, and the environmental conditions, a different view emerges. The waterjet is subjected to a constant forcing frequency by the impeller and shaft, and to a lesser degree the engine.

Assuming the forcing frequency is related to the blade passing frequency of the waterjet impeller, 10^8 cycles is achieved in only 300 hours in a 6 blade waterjet rotating at 900 RPM. KaMeWa [7.4] recommend using levels of 10^5 cycles for reversing and pitching forces and 10^6 cycles for steering forces. On propeller driven craft, shaft RPM tends to be lower and the number of blades fewer [5.10]. Given the poor fatigue characteristics of aluminium, discussed in section 3.8, the stress levels within the duct and surrounding structure need to be low. The jet duct is immersed in seawater, which further reduces the allowable stress level [3.21], fig.3.11. Therefore, it is clear that design stresses must be set at a very low value, to offset the lower fatigue strength of aluminium. The designer's main problem is what forces are imparted within the duct. The vibration modes in this complex structural arrangement will also influence the stress levels. The displacement and velocity of the panels of plating, and stiffer fabricated structure, will augment the stress levels even more. The mechanism of failure must be understood in order to arrive at a solution to the problem.

7.2 FBM Tricat Design

The following description sets out the design steps that were taken for the Tricat catamaran ferries being built by FBM. These steps were to reduce or eliminate altogether the problems of cracking around the waterjets and transom. The Tricat fast ferry is propelled by two KaMeWa waterjets each powered by a Solar Taurus gas turbine rated at 4200 kW, fig 7.1. The hull structure is of welded aluminium. While the theoretical tools available to check the fatigue life of the design structure were limited at the time of conception, the following areas were explored:

1) Careful detail design to avoid discontinuities and other stress raising features [7.2]. (This was discussed in chapters 4 & 5). The lower the stress concentration, the increase in fatigue life of the structure.

2) Calculation of the natural frequencies of vibration of vulnerable areas. This will identify the most prone areas within the structure and steps may then be taken to reduce the effect of the vibration.

3) FEA model to examine the stresses and deflections of the whole aft end of the ship caused by the static loads from the waterjets. This will help the designer to locate areas of high stress as well as stress raising features [7.5].

7.3 Choice of Aluminium Type and Grade

At the time of the original Tricat design, the choice of aluminium was limited. However a new grade developed by Pechiney in France called 5383 [3.28], see section 3.10, was available but at considerable cost. Since it was a new alloy, the development costs needed to be recouped. Therefore, owing to the then higher cost of the improved 5383, the choice of aluminium was standard 5083-O grade. The reason for using the O temper was the production process. Being a waterjet duct, the plate will have to be rolled into the shape of a cylinder [7.4], and in some regions the radius will be small.

The dangers of using a small radius have been discussed in section 4.5 [3.17] [3.24] [4.11]. Localised bending of the plate can promote plastic deformation and will lead to ductile fracture [4.12]. The alloy is a 5000 series and is non-heat treatable, see 3.5, and the O temper indicates that there is no strain hardening of the alloy to improve its mechanical characteristics, table 3.4. Therefore, the bending and rolling process, during manufacture which strain hardens the plate, will effect the non-strain hardened temper.

Once the plate has been rolled, the temper changes from an O grade to either a H111 or H116 temper, or higher, if a high degree of bending takes place. This would occur owing to poor manufacture or poor detail design. Where as if the temper had initially been H116, the plate will finish closer to H321. Over strain hardening the alloy to a H321 has shown to be deleterious in certain conditions [3.14] [3.15]. In addition, the high magnesium content in the 5083 can lead to intergranular and stress corrosion cracking when the alloy is strain hardened during cold working [7.6]. It also promotes intergranular precipitates of the beta phase which is anodic to the bulk of the plate and initiates local galvanic cells. This was also discussed in section 3.5, regarding the use of H321 temper which has lost its approval for use in structural components [3.17] [3.24].

In terms of production, that is when the alloy is rolled into the shape of the large cylindrical tube, which forms the duct, fig.7.7, it will be strain hardened by the process of being rolled into a defined shape. The process for forming and shaping the duct into the correct shape uses rollers and/or presses. This manufacturing process can promote potential sites of crack initiation, see sections 4.1.1 & 4.5. The geometry of the duct dictates high amounts of double curvature, which will strain the alloy even further when rolled into shape. The amount of strain that an alloy is able to absorb before plastic deformation sets in must be identified from the manufacturing and production process.

7.4 Designing out Stress Raisers

The Tricat, shown in fig.7.1, is a traditional longitudinally framed vessel. This is made from plating, forming the outer skin, which is stiffened by longitudinal stiffeners, which is then itself supported by transverse frames, fig.7.2. It can be seen in fig.7.2, that in the simplified hull form shown to identify structural members, the number of structural members, which must pass through or be in contact with another member is significant. Therefore, one objective is to achieve a design which minimises the number of cutouts.

These frames that follow the shape of the hull can become very complex in confined areas of the vessel, notably the waterjet void. A production friendly method of fabrication of these frames can be achieved to improve the fatigue life with careful selection of geometry. Utilising sharp or hard corners for a bottom frame that joins a side frame of the vessel, is production friendly. However, this will increase the risk of cracking owing to a stress concentration at the junction, see fig.5.8a. This method of joining gives an SCF of 4.2. With a reduction in allowable design stress of around 90% [3.26] as discussed in section 3.9, an SCF is to be as low as possible. In fig.5.8d, an SCF of 1.2 is obtained when using a smooth radius for transition from one member to another. This reduction in SCF is also shown in fig.5.6f, for a similar joint. Therefore, taking into account the possible 90% reduction in allowable design stress, the method of joining which yields the lowest SCF is to be used. The size of the jet void in relation to the while vessel, is small. Therefore, a design for production structure in the jet void is counterproductive.

At this stage in the design process, the designer can investigate the stress intensity factor (SIF). This is determined using equation 2.3. Establishing the fracture toughness for the alloy by CTOD [2.25] in the as-welded condition, as discussed in section 2.9, ensures representative values. It also ensures that a realistic engineering critical assessment (ECA) can be undertaken to calculate, for example, tolerable crack size [7.8]. The time scale and funds available at the time of the Tricat design precluded this CTOD procedure and ECA.

7.4.1 The Tricat's Production Friendly Design

For the Tricat, there was insufficient time available for a full and detailed analysis of the entire waterjet void, the transom, the aft peak void and the engine room. However, knowing that cutouts in framing have a deleterious effect, reducing the amount of cut outs in the frames was a priority. A simple and production friendly way of achieving this is to switch to all transverse framing, rather than traditional longitudinal. Transverse frames would eliminate all cutouts for the longitudinal. This has a secondary benefit. In section 4.7, it was noted that stop/starts of welds create geometric stress concentrations [4.20]. These localised stress concentrations reduce fatigue life by hot spot stress and notch stresses noted in 6.1 and 6.1.1 respectively. Therefore, changing from a longitudinally framed to a transversely framed structure reduces the likelihood of promoting stress raisers owing to the weld bead profile [7.7]. This also avoids the inevitable stopping of longitudinals as they run aft and up the inlet duct, without a load path.

It can be seen in fig.7.3 that the transverse web frame still shows cutouts. The reason for these scallops (cutouts) is to eliminate a more onerous stress raiser: that of a biaxial weld. The scallop is to allow the welded seam of the hull shell plating to pass through the transverse web frame without crossing it. This aspect was discussed in section 5.5.4. This prevents a tensile load in the weld of the frame from crossing over a shell butt weld. This shell butt weld will experience tensile and compressive stresses from global loads [1.4] [1.10] [1.11]. Two welds, which are at right angles to each other, can increase the load at the junction by a factor of $\sqrt{2}$, an increase of 41.4%. This is before any SCFs are accounted for.

It is common practise to see scallops on all transverse frames and any structural members which would prevent a biaxial welded joint. It could be argued that this beneficial effect on the fatigue life of welded joints and structure can be applied to all the frames. In house studies at FBM Marine demonstrated this to lead to a heavier structure and cost prohibitive.

Transverse framing of the waterjet void has other benefits too. Owing to the shape of the hull, the closely spaced thick heavy transverse web, which now replaces the longitudinal, is an arc of a circle. In this type of complex geometry, it is standard practice at FBM to build a separate steel jig to build the structure. This also gives the welder more control. This means without cutouts, the welder can also minimise the number of stop-starts, which influences the fatigue life. Providing plenty of access for welding will ensure the welder is able to produce good quality welds.

In some of the smaller webs, the welder is able to achieve the run of weld in one long sequence, thus eliminating the stop-start altogether. It also makes welding access to the most awkward area of a waterjet easier – that being the underneath part of the duct aft, of the inlet. Hence, a closely spaced pack of transverse frames encompass the inlet and duct. This can be seen in fig.7.4 and shows the complexity, as well as the confined space for the welder, when the structure of the waterjet is assembled.

Because of the inevitably large depth of these transverse frames to provide suitable structural strength, in the absence of longitudinal stiffeners, they are over sized. This means the frames are stiff enough without rider bars; so riders were eliminated thus avoiding a large amount of welding and distortion, section 4.9. This also eased access in between the frames. Finally, to improve the fatigue resistance even further, paint with epoxide primers was applied to the internal bilge areas to avoid sea water contamination of the aluminium, fig.7.5.

The effect of sea water on the mechanical properties of aluminium, particularly along the heat affected zones caused by welding, has been discussed in section 3.9, and shown in fig.3.11. Painting the voids protects the aluminium. Painting the void space, also protects the aluminium from the corrosive effects of sea water [2.34], which can also increase crack growth, see 2.11.

7.5 Natural Frequencies

A cyclic load from a source internal or external to the vessel could initiate fatigue cracking. It has been demonstrated in [1.1] [1.11] that global forces are to be considered. However, with respect to the detail analysis, the source of the cyclic load will be secondary and tertiary in nature. The main source of loading will be mechanical and hydrodynamic [7.4] [7.5], that is: main engine, shafting, impeller etc. At an early stage of the design of the duct for Tricat, the basic parameters of each mechanical source were know. Shaft and engine RPMs for example, and loads from the jet manufacturer. From these known sources, it was able to ascertain the resonant frequencies within the structure from vibration analysis.

The criteria is that the structure designed is to be unaffected by the resonant frequencies as much as practicably possible. With regards to the Tricat design, a detailed analysis of the proposed structure was undertaken by DNV. The computer programme developed by DNV was used to evaluate the natural frequency of vibration of plate panels and plate stiffener combinations. Areas such as the transom, inlet duct, aft peak bulkhead and bottom plating were investigated and any panels which appeared to be close to the blade passing frequency were modified by changing the geometry. The addition of a simple lightweight stiffening member to change the aspect ratio of a plate yields excellent results. Since HSC craft are weight sensitive, solutions that minimise weight growth are essential. The DNV software program took into account the appropriate edge constraints and the effect of water on one side.

As with any computer simulation, validation is required to ascertain the accuracy of the analysis. In the same manner as the FE analysis in chapter 6. During sea trials of the Tricat, the whole of the jet duct and void, measurements were taken with an accelerometer. An output from the post processing is shown in fig.7.6. The analysis was compared against the DNV predictions and guidelines, which were issued by DNV during the rule development of the HSLC rules [3.24]. This procedure is now embodied into DNV rules [7.5]. The actual velocities of panels of plating and structure were close to the predicted values by the computer program. A more detailed description and analysis of the sea trials and results is in [7.9].

The criterion set by DNV, was a maximum of 20mm per second for any structure. It can be seen in fig.7.6 that the blade passing frequency is producing a velocity of 7.5 mms^{-1}. This is within the acceptance criterion. The result of the sea trail gave confidence in the structural stiffness of the jet duct and void and satisfied that which is outlined in section 7.2.

7.6 Establishing Load Paths

In the case of high speed ferries such as the Tricat, prescriptive rules exist from Classification Societies [3.17] [3.24] enable the designer to establish a common standard. The Classification Society rules are based upon extensive research over many years. With regard to the waterjet loads, the manufactures of the waterjet supply the given loads from the waterjet that must then be absorbed into the vessel. The waterjets chosen for the Tricat design were KaMeWa. KaMeWa supply the waterjet loads, thus making the analysis easier.

The natural temptation is to assume that forces applied at the transom will be absorbed by the hull more or less immediately, i.e. at the transom. However, as waterjet forces are concerned, most of the structure in the transom area is, redundant, [3.26] [7.9]. The reason for this is that the waterjet duct is a large cylinder which has a diameter of ranging from 600 to 1500mm. In the case of the Tricat, it is 900mm. This duct, therefore, is very stiff. The stiffness of the duct is greater then the surrounding and supporting structure. Intuitively, the load is attracted to these stiffer regions of the of structure. The duct, generally, extends from the transom via the watertight bulkhead (WTB) into the engine room.

Representing this in a simple structural analysis, the duct is a propped cantilever. The engine room structure represents the built in part of the boundary conditions. The WTB being the simple support and the transom the propped end. The transom is merely a watertight diaphragm that flexes as the waterjet loads are transferred from the waterjet nozzle steering system to the duct. Therefore, the transom is a flat unstiffened panel of plating, welded to the hull bottom and sides.

7.6.1 The Various Load Cases

Before examining the load diffusion into the hull structure, the different load components applied by the jet unit were examined [3.26] [7.5] [7.9]. There are three basic load cases:

- Axial thrust:
- Steering loads:
- Crash stop loads.

Axial thrust occurs whenever the vessel is propelled forwards, with the maximum load applied during peak acceleration. A more or less steady thrust is applied along the jet axis. Steering forces apply lateral shear forces to the nozzle system, producing a combination of lateral shear and sideways bending moment at the transom, fig.7.7. While relatively small in magnitude [7.4], these loads may be significant for fatigue in some cases. In terms of severity, the crash stop is the most onerous. A combination of axial and vertical forces and a vertical bending moment will apply at the transom.

It is this load case which generate design problems and lead to fatigue cracking. All these loads pass through the nozzle/flange attachment at the transom and it is at this stage that they come into contact with the hull. The process of load diffusion into the hull starts at this point.

7.6.2 Structural Stiffness

The conventional wisdom has been to consider of the hull as stiff, with the nozzle/duct system as secondary structure - a view reinforced by looking at any shipyard engineering drawings. In fact the stiffness of the duct is very high due to the very thick plating used (appx. 20 mm), and the large diameter of the conical portion immediately forward of the transom; since this is essentially a very thick walled pipe. It is the simple propped cantilever concept that has been overlooked and, in the case of the waterjet, it means that the loads tend to stay in the stiffer duct.

The transverse webs, including the transom, are only effective in absorbing the vertical shear loads. Thrust and bending moment cannot diffuse directly into the hull. The closer packed transverse frames shown in fig.7.4, transfer these vertical loads, in shear, directly into the hull shell plating. The choice to use transverse framing has the additional benefit of load transfer of the waterjet loads.

7.7 The FEA

The FE model consisted of the hull structure and the engine room structure up to the forward engine room watertight bulkhead as well as the waterjet duct. This aids in the removal of any possible influence of boundary conditions and helps to prevent excess stiffness of the FE model, see 6.3 & 6.4.4. This requires care to ensure that the extra displacement constraints prevent rigid body motion without over constraining the structure [6.6]. Thereby producing unwanted deformation.

The model was created using a FE software package called COSMOS/M version 2.0, which is a product of SRAC, Santa Barbara, California, USA. Four types of elements were used: shell3, shell4, 3D Beam and Solid. The following description of each element type is from the user manual of COSMOS/M [6.15].

7.7.1 Element Types

Shell Element Type

As discussed in 6.2.4, thin shell elements are suitable for solving elastic structural stresses [6.16] [6.17]. The shell elements used in this model are SHELL3 and SHELL4. These are 3-node triangular and 4-node quadrilateral thin shell elements with membrane and bending capabilities for the analysis of three-dimensional structural and thermal models [6.8] [6.15] [6.18]. This type of element is ideal for the analysis of the waterjet duct, owing to its six degrees of freedom and the special features of buckling and in plane loading. The 3-noded shell element allows for complex curvature. A more detail explanation of the element types is in appendix C.

Beam Element Type

Referring to 6.2.3 with regards to Beam Elements, the choice available in the COSMOS/M suite is varied. The type of element chosen is called a BEAM3D [6.15], which is a 2-node uniaxial element for three-dimensional structural and thermal models. This type of element is ideal for representing the rider bar of transverse Tee frames, as well as application of moments.

Solid Element Type

The elements discussed in 6.2.6 outline the use of 8 and 20 noded 'brick elements. For this analysis, an 8 node 'brick' type of element was considered to be sufficient to obtain the accuracy required, since the 20 noded element would increase the computing time for a small gain in the desired accuracy. Since the FE model is complex, it is worth noting that higher order elements require an increase in computing time and also can produce strange nodal vectors [6.23]. Using a lower order element reduces the risk of this occurring.

7.7.2 Boundary Conditions

As described in section 7.7, the model included the waterjet duct and all the surrounding structure, as shown in fig.7.8. The FE model had symmetry about the vessels centreline and about the forward engine room watertight bulkhead, (WTB). This gives the model the effect of being as stiff as the region of the model along the line of nodes which are being constrained, without having to model any more of the structure. A simple support along the line on the forward engine WTB only, enables the FE model to be held without affecting rotation. This is in line with the findings of 6.4.3, which clearly show that the applied loads and boundary constraints must be as far away from the area of concern as possible. The FE model consisted of 25,000 nodes, 13,000 elements and 110,000 degrees of freedom. The mesh, which represented the hull structure, is coarse compared to the mesh density of the waterjet duct. The meshing from a coarse to a fine mesh requires a smooth transition, including localised areas of fine meshing, as recommended in 6.4.2.

Owing to the shape of the waterjet duct, shell4 element would exhibit a degree of warping and twist. Therefore in these regions of high curvature, the shell3 element is used since three nodes in space will always be in plane and fair with each other.

7.7.3 The FE Results

The finite element model, was analysed under each of the three given waterjet load cases in 7.6.1, applying the loads at the transom. A more detailed analysis of the results can be found in [7.9]. The conclusions from the FE model are thus:

- Acceleration loads produce an almost purely axial deflection, though there is some slight rotation at the transom due to the support stiffness provided by the bottom shell. This was seen on sea trials to be in the order of 1-3mm.

- Steering forces produce a lateral rotation of the transom. This causes the transom plating to rotate with the nozzle system. (A flat unstiffened transom flexes, unlike a traditionally stiffened transom).

- The crash stop case produces a rearward and upward motion of the nozzle, as well as rotation at the transom; the entire FE model bends from its support point (at the forward engine room bulkhead). This deflection was observed during sea trials.

The crash-stop stresses in the duct forward of the conical portion show a roughly linear bending distribution, as the loads transfer forward through the duct, fig.7.9. The stresses in this region can be compared to the predictions from treating the conical duct as a propped cantilever beam under an end moment. If the transom absorbs no bending moment, then:

- Shear transfer will take place into the transom;
- Bending and axial loads will pass down the conical portion into the duct within the hull structure.

7.7.4 Calculated Stresses

From the FE plot shown in fig.7.9, the Von Mises stress distribution indicates a maximum stress in the region of 44 MPa - around the circumference of the jet duct in way of the cone interface. This is the region where the aluminium jet duct butts into the large cone section, which is supplied by the manufacturer, fig.7.7. Whilst the stress may be low, one third of yield [3.16] [3.17], the value was considered too high when taking into account the fatigue and sea water environment in which the duct is immersed. In chapter 3 the effects of fatigue are shown to have a detrimental effect on aluminium, compared to steel. SN curves of aluminium do not have a fatigue limit the way steel does. Comparing the stress of 44 MPa with fig.3.10 in air, the actual fatigue limit has been reached with no residual factor of safety. When comparing the allowable design stress in sea water, fig.3.11, the stress of 44 MPA has now been exceeded by a factor of 2. Clearly this is unacceptable. There is no longer a factor of safety on the design stress limit. This is also confirmed in [3.26].

In light of these results, further detailed analysis was necessary to eliminate the possibility of a fatigue failure in way of the flange that joins the two sections of the waterjet together. The FE model shown in fig.7.9 is coarse in nature, relative to the thickness of the actual plating used. Therefore, a finer mesh is required to analyse this region in more detail, see section 7.8.

7.7.5 Transom Stresses

These stresses are solely due to the displacements caused by the nozzle being attached directly to the cone. Given the nozzle deflections, the stresses can be examined using a simple beam model of the plating in this area [7.10]. It was shown in [7.9] that the stress values decrease with decreasing plate thickness. This was expected given the lack of load transfer via the transom. With this pattern of high deflection-induced stresses, it is clear that a flexible transom, designed to accept in-plane forces but to flex under out-of-plane loads, is desirable; see 7.6.2 for discussion on structural stiffness.

The flexible transom is complicated by the need to provide high material strength in the region between the nozzle and the bottom skin. Welding at the nozzle/transom and transom/ bottom junctions will reduce the aluminium properties in this area, as discussed in sections 7.7.4 and 3.9. The FE analysis [7.9] indicated stresses in this transom area to be 21 MPa, membrane, and 188 MPa surface stress. Therefore, careful selection of alloy and attention to detail with regards to the geometry and the weld sequence must be borne in mind. An estimated stress of 188 MPa [7.9] is greater than the as-welded design stress allowed by Classification Societies, see table 3.4, for 5083 plate.

Therefore, it was decided to choose a different alloy. The alloy chosen was 6082-T6. This alloy has an unwelded design stress of 240 MPa, table 3.6, which is greater than the estimated stress of 188 MPa. This alloy is a heat treatable and is used extensively for extrusions and profile sections [3.5] [3.7] [3.12] [3.13]. An extrusion, was shaped in the angle of the transom-hull bottom plate. It was L shaped. Using this extrusion, would remove the need for welding in this region, the apex, thereby utilising the unwelded strength properties of the alloy. It is worth noting that Classification Societies [3.17] [3.24] restrict the use of 6082 alloy below the waterline. However, owing to the FEA results, the use of 6082 was permitted.

During sea trials of the Tricat, the jet duct, transom and hull plating was strain gauged. The stresses recorded were close to those predicted by FEA. The maximum stress recorded was about 120 MPa, compared to that of 188 MPa predicted by FEA. The stress in the duct and transom, at some distance away from the extruded joint, also showed good correlation to the FEA. Measured stresses of 20 MPa compared to 20-25 MPa. The large discrepancy of the estimate 188 MPa to the actual observed 120 MPa, can be explained by the theory in section 6.3. The region of the FE model, around this section of the model was coarse. It is also a major structural discontinuity. A discontinuity like this can represent a singularity. Therefore, a much finer smoothed mesh is this region is required and recommended.

The analysis in [3.24] [7.9] shows that the transom/hull bottom plating corner joint acts as a pivot for the plating, which is being caused to rotate by the nozzle. This then has the affect of bending the plate into an S shape, fig.7.10. It is this short distance between the flange and the hull bottom, that the FE model requires a finer mesh. A simple solution would be to increase the distance of this plating to allow greater flexibility of the plate. This would reduce the stress. However, the situation is made somewhat more complex by the desire to keep the waterjet as low as possible in the hull, relative to the waterline, for zero head. This invariably means that the distance, from the transom hull bottom corner join to the jet ring on the transom, is very small. This is not conducive to allowing this region of the transom to flex into a desired S shape.

Post welding treatment, as discussed in section 5.8 can be utilised to further reduce the onset of fatigue cracking. The production drawing shows an undercut of the weld toe both sides of the transom plate. This applies to the transom which is 5083 plate, rather than the extruded section. The undercut is the same as shown in fig.7.13 on the flanged joint.

7.8 Jet Duct Flange

Another area of interest is raised by transfer of load forward of the cone. The bolted connection at the cone's forward end must now be capable of absorbing a much higher set of loads than if the load was transferred at the transom. This requires analysis of the flange and duct wall under the resultant bolt loads, taking into account transfer of both axial and bending loads. It has been shown in fig.7.9 that the stress at this junction of the two units is high and requires careful analysis.

The problem with this type of analysis is that the two units are flanged and bolted together; a flanged and bolted connection is very difficult to achieve with FEA [7.9]. This is because the stress is no longer linearly proportional to the strain. Therefore, non-linear analysis is required [6.19]. To overcome this dilemma a different approach was necessary. From the coarse model in fig.7.9, the nodes around the entire circumference were plotted with their corresponding displacements and rotations.

What was required was a method to simulate the actual loads on the flange and how the transfer of these loads would occur in a bolted connection. The solution is relatively straightforward once the mechanism is understood. A bolt transfers load through shear, tension and compression.

For the detailed analysis of the jet duct flange joint, solid elements were used. These proved to be effective in obtaining good SCF correlation between experiment and theory, as discussed in 6.4.5. Only the jet duct flange is modelled. At first, it would seem natural to model the flange of the duct bolted to the flange of the cone section. However, as pointed out, this is difficult owing to the non-linearity effects. Therefore, modelling the jet duct flange alone maintains elasticity with the model. The welded joint is also modelled to establish the notch stress for the SCF. A partial substructure model was performed, owing to the complex shape.

The element size for this analysis was in the order ½ plate thickness, recommended in 6.4.6. This would give sufficiently accurate results to obtain a SCF and further guidance for the designer concerning the flanged joint. The next step was to ensure that the finer mesh model was behaving correctly. The only validation was to use the original FEA results on the coarse model as a reference for validation. If the stress on the fine solid mesh model, at some distance away from the area under scrutiny, is of the same order of magnitude as the coarse model, this would give sufficient confidence that the solid mesh model is behaving correctly.

It can be seen in the Von Mises plot fig.7.11, that the value of the stress in the jet duct, 42 MPa, is comparable to that shown in fig.7.9; at some 3 or 4 plate thickness distance. This gives confidence in the behaviour of the solid fine mesh model. The regions of high stress can be seen to be in way of the holes for bolting the flange to the jet cone, and the fillet of the welded joint. In order to establish the direction of the load path, a stress plot in the longitudinal plane of the duct, is required, fig.7.12. If the stresses are of similar value then this would indicate that the loads are acting in plane rather than out of plane. In fig.7.11, the stress along the fillet weld is in the order 180-190 MPa.

The stress plot in fig.7.12 does indeed indicate that the primary load is in the longitudinal direction, i.e. in-plane; since the stress of 192 MPa in this longitudinal direction, σ_z, is comparable to the Von Mises stress. This causes the flange to rotate, forcing the fillet weld into compression and tension. The bearing stress around the bolt holes is also high owing to this rotation; 318 MPa compressive. From the stress plot in fig.7.12, the SCF at the flange joint can be calculated using the same procedure as described in 6.4.7 and is approximately 4.8. This value is high, especially when taking into consideration the environment that the duct is in, i.e. the immediate proximity of the sea water environment, and the vibration from the impeller, fig.7.6. The analysis of this welded joint and its conclusions is the same for the transom stress in 7.7.5. However, this detailed joint has a more pronounced notch and hence hot spot stress. The design of the flanged joint required input from production. FBM production used test specimens of the joint to establish parameters of joint details, weld procedure etc, to ensure a weld that would pass an NDT examination.

In addition to the flanged, the weld profile, as discussed in 4.7.1, influences the fatigue of the joint. The inside of the duct, where the plates butt together, will have the weld bead extending into the duct void, where the water passes through. Clearly, removing this weld profile would be desirable for the flow of the water thought the duct. In section 4.7.1, it is shown that a dressed weld exhibits improved fatigue strength compared to an as-welded profile, fig.4.16. To dress this weld bead on a curved surface is difficult. Therefore, a warning was placed on the production drawing to dress the weld bead as much as practicably possible without affecting the parent plate. This attention to detail prevented undercutting into the parent plate.

This flange joint to the duct in the FE model, is the fillet weld, and given the high SCF, the geometry of the weldment needs to be addressed to smooth out the peaks. This means the fillet weld must be welded with a smooth and defined shape to the weldment and with extreme care. The design of the joint must be that easy access to the root of the weld is possible, to ensure 100% penetration.

In section 4.6, the skill of the welder was shown to influence the fatigue life of a joint [4.18] [4.19]. Therefore, FBM use the most highly trained, qualified, and experienced welders for these joints.

7.8.1 Post Weld Treatment

Post weld treatment is also required. The post weld treatment is in the form of smoothing off the toe of the weld, see 5.8.1 and recommend [3.17] [3.24], fig.5.13. This removes residual notch stresses, see 6.1.2, as can be seen by the production drawing of this region of the flange, fig.7.13. The stress of 192 MPa shown in fig.7.12 is also beyond the yield of aluminium in this welded joint. Therefore the shape of the weldment is just one of several options that were available during the design process. The thickness of the flange and the plating surrounding the flanged was also increased considerably, from 15mm to 25mm. The flange was also increased in thickness to 35mm. Since this would help to reduce the bending in the flange and its behaviour would change from bending to that of shear. This is now standard on all FBM waterjet ducts, with thicker plating in way of the flanged joint and the flange to be thicker still.

The stress in way of the bolts whilst being high, is acceptable and just within the bearing stress limits of the alloy. The bolt holes must be drilled with care to prevent unnecessary score marks or misalignment which create an unwanted flaw. This would initiate the first stages of fatigue cracking through fracture. The mechanism and analysis of fracture was discussed in 2.9.2 and 2.9.3. The analysis of bolt holes under cyclic loading is address further in [1.16] [7.11].

7.9 Conclusions

A method of analysis for fatigue suitable for use within the time frame of a working shipyard has been addressed. Current methods [1.16] [7.11] are too time consuming for the shipyard designer faced with timescales that are often unrealistic. The analysis focused upon the fact that standard methods of fatigue analysis only provide guidance to simple structures acting under uniaxial loading [1.16] [7.11].

In the case study of the Tricat, the calculated stresses and SCF enabled the design to focus on published data that enhanced fatigue life by:

- Correct alloy selection and temper
- Using realistic allowable design stresses in air or sea water
- Complex structures can be model using FEA with guidelines
- Establish a coarse mesh FE model
- A fine mesh model with ½ t element size gives acceptable results
- Calculating the SCF from FEA provides choice for detail design
- Reducing the amount of cut outs as much as possible
- Painting the welded structure for protection
- Weld profile to be as smooth as possible
- Post weld mechanical treatment to reduce notch stresses
- Vibration study to establish natural frequencies in the structure
- Weld procedure and detailing is essential to reduce notch stress
- Using skilled fabricators

8. Conclusions

8.1 Discussion

High speed vessels have been shown to exhibit fatigue cracking, especially in the region of the transom. This thesis has demonstrated that with regards to aluminium used on high speed vessels, a single factor for fatigue cracking is unrealistic. The reason for a structural failure through fatigue requires a broader knowledge of the influences and mechanisms that affect ship structures. The concepts of crack initiation and crack growth have been shown to influence stress intensity factors, which directly affect the onset of cracking. Having understood these concepts, the designer is able to focus upon these areas of the design to ensure that crack initiation and crack growth, is reduced to a minimum. Understanding crack closure for example could result in a structure that maintains a constant compressive stress in regions of high stress concentrations. This would prevent a crack, from whatever source, propagating.

This thesis presents a review of factors that influence fatigue cracking as well as the mechanism of fatigue and how to analyse crack growth and stress concentrations. The mechanism of fatigue is cyclic loading. All high speed vessels experience cyclic loading from various sources. Globally, it is from the sea and frequency of encounter in heavy seas. Locally it is from mechanical and hydrodynamic sources. For local analysis, the expected loads are available from the manufacturers of such items. Using this data, the designer can establish early in the design from simple vibration analysis, areas of the structure that require attention - much of which may be intuitive. Aluminium is a material chosen for its lightweight and strength properties. However, the manufacturing process of the alloy can initiate small flaws in the microstructure of the alloy matrix. The grade of aluminium and its temper also affects the crystalline structure. A temper that has a high degree of strain hardening, for higher mechanical properties, H321 for example, has a reduced capacity for bending and forming. This temper also promotes delamination of the matrix by its poor corrosion properties. This is shown to have a significant effect on the fatigue properties of the alloy.

If the designer is unaware of the implications of choosing certain alloys and their tempers, fatigue cracking will occur well before that expected during normal service conditions.

Fatigue cracking is generally attributed to poor detail design. Choosing the wrong grade of alloy for fabrication will promote fatigue cracking in advance of any detail design. The design detail may be from the result of using BS8118 [1.16]. However, given that the manufacturing process also reduces the capacity by changes in the crystalline structure by dislocations, failure may occurring owing to the method of production. To fabricate structures for high speed vessels, plate is rolled and bent in to complex shapes. This process can promote crack initiation if the plater is unskilled or unaware of the implications of rolling with different tempers. Rolling the plate into a radius that is too tight will overstrain the alloy. Once the alloy is overstrained, it will create voids in an already dislocated matrix. These voids become sites of crack growth leading to ductile failure. The influence of welding on aluminium has a deleterious effect on the mechanical properties. The effect can be a reduction as much as 50% in air and as much as 90% when seawater is taken into account. During welding by MIG or TIG, poor joint preparation will lead to porosity in the weld. Porosity in welds can reduce the fatigue life by a factor of 200. The skill of the welder is also a factor. If the welder produces a weld that has poor penetration it reduces the fatigue life of the weldment. A weld bead that is too large will form a localised discontinuity. This leads to notch stresses in the weld. These notch stresses increase the stress concentration factor at the weld toe, thus reducing the allowable design stress.

The structures of high speed vessels are complex. To allow the passing of smaller longitudinal stiffening members through larger transverse members requires cutouts. A cutout creates a structural discontinuity in the member that is being penetrated. It is shown that the shape of cutouts has a significant affect on the stress concentration factor surrounding the cutout. Therefore the designer needs to establish the SCF of cutouts used in the structure. From parametric studies, redesigning cutouts for longitudinals can result in SCFs being reduced by a factor of more than 2. The joining of two main structural members to form a transverse frame system has many solutions with regards to reducing discontinuity effects.

Each method has its own SCF and is presented in chapter 5. Such joints also affect production cost. Hence the designer needs to balance the choice of design variables to yield an acceptable SCF and at an optimal cost. Establishing the SCF for non-standard structures is addressed in chapter 6. Where data is unavailable, the use of FEA enables the designer to model and calculate the SCF for any given joint. The use of FEA for design is complex and requires understanding the limitations of the program. Simple guidelines for using FEA are given in chapter 6. These include:

- Establish a model with a coarse mesh
- Understand the element types being used, by simple verification
- Maximum element aspect ratio to be 5:1
- Validate the coarse mesh model with beam theory, where possible
- Use a finer mesh in regions of higher stress
- Smooth out the transition from coarse to fine mesh
- Beware of using a mesh that is too coarse in way of singularities
- Solid elements produce consistent results for detailed analysis
- Element size of ½ t produces results that agree with experimental data
- Element size of ¼ t in way of notch stresses give consistent results
- Using a mesh that is too fine may give incorrect results
- Applied loads are to be transferred into the model smoothly and sufficiently far away from discontinuities
- The boundary conditions are to be sufficiently far way from the area of inspection, to prevent unwanted influences

In summary, it is clear that while guidelines such as BS8118 [1.16] and ECCS [7.11] are useful for the design of high speed vessels, it needs to be understood that there are many other influencing factors that can affect the fatigue life of a structure. Isolating a single factor, for analysis, ignores the wider implications of the deleterious effects of production and environmental conditions.

8.2 Recommendations For Future Work

The case study of the waterjet shows how a common fatigue problem within shipbuilding can be overcome with guidance. In chapter 2 the theory of crack growth and propagation could be presented in a manner that gives useful information to the designer without having to be immersed in the theory of fracture mechanics.

The study of common shipyard joints in chapter 5 could be taken a stage further with fracture mechanics. The use of fracture mechanics as a tool for the designer, would give far greater confidence into the understanding and behaviour of how and where cracks may occur. With such information, simple crack arrestors maybe employed to prevent further cracks, or to guide the crack into a region of high structural redundancy, thereby increasing the fatigue life of the joint.

Further work is needed to extend the fitness-for-purpose acceptance criteria to include less harmful imperfections that could still be controlled during fabrication. As more is learnt about the link between weld quality and fatigue life, so the prospects for improved quality justifying increased design stresses should improve.

The effect of thickness and load paths on such joints using fracture mechanics would also be an invaluable source of information. Instead of presenting the data in the form of the complex BS8118, a much more user-friendly matrix of joints with their implications, would be cost and time effective for the designer. A quick glance at a matrix of joints, with all the given parameters of how, what and where, would take out the complexity but not the theory, thereby leaving the designer far more choice and time to research and redesign joints in a project lead time frame.

Further research into multiaxial fatigue is paramount. The standard literature available such as ECCS and BS8118 only addresses single plane loading on very simple two or three-dimensional structure. This may be sufficient for bridges and similar structures. High speed marine vessels however, are made from complex three-dimensional structure with loads being imposed in six degrees of freedom, require a far greater understanding and research into its effects.

It may be shown that using current recommendations in BS8118 are non-effective when considering multiaxial loads or even deleterious. Until this aspect is investigated, the designer may be doing more harm than good.

8.3 Conclusion

This thesis has dealt with the fatigue design aspects of high-speed marine vessels made from aluminium alloys by:

- Highlighting fundamental aspects of fatigue crack initiation and growth geometry;
- Discussing the key characteristics of the 5000 and 6000 series aluminium alloys as pertaining to their marine usage;
- Exploring the effects of the ship production environment and related fabrication processes on the fatigue performance of the structure;
- Illustrating the manner in which details such as cutouts are designed influence structural performance;
- Establishing a methodology for using FEA to provide consistent results for analysis; and
- Applying the above concepts in the context of a part of the structure of a Tricat vessel.

9. List of References:

1.1 Violette F.L.M., Polezhayeva H.A., H.W. Chung, Cheng F.Y, "Basic Parameters Governing The fatigue of Alumnium Ships", The 3rd International Forum on Aluminium Ships, 27-28th May 1998, Norway. Published by Quantic Media Ltd, Kent, UK.

1.2 Bryce R., Taylor D., "Underwriting High Speed Craft", International Symposium & Seminar on The Safety of High Speed Craft, February 6 & 7 1997, London, UK, The Royal Institution of Naval Architects.

1.3 International Code of Safety for High-Speed Craft (HSC Code) 1995, IMO-187E, International Maritime Organisation, London.

1.4 Berstad A.J., Larsen C.M., "Fatigue Crack Growth in The Hull Structure of High Speed Vessels", Proceedings of Fourth International Conference on Fast Sea Transport, Fast '97, Sydney, July 1997.

1.5 Farinetti V., "General Considerations on High Tensile Steel Vs Aluminium Alloy and Technical Aspects Related to The Aluminium Construction", The 3rd International Forum on Aluminium Ships, 27-28th May 1998, Norway. Published by Quantic Media Ltd, Kent, UK.

1.6 Kecsmar J., Warren N.F., "Practical Design Aspects in The Hydrodynamics of Fast Craft", International Conference on Hydrodynamics of High Speed Craft, 24-25th November 1999, London, UK. The Royal Institution of Naval Architects.

1.7 Groves S., "Recent Developments in Fast Ferry Design, Construction and Operation – Key Underwriting Issues", An Address Delivered to The Insurance Institute of London, 23rd October 2001.

1.8 Morris J.A., "A Three Dimensional Structural Analysis of a Large Wave Piercing Catamaran Design", IMAS 91 High Speed Marine Transportation, The University of New South Wales, Sydney Australia, 11-13 November 1991, The Institute of Marine Engineers.

1.9 Govindasamy B.N., Hughes C.T., Olbjørn E.H., "Classification of High Speed Marine Transportation With Particular Emphasis on Structural Strength", IMAS 91 High Speed Marine Transportation, The University of New South Wales, Sydney Australia, 11-13 November 1991, The Institute of Marine Engineers.

1.10 Berkovits A., Di S., Kelly D., Kastak D., Chowdhury M., Goss P., "Development of a Generic Ship Model For The Study of Fatigue in Welded Aluminium Catamaran", Proceedings of Fourth International Conference on Fast Sea Transport, Fast '97, Sydney, July 1997.

1.11 Heggelund S.E., Moan T., Hoff J.R., Oma S., "Practical Calculations of Global Design Loads and Load Effects For Large High Speed Catamarans", Fast 2001, 6th International Conference on Fast Sea Transportation, 4-6th September 2001, Southampton, UK.

1.12 Tveiten B.W., Moan T., "Fatigue of Aluminium Stiffener-Girder Connection", Proceedings of Fourth International Conference on Fast Sea Transport, Fast '97, Sydney, July 1997.

1.13 Fredriksen A., "Fatigue Aspects of High Speed Craft", Proceedings of Fourth International Conference on Fast Sea Transport, Fast '97, Sydney, July 1997.

1.14 Rules for Classification of High Speed, Light Craft and Naval Surface Craft, Det Norske Veritas, Høvik, Norway, 1999.

1.15 ShipRight: Design, Construction and Lifetime Ship Care Procedures Fatigue Design Assesment Procedure, January 1996, Lloyd's Register of Shipping, London, UK

1.16 BS8118, Structural Use of Aluminium, Part 1: Code of Practice for Design, 1991, BSI – British Standards Institution, London.

1.17 Hudson D., "Current Boat Building Materials", Advanced Composites Seminar, SP Technologies Publication.

1.18 Hopf K.A., "A Comparison of FRP Tooling Process", Number 71, June/July 2001, Professional Boat Builder Magazine, Brooklyn, ME 04616-0078, USA.

1.19 Rudgley G., Warren N.F., "Designing a Special Purpose SWATH to The HSC Code", International Symposium & Seminar on the Safety of High Speed Craft, February 1997, London, UK, The Royal Institution of Naval Architects.

2.1 Pook L.P., "The role of crack growth in metal fatigue", The Metal Society London, 1983.

2.2 Benallal A., Cailletaud G., Chaboche J.L., Marquis D., Novailhas D., Rosset M., "Description & Modelling of Non-Proportional Effects in Cyclic Plasticity", Biaxial & Multiaxial Fatigue, Edited by M.W. Brown & K.J. Miller, Mechanical Engineering Publications Ltd, London, University Press Cambridge, 1989.

2.3 Frost N.E., Marsh K.J., Pook L.P., "Metal Fatigue", Oxford University Press, 1974, ISBN 019 8561148

2.4 Cyclic Deformation and Fatigue of Metals, Edited by E. Bílý, Material Science Monographs 78, Elsevier 1993, ISBN 0 444 98790 8

2.5 Peralta P., Laird C., Ramamurty U., Suresh S., Campbell G.H., Mitchell W.E. "Fatigue Crack Nucleation in Metallic Materials" - Small Fatigue Cracks: Mechanics, Mechanisms and Application Proceedings of the 3rd Engineering foundation International Conference, Hawaii, Dec 6-11, 1998.

2.6 Anderson J.C., Leaver K.D., Rawlings R.D., Alexander J.M., *"Materials Science, 3rd Edition"*, 1985, Van Nostrand Reinhold (UK). ISBN 0-442-30626.

2.7 Liebowitz H., "Fracture" – An Advanced Treatise, Volume 1, Academic Press Inc. New York, 1968.

2.8 McGregor Tegart W.J., "Elements of Mechanical Metallurgy", MacMillan Series in Materials Science, The MacMillan Company, New York, Second Printing 1967.

2.9 Felbeck D.K., Atkins A.G., "Strength and Fracture of Engineering Solids", Prentice-Hall Inc, N.J. USA, 1984, ISBN 0 13 851709 6

2.10 Honeycombe R.W.K., "The Plastic Deformation of Metals", Edward Arnold Publishers Ltd., 1968

2.11 Piascik R.S., "The Growth of Small Cracks in Airframe Structure", Small Fatigue Cracks: Mechanics, Mechanisms and Application Proceedings of The 3rd Engineering foundation International Conference, Hawaii, Dec 6-11, 1998.

2.12 Fuchs H.O., Stephens R.I., "Metal Fatigue in Engineering", A Wiley-Interscience Publication, 1980, ISBN 0 471 05264 7

2.13 Broek D., "Elementary Engineering Fracture Mechanics", Noordhoff International Publishing, Leyden, 1974.

2.14 "Fatigue Crack Propogation", A Symposium Presented at the 6th Annual Meeting American Society for Testing and materials, June 26-1st July 1966, ASTM Publication.

2.15 "Fatigue Design Hand Book", Advances in Engineering, Vol 4, Society of Automotive Engineers Inc., 1968

2.16 Kosteas D., "Fatigue Behaviour and Analysis", Lecture 2401, Advanced Level, Training in Aluminium Application Technologies, European Aluminium Association, 1994.

2.17 Etube L.S., "Fatigue and Fracture Mechanics of Offshore Structures", Professional Engineering Publication, 2001. ISBN 1 86058 312 1

2.18 Ishihara S., McEvily A.J., "Analysis of Small Fatigue-Crack Growth Under Two-Step Loading Conditions", Small Fatigue Cracks: Mechanics, Mechanisms and Application Proceedings of the 3rd Engineering foundation International Conference, Hawaii, Dec 6-11, 1998.

2.19 deKoning A.U., "Prediction of Fatigue Crack Crowth", The Assessment of Cracked Components by Fracture Mechanics, Mechanical Engineering Publication Ltd., 1989.

2.20 Trantina G.G., Johnson C.A., "Probabilistic Defect Size Analysis Using Fatigue and Cyclic Crack Growth Rate data", Probabilistic Fracture Mechanics and Fatigue Methods – Applications for Structural Design and Maintenance, American Society for Testing Materials, 1983.

2.21 Kosteas D., "Applied Fracture Mechanics", Lecture 2403, Training in Aluminium Application Technologies, European Aluminium Association, 1994.

2.22 Latzko D.G.H., "Linear Elastic Fracture Mechanics: A Summary Review", - Post-Yield Fracture Mechanics, Applied Science Publishers Ltd., 1979, ISBN 0 85334 775 1

2.23 Rolfe S.T., Barsom J.M., "Fracture and Fatigue Control in Structures", Prentice-Hall Inc, N.J. USA, 1977

2.24 Turner C.E., "Methods for Post-Yield Fracture Safety Assessment", - Post-Yield Fracture Mechanics, Applied Science Publishers Ltd., 1979, ISBN 0 85334 775 1

2.25 Robinson J.N., Tetelman A.S., "Measurement of K_{IC} on Small Specimens Using Critical Crack Tip Opening Displacement", Fracture Toughness and Slow-Stable Cracking. Proceedings of the 1973 National Symposium on Fracture Mechanics Part 1, ASTM.

2.26 Roos E., "Component Tests and the R-Curve Approach for Through Cracks", The Assessment of Cracked Components by Fracture Mechanics, Edited by Larsson L.H., Mechanical Engineering Publication Ltd., 1989, ISBN 0 85298 677 7

2.27 Heyer R.H., "Crack Growth Resistance Curves (R-Curves) – Literature Review", Fracture Toughness Evaluation by R-Curve Methods, American Society for Testing and Materials, 1973.

2.28 Larsson L.H., "The Basic Principles of Fracture Mechanics and an Overview of ASFM6", The Assessment of Cracked Components by Fracture Mechanics, Edited by Larsson L.H., Mechanical Engineering Publication Ltd., 1989, ISBN 0 85298 677 7

2.29 Beerers C.J., Bell K., Carlson R.L., "Fatigue Crack Closure and The Fatigue Threshold", - Fatigue Crack Growth Threshold Concepts – The Metallurgical Society of AIME, Proceedings International Symposium on Fatigue Crack Growth Threshold Concepts, Pennsylvania, October 1983.

2.30 Suresh S., Ritchie R.O. "Near-Threshold Fatigue Crack Propagation: A Perspective on the Role of Crack Closure", - Fatigue Crack Growth Threshold Concepts – The Metallurgical Society of AIME, Proceedings International Symposium on Fatigue Crack Growth Threshold Concepts, Pennsylvania, October, 1983.

2.31 Monahan CC., "Early Fatigue Crack Growth at Welds", Computational Mechanics Publications, Southampton UK and Boston USA, 1995.

2.32 Davidson D.L., "Fatigue Crack Tip Constraint and Closure as a Function of Crack Length", Small Fatigue Cracks: Mechanics, Mechanisms and Application Proceedings of the 3rd Engineering foundation International Conference, Hawaii, Dec 6-11, 1998.

2.33 Sadananda K., Vasudevant A.K., "Analysis of High Temperature Fatigue Crack Growth Behaviour", Vol. 19 Supplement No. 1 1997, International Journal of fatigue.

2.34 Radon J.C., "Corrosion Fatigue of Aluminium Alloy RR58", – The Influence of Environment on Fatigue, Institute of Mechanical Engineers Conference Publications, 1977- 4

2.35 Howard Rogers T., "Marine Corrosion", Newnes International Monographs on Corrosion Science and Technology, 1968.

3.1 Aluminium Federation Ltd., Birmingham, UK.

3.2 Encyclopædia Britannica, Vol. 1, Printed in Great Britain, 1951.

3.3 Pike D.V., "The Application of Light Aluminium Alloys to Structural Engineering", The Structural Engineer, July 1945.

3.4 "Methods for tensile testing of Metals – Non-Ferrous Metals", British Standard 18 Publication, British Standards Institution, London, UK.

3.5 "The Aluminium File – A Part Work for Engineering Designers", spring 1995, The Aluminium Rolled Products Manufactures Association, Birmingham UK.

3.6 *"Job Knowledge for Welders"*, Welding Knowhow, TWI Connect, TWI Abington Hall, Abington, Cambridge, Issue No.80, October 1996

3.7 "Aluminium and The Marine Environment", April 2002, Publication by Hydro Aluminium, Vekst, Norway.

3.8 Warren, N.F., "Metal Corrosion in Boats", 2nd Edition, 1998, Adlard Coles Nautical, ISBN 0 7136 4869 4

3.9 Hynds P., "Materials and Techniques – Advance Alloy Advantages", Speed at Sea, October 2000, Speed at Sea Publishing, Enfield, UK.

3.10 Nordhammar H., "Experience From The Construction and Operation of The Stena HSS Catamarans", The 3rd International Forum on Aluminium Ships, 27-28th May 1998, Norway. Published by Quantic Media Ltd, Kent, UK.

3.11 Deutschman A., Michels W., Wilson C., "Machine design, Theory and Practice", Macmillan Publishing Co. Inc., 1975, ISBN 0-02-979720

3.12 "The Aluminium Hand Book – Apollo Metals", Apollo Metals PLC Publication, Birmingham, UK.

3.13 "Aluminium and the Sea", Pechiney Rhenalu Handbook.

3.14 "Aluminium Debacle Shakes U.S. Shipbuilders", Ship & Boat International, July/August 2002. Publication of the Royal Institution of Naval Architects.

3.15 "Northwest Boatbuilders Experience Aluminium Problems", Pacific Maritime Magazine, March 2002, Published by R.H. Philips Company, Seattle, U.S.A.

3.16 "Structural Use of Aluminium" Part1 Code of Practice for Design, BS 8118, part 1, Table 2.2

3.17 Lloyds Register Rules and Regulations For the Classification of Special Service Craft, 1996

3.18 Published figures Supplied by Pechiney Rhenalu, Issoire, France

3.19 "Non-Ferrous Metals and Alloys", Kempe's Engineers Year-Book 1993, Edited by Sharpe C., 98th Edition, Vol. 1, Benn Business Information Services Ltd.

3.20 Kosteas D., "Aluminium: Physical Properties, Characteristics and Alloys", Lecture 1501, Training in Aluminium Applications Technologies, European Aluminium Association, 1994.

3.21 Aluminium Alloy, Part B, Chapter 8, Marine Survey Procedures Manual, August 2002, Lloyd's Register of Shipping.

3.22 Raynaud G.M., "New Aluminium Products for High Speed Light Crafts", Pechiney Rhenalu, Issoire, France.

3.23 Callan J.T., "Marine Grade Aluminium Alloys for High-Speed Craft Construction", Paper 13, IMAS 91, High Speed Marine Transport, University of New South Wales, Sydney Australia, 11-13 November 1991.

3.24 Rules for Classification of High Speed, Light Craft and Naval Surface Craft, January 2002. Det Norske Vertias, Norway.

3.25 Wood W.A., "Fracture of Metals", Fracture, The Proceedings of the 1St Tewksbury Symposium, University of Melbourne, Australia, 1963.

3.26 Verbeek R., "Waterjet Fotces and Transon Flange Design", International Symposium on Waterjet Propulsion – Latest Development, Dec 1994, London. The Royal Institution of Naval Architects.

3.27 Sampath D., Moldenhauer S., Schipper H.R., Schrijuars A.J., Haszler A., Weber G., Mechsner K., Tack L., "New Semi-Fabricated Aluminium Alloy Products for Marine Applications", The 3rd International Forum on Aluminium Ships, 27-28th May 1998, Norway. Published by Quantic Media Ltd, Kent, UK.

3.28 Ehrstrom J.C., Cottignies L. "Fatigue Resistance of High Strength Aluminium Alloy Weldments", The 3rd International Forum on Aluminium Ships, 27-28th May 1998, Norway. Published by Quantic Media Ltd, Kent, UK.

4.1 Chen Q., Kawagoishi N, , Nistani H., Goto M. & Kondo E. "Initiation and Growth Behaviour of a Small Fatigue Crack in Nickle-Base Super Alloy at Elevated Temperatures", Small fatigue Cracks: Mechanics, Mechanisms and Applications, 1999.

4.2 Sadananda K., Vasudevant A.K., "Analysis of High temperature fatigue Crack Growth Behaviour", International Journal of Fatigue, Vol. 19, Supp. No.1, 1997.

4.3 Ochi Y., Kubota M., Shibata R., "Initiation and Propagation Behaviour of Small Fatigue Cracks in HIP-Treated Aluminium Alloy: AC4CH", Small fatigue Cracks: Mechanics, Mechanisms and Applications 1999.

4.4 Svensson R., "Water-jet Propulsion of High-Speed Craft", IMAS 91 High Speed Marine Transportation, The University of New South Wales, Sydney Australia, 11-13 November 1991, The Institute of Marine Engineers.

4.5 "5383 High-Tech Products Key for The High Speed Light Craft Industry", Pechiney Rhenalu Publication, Pechiney Rhenalu Issoire France.

4.6 Ewalds H.L., Wanhill R.J.H., "Fracture Mechanics", Arnold/DUM, London/Delft, 1984

4.7 "Specification for The Delivery of Aluminium Alloy Sheets and Plates" Pechiney Rhenalu Publication, Pechiney Rhenalu Issoire France.

4.8 Brager Ø., "Alloy Development", The 3rd International Forum on Aluminium Ships, 27-28th May 1998, Norway. Published by Quantic Media Ltd, Kent, UK.

4.9 Dodd B., Bai Y., "Ductile Fracture and Ductility – With Applications to Metalworking", Academic Press Inc. Ltd., 1987, ISBN 0 12 219125 0

4.10 Woodward R., "The Rolling of Aluminium: The Process and The Product", Lecture 1301, Training in Aluminium Applications Technologies, European Aluminium Association, 1994.

4.11 FBM Babcock Marine Standard Booklet, March 2002, FBM Internal Publication.

4.12 Dahl W., Dormagen D., "Micromechanisms of Crack Initiation and Propagation", Elastic-Plastic Fracture Mechanics, Reidel, Dordrecht/ Boston/Lancaster, ASTM 4, 1985.

4.13 Mundry F., "Rationalization of Size Effects in Fracture Toughness Tests Using Local Criteria for Fracture", The Assessment of Cracked Components by Fracture Mechanics, Edited by L.H. Larsson, Mechanical Engineering Publication Ltd., 1989, ISBN 0 85298 677 7

4.14 Bik W.A.Th., "Aluminium, How to be Used in an Aluminium Construction", The 3rd International Forum on Aluminium Ships, 27-28th May 1998, Norway. Published by Quantic Media Ltd, Kent, UK.

4.15 Bruce R., Taylor D., "Underwriting High Speed Craft", International Symposium & Seminar on–The Safety of High Speed Craft, February 6 & 7 1997, London, UK. The Royal Institution of Naval Architects.

4.16 McKeown D., "Welding Checkmate", Welding & Joining, TWI Publication, October 1996

4.17 No.47 Shipbuilding and Repair Quality Standard, Rev 1 August 1999, M46A, International Association of Classification Societies.

4.18 James M.N., Paterson A.E., Sutcliffe N., "Constant and Variable Amplitude Loading of 6261 Aluminium Alloy I-beams With Welded Cover plates – Influence of Weld Quality and Stress Relief", International Journal of Fatigue Vol. 19, No.2, 1997.

4.19 James M.N., Paterson A.E., "Fatigue Performance of 6261-T6 Aluminium Alloy – Constant and Variable Amplitude Loading of Parent Plate and Weld Specimens", International Journal of Fatigue Vol. 19, No.2, 1997.

4.20 Faults in Fusion Welds in Constructional Steels, Wall Chart C 304, The Welding Institute.

4.21 Dawes M.G., "Application of Fracture Mechanics to Ductile and Brittle Fracture in Welded Structures", The Assessment of Cracked Components by Fracture Mechanics, Edited by L.H. Larsson, Mechanical Engineering Publication Ltd., 1989, ISBN 0 85298 677 7

4.22 Van Horn K.R., Editor, "Aluminium Vol. III Fabrication and Finishing", 3rd Printing, 1967, American Society for Metals.

4.23 Gittos M.F., "Welding Al-Mg-Si Alloys", The Welding Institute Research Bulletin, Vol.27, July 1986. The Welding Institute Publication, Cambridge.

4.24 Aluminium Extrusion Manual, 2nd edition March 2002, Sapa Publication

4.25 "No. 21. Weldability of metals-Aluminium alloys", TWI Connect, issue no. 80, TWI Publication, October 1996. The Welding Institute Publication, Cambridge.

4.26 "No. 42 Defects/Imperfections on Weld – Porosity", TWI Connect No.101, July/August 1999, The Welding Institute Publication, Cambridge.

4.27 Ashton R.F, Wesley R.P., Dixon C.R., "The effect of porosity on 5086-H116 aluminium alloy welds", Welding Research Supplement 95-s, March 1975.

4.28 Radaj D., "Design and Analysis of Fatigue Resistant Welded Structures", Abington Publishing, 1990. ISBN 1 85573 004 9

4.29 "No.41 Weld Defects/Imperfections in Welds – Lack of Sidewall and Inter Run Fusion", Issue 100, TWI Connect, May/June 1999, The Welding Institute Publication, Cambridge.

4.30 Maddox S.J., "Fatigue Strength of Welded Structures", Abington Publishing, 2nd edition, 1991, ISBN 1 85573 013 8.

4.31 James M.N., Lambrecht H.O., Paterson A.E., "Fatigue Strength of Welded Cover Plates on 6261 Aluminium Alloy I-beams", International Journal of fatigue, November 1993

4.32 Pope J.A., "Metal Fatigue", Chapman & Hall Ltd., 1959

4.33 Hans-Fredrik, H., "Short fatigue crack propagation at spot welds: Experiments and simulations", Small fatigue Cracks: Mechanics, Mechanisms and Applications, 1999.

4.34 Bertini L., Fontanari V., Straffelini G., "Influence of Post Weld Treatments on The Fatigue Behaviour of Al-Alloy Welded Joints", International Journal of fatigue, Vol.20, No.10 1998.

4.35 Nordmark G.E., "Peening Increases Fatigue Strength of Welded Aluminium", 1963, Metal Improvement Company Publication.

4.36 "Weldability of Dissimilar 5000 and 6000 Aluminium Alloy Combinations", Summary Report SR0007, June 2000, EWI Publication. Edison Welding Institute, USA.

4.37 "No.37 Distortion – Correction Techniques", TWI Connect, Issue no.91, Sep/Oct 1998, The Welding Institute Publication, Cambridge.

5.1 Forrest P.G., "Fatigue of Metals", Pergamon Press, 1962.

5.2 McClintock F.A., Argon A.S., "Mechanical Behaviour of Materials", Addison - Wesley Publishing Company Inc., 1966.

5.3 Timoshenko S., "Strength of Material – Part II, Advanced Theory and Problems", 3rd Edition, Van Nostrand Reinhold Company, 1958.

5.4 Iida K, Matoba M, "Fatigue Strength of Hold Frame Ends in Ship Hulls", IIW-Doc XIII-950-80, International Institute of Welding, 1980.

5.5 Matoba M, Inoue K., "Some Stress Intensity Factors For Hull Members in Relation to Fatigue Crack Propagation", IIW-Doc XIII-1081-83, International Institute of Welding, 1983.

5.6 2000 HSC Code, International Maritime Organisation, London 2001.

5.7 Faulkner D., "Welded Connections in Warships Structures", Quarterly Transactions of Royal Institution of the Naval Architects, January 1964, Vol. 106, No.1

5.8 "FPSO-Fatigue Capacity Summary Report on Stress Concentration Factors and Analyses", Technical Report No. 2000-3264, revision no.2, 29th August 2000, Det Norske Veritas.

5.9 Paetzold H., "Fatigue Strength Behaviour of Selected Details From Ship Design", Beriche 159, Publication Institute für Schiffbau, Universität Hamburg, 1985.

5.10 NF Warren, J Kecsmar, N Sims, "Waterjet Propulsion- A Shipbuilders View", RINA Waterjet Conference - Latest Developments, December 1994. Publication of The Royal Institution of Naval Architects

5.11 Violette Dr. FLM, "A Total Approach to the Fatigue Performance of Ship Structural Details", Lloyds Register, Royal Institution of Naval Architects – London Branch, 11th November 1998.

5.12 Polezhaeva H., Malinowski W., "Fatigue Strength of Aluminium Structural Details of Special Service Craft", The 6th International Conference of Fast Sea Transportation, September 2001, Fast '01, Southampton, UK

5.13 Nordmark, G.E. Mueller L.N., Kelsey R.A., "Effect of Residual Stresses on Fatigue Crack Growth Rates in Weldments of Aluminium Alloy 5456 Plate", ASTM STP 776, American Society for Testing & Materials, 1982.

5.14 Galatolo R., Lanciotti A., "Fatigue Crack Propagation in Residual Stress Fields of Welded Plates", International Journal of Fatigue, Volume 19, 1997.

5.15 Andersen M., Birk-Sørensen M., Friis Hansen P., " Probabilistic Fatigue Analysis of Shape-Optimised Slot design", Accepted for publication in Journal of Ship Production, 1995.

5.16 Birk-Sørensen M, "A Comparative Study on Fatigue Life Optimisation of The Intersection Between a Longitudinal and a Web Frame in the B&W Mark V Bulk Carrier", Technical university of Denmark, Department of Ocean Engineering, 78s, 1995.

5.17 Clark S.D., Shenoi R.A. Price W.G., Temarel P., Hudson D.A., Hawkins G.L., "Design of Aluminium Structures Subjected to High Frequency, High Cycle Loadings", University of Southampton, EPSRC/MTD Programme on High Speed Craft, TAG2, April 1999

5.18 Fyfe A, Hawkins G.L, Shenoi R.A, Price W.G, Temarel P, Read P.J.C.L, Kecsmar J., "Fatigue Performance of Welded Aluminium Tee Connections", Proceedings of Fourth International Conference on Fast Sea Transport, Fast '97, Sydney, July 1997

5.19 Nordmark G.E., "Peening Increases Fatigue Strength of Welded Aluminium", Metal Progress, November 1963.

5.20 "The Application of Controlled Shoot Peening for the Prevention of Stress Corrosion Cracking", A Technical Review, Metal Improvement Company Inc. 1991.

6.1 Van Delft D.R.V., "A Two Dimensional Analysis of The Stresses at The Vicinity of The Weldtoes of Welded Tubular Joints", Delft University of Technology, Report 6-81-8, 1981.

6.2 Neimi E, "Stress Determination for the Fatigue Analysis of Welded Components", The International Institute of Welding, Abington Publishing, Cambridge UK, 1995

6.3 Hicks J.G., "Welded Joint Design", 2nd Edition, Abington Publishing, 1997, ISBN 1 85573 337 4

6.4 Courant R., "Variational Methods for the Solution of Problems of Equilibrium and Vibrations", Bulletin of the American Math Society 1943.

6.5 Turner M.J., Clough, R.W. Martin H.C., Topp L.J., "Stiffness and Deflection of Complex Structures", Journal of Aeronautical Science, Vol. 23, 1956.

6.6 Burnett D.S., "Finite Element Analysis – From Concepts to Applications", Addison-Wesley Publishing Company, 1987, ISBN 0 20110806 2.

6.7 Cook R.D., Malkus D.S., Plesha M.E., "Concepts and Applications of Finite Element Analysis", 3rd Edition, John Wiley and Sons, 1989.

6.8 Moaveni S., "Finite Element Analysis – Theory and Application with ANSYS", Prentice-Hall Inc., 1999, ISBN 0 13 785098 0

6.9 Woodford C.H., "The Availability of Finite Element Software for Use With Thin-Walled Structures" - Finite Element Analysis of Thin-Walled Structures, Editor J. Bull, Elsevier Applied Science, 1988, ISBN 1 85166 136 0.

6.10 Zienkiewicz O.C., Taylor R.L., "The Finite Element Method", Vol. 1: The Basis, 5th Edition, Butterworth Heinemann, 2000, ISBN 0 7506 5049 4

6.11 Irons B.M., "Numerical Integration Applied to Finite Element Methods", Conference on the Use of Digital Computers in Structural Engineering, University of Newcastle, 1966.

6.12 Bazeley G.P., Cheung Y.K., Irons B.M., Zienkiewicz O.C., "Triangular Elements in Plate Bending, Conforming and Nonconforming Solutions", Proceedings 1st Conference on Matrix Methods in Structural Mechanics, AFFDLTR-CC, Wright-Patterson AF Base, Ohio, USA, 1966.

6.13 Irons B.M., Razzaque A., "Experience with the Patch Test for Convergence of Finite Element Method", Mathematical Foundations of The Finite Element Method, Academic Press, 1972

6.14 NAFEMS, National Agency for Finite Element Methods and Standards, "Guidelines to Finite Element Practice", Crown Copyright, 1984, ISBN 0 903640 16 3, National Engineering Laboratory, East Kilbride, Glasgow.

6.15 COSMOS/M User Guide, version 2.6, Structural Research and Analysis Corporation, Los Angeles, California, USA.

6.16 Timoshenko S., Woinowsky-Krieger S., "Theory of plates and Shells", 2nd Edition, McGraw-Hill International Editions, Engineering Mechanics Series, 1989, ISBN 0 07 Y85820 9

6.17 Ural O., "Finite Element Method", Intext Educational Publishers, 1973.

6.18 Holland I., "Finite Element Method in Plane Stress Analysis" - Finite Element Methods in Stress Analysis, Editor I. Holland, K. Bell, Tapir Forlag, 3rd Edition. 1972.

6.19 Zienkiewicz O.C., Taylor R.L., "The Finite Element Method", Vol.2: Solid Mechanics, 5th Edition, Butterworth Heinemann, 2000, ISBN 0 7506 5055 9

6.20 Norrie D.H., G DeVries., "An Introduction to Finite Element Analysis" Academic Press, 1978, ISBN 0 12 521660 2

6.21 Moe J., "The Finite Element Technique – A New Tool in Structural Analysis" - 'Finite Element Methods in Stress Analysis', Editor Holland I., Bell K., Tapir Forlag, 3rd Edition. 1972.

6.22 Iverson P.A., "Some Aspects of the Finite Element Method in Two-Dimensional Problems" - Finite Element Methods in Stress Analysis', Editor, Holland I., Bell K., Tapir Forlag, 3rd Edition. 1972.

6.23 Grandin Jr H., "Fundamentals of The Finite Element Method", Macmillan Publishing Company, 1986, ISBN 0 02 345480 6

6.24 Rockey K.C., Evans H.R., Griffiths D.W., Nethercot D.A., "The Finite Element Method – A Basic Introduction", Crosby Lockwood Staples, 1975, ISBN 0 258 96821 4

6.25 "Dectecting and Avoiding Numerical Difficulties", E. Akin, 'Finite Element Analysis of Thin-Walled Structures', Editor J. Bull, Elsevier Applied Science, 1988, ISBN 1 85166 136 0.

6.26 Stenseng A., "Cracks and Structural Redundancy", The Society of Naval Architects and Marine Engineers, Marine Technology, Vol.33, No.4, Oct 1996.

6.27 Andrews D., "Finite Element Analysis and the Design of Thin-Walled Ship Structures" - Finite Element Analysis of Thin-Walled Structures', Editor J. Bull, Elsevier Applied Science, 1988, ISBN 1 85166 136 0.

6.28 Røren E.M.Q., "Finite Element Analysis of Ship Structures" - Finite Element Methods in Stress Analysis', Editor Holland I., Bell K., Tapir Forlag, 3rd Edition, 1972.

6.29 Iversen P.A., "Some Aspects of the Finite Element Method in Two-Dimensional Problems" - Finite Element Methods in Stress Analysis, Editor: Holland I., Bell K., Tapir Forlag, 3rd Edition, 1972.

6.30 Brebbia C.A., Conner J.J., "Fundamentals of Finite Element Techniques for Structural Engineers", Butterworth Co. (Publishers), 1973.

7.1 Cruise Ferry Information. No 9, 1991, Ship Pax Information, Sweden.

7.2 Svensson R., "Experience with Waterjet Propulsion in the Power range up to 10,000 kW", Society of Naval Architects and Marine Engineers Power Boat Symposium, Feb 1985, Florida.

7.3 Welford S., "A Capable Fishers Protection Vessel", Ship & Boat International, Sept 1992, p 27, Royal Institution of Naval Architects Publication.

7.4 "Design of Inlet Duct", KaMeWa Guideline Notes, KaMeWa, Sweden.

7.5 "Strength Analysis of Hull Structures in High Speed and Light Craft", Classification Notes, No.30.8, August 1996, Det Norske Veritas, Norway.

7.6 Allday W.J., "Methods of Avoiding Common Problems With Aluminium Structure", Vol.1, FAST '91. Proceedings 1st International Conference on Fast Sea Transportation, Trondheim, Norway, June 1991,

7.7 Youn J.G., Kim H.S., Park D.H. "Effect of Joint Details on The Fatigue Properties of a Slot Structure", International Institute of Welding Document, XIII-1671-97, Presented July 1997, San Francisco, USA.

7.8 Speck J.B., "Fracture Assessments Established in The Integrity of FSPO Mooring Chain Stoppers", The Naval Architect, October 2002.

7.9 Warren N.F., Kecsmar J., Sims N., "Waterjet Propulsion-A Shipbuilders View", paper 4, Royal Institution of Naval Architects International Symposium on Waterjet Propulsion, Latest Developments, 1&2 December 1994 London,

7.10 Kecsmar J., "FEA Analysis of Jet Duct/Transom Plating", FBM Marine Internal Report, 1996.

7.11 "European Recommendations For Aluminium Alloy Structures – Fatigue Design", No.68, First Edition, 1992, European Convention of Constructional Steelwork, Brussels, Belgium.

10. List of Figures

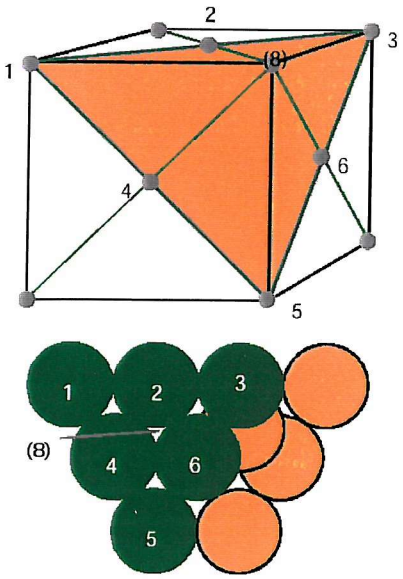

fig.2.1

The FCC Cubic system of Copper

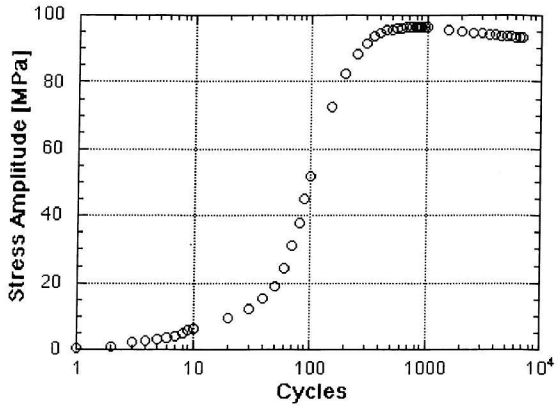

fig.2.2

Hardening of Copper subjected to Cyclic Loading

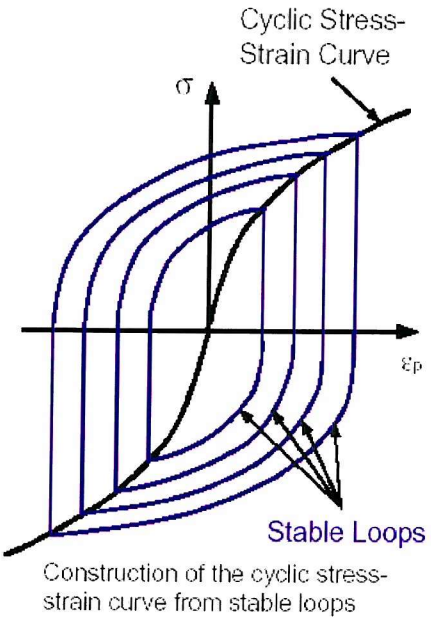

fig.2.3

Definition of a Cyclic Stress-Strain Curve

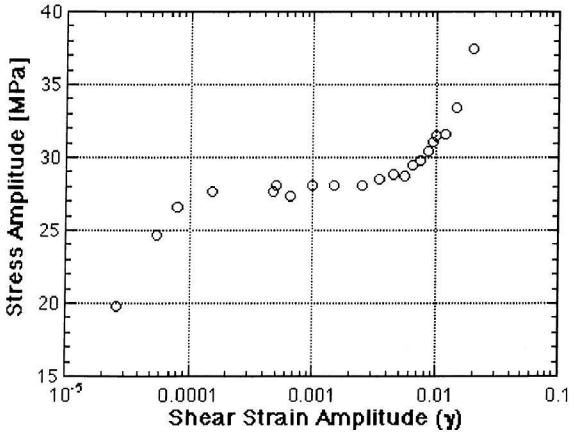

fig.2.4

CSSC for Copper

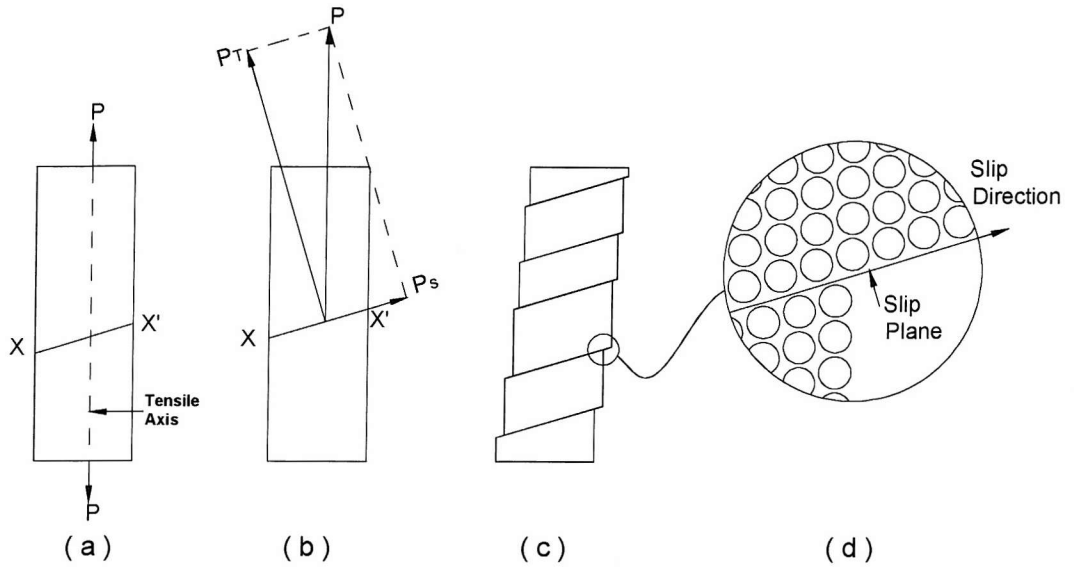

fig.2.5

Formation of a Slip Plane

fig.2.6

Slip Planes on the Surface of a Specimen

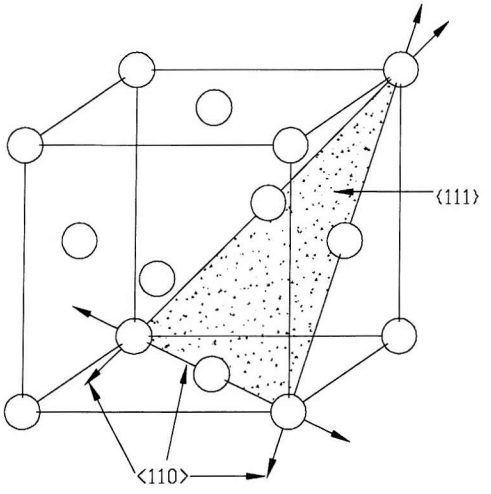

fig.2.7

One of the 4 {111} Slip Planes with its 3 <110> Slip Directions in an FCC Structure

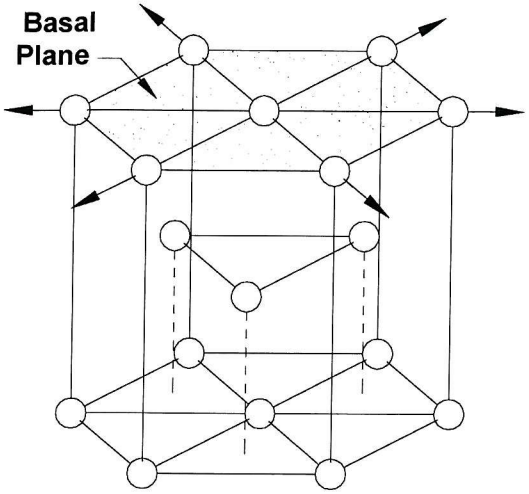

fig.2.8

The Single Slip Plane (Basel Plane) in the CHP Structure With its 3 Slip Directions

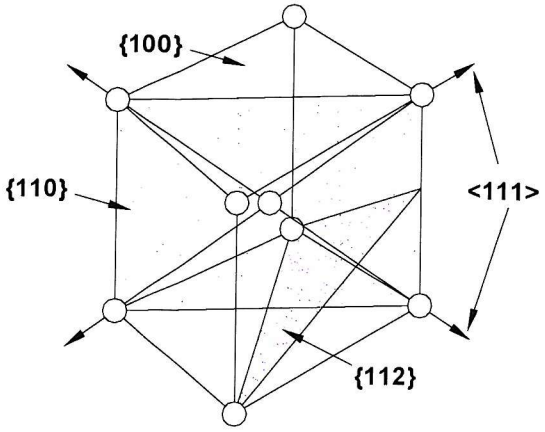

fig.2.9

The 3 Planes of High Packing Density {100},{110},{112} In the BCC Structure, with 2 Slip Directions <111>

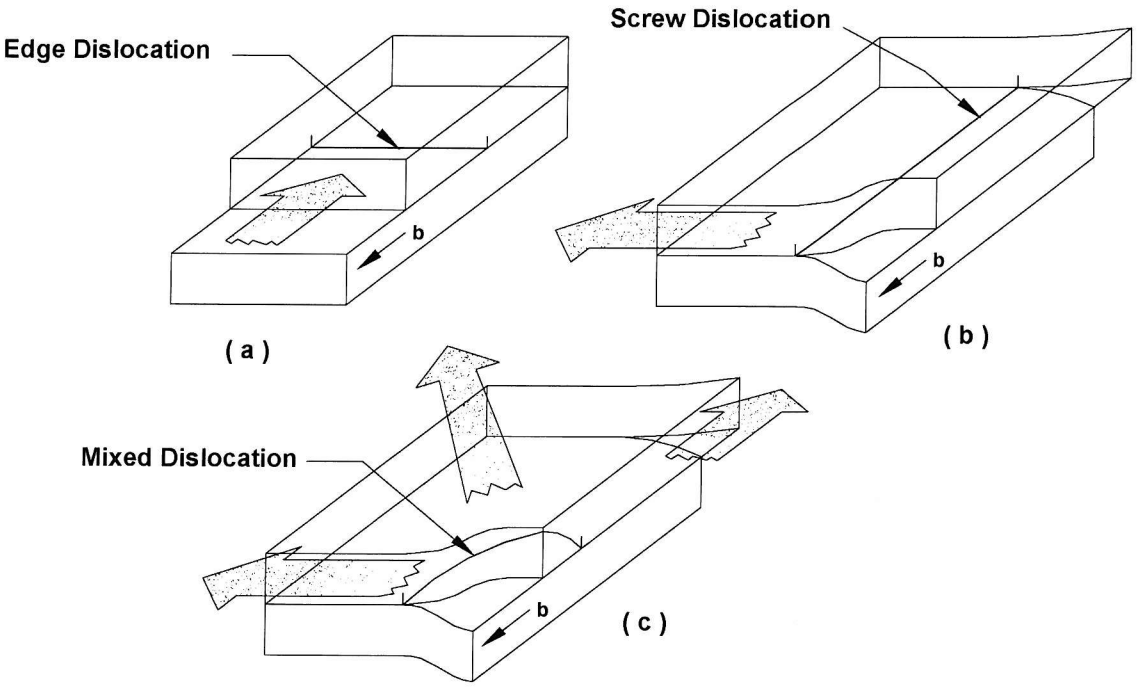

fig.2.10

The motion of (a) Edge Dislocation; (b) Screw Dislocation (c) Mixture of Screw and Edge Dislocation

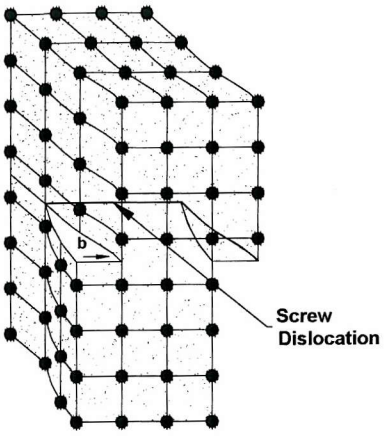

fig.2.11

Screw Dislocation

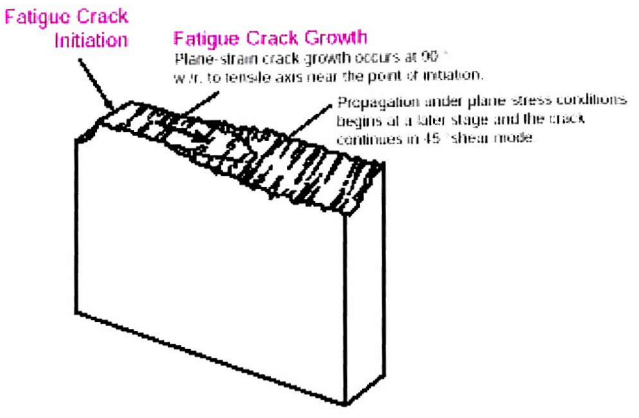

fig.2.12

Schematic of a Fatigue Fracture Surface

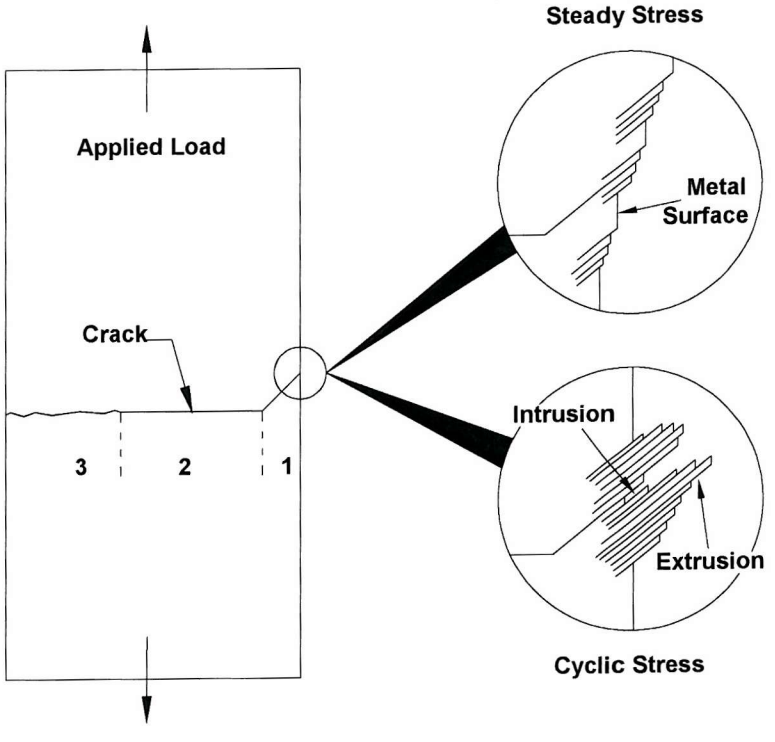

fig.2.13

The 3 Stages of fatigue Failure

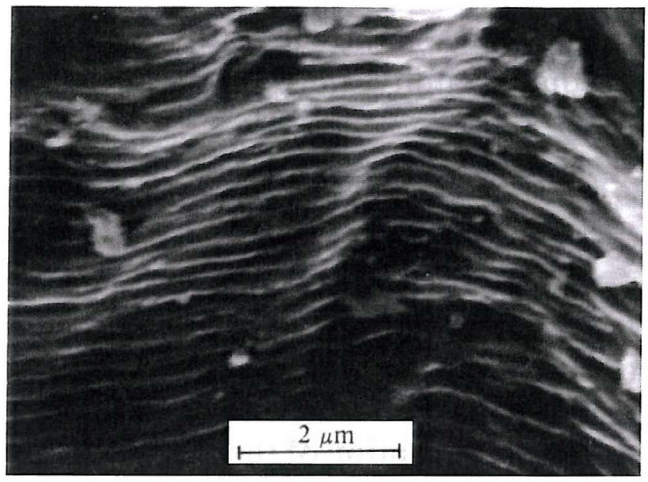

fig. 2.14

Fatigue Striations in Stainless Steel

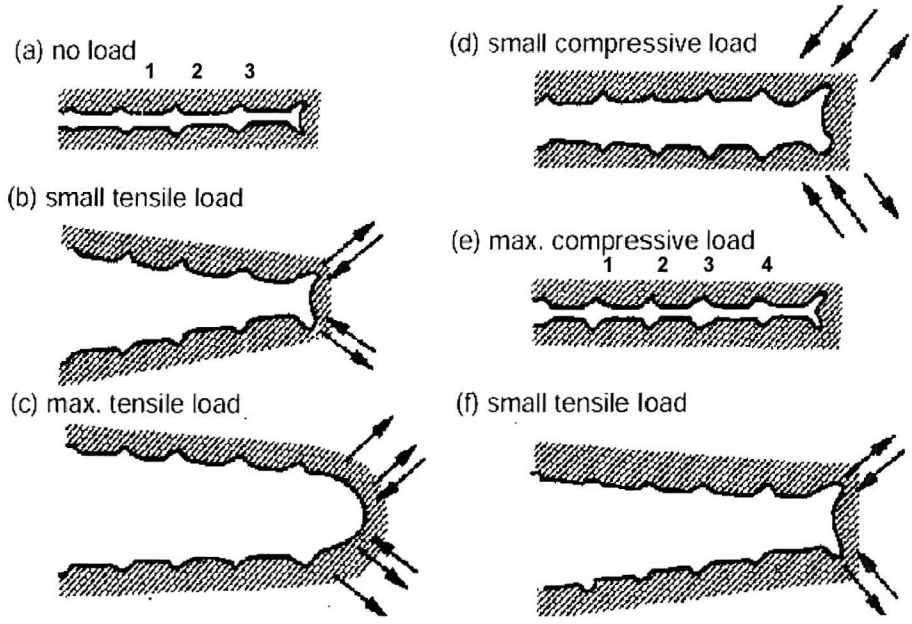

fig.2.15

Formation of a Fatigue Striation During One Cycle

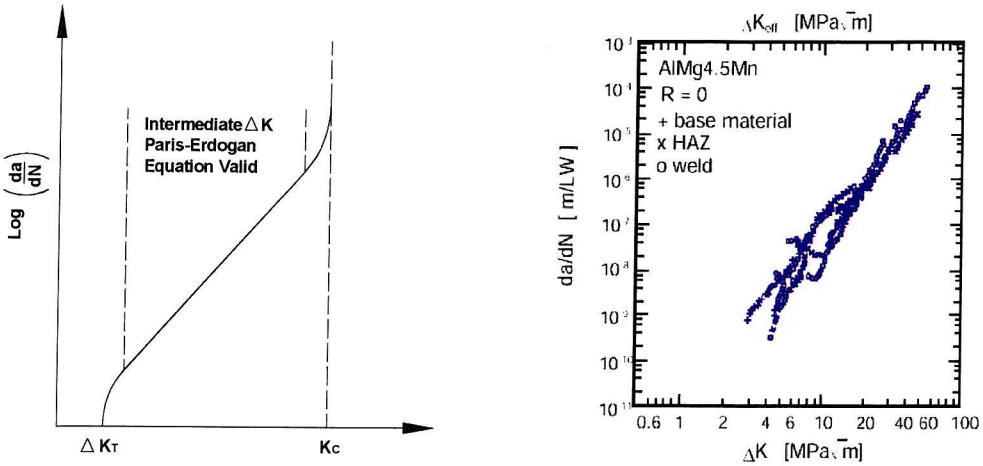

fig.2.16

Theoretical and Experimental Crack Growth Rate of Aluminium

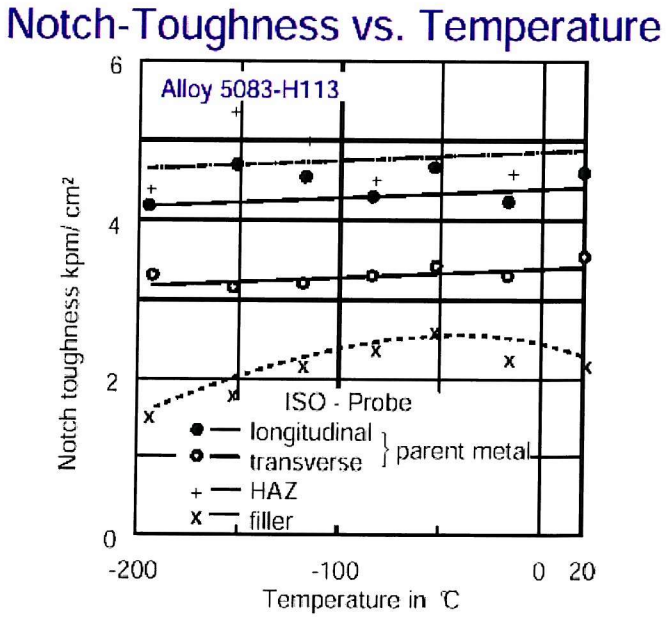

fig.2.17

Notch Toughness of Aluminium

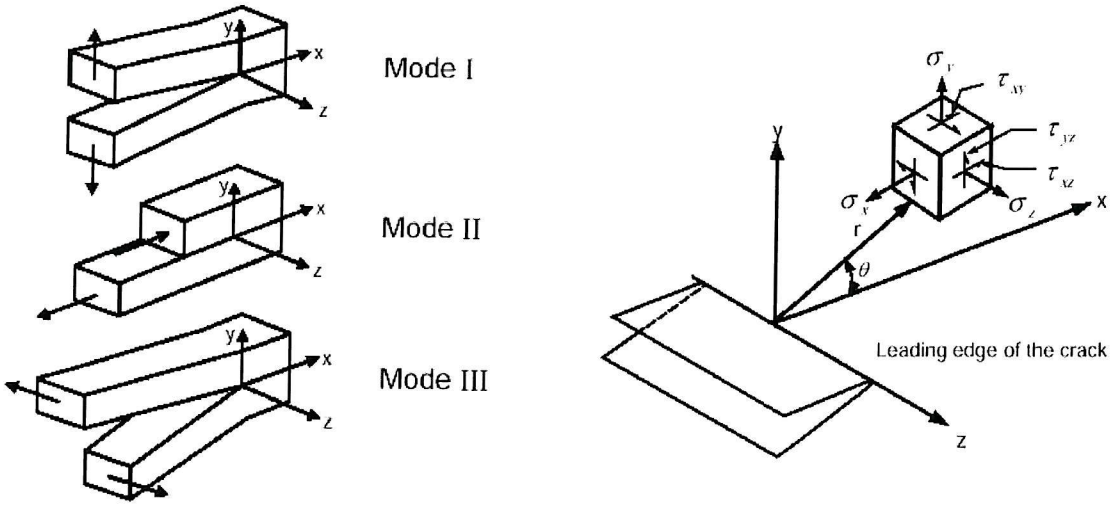

fig.2.18

The 3 Modes of Crack Displacement & Coordinate System

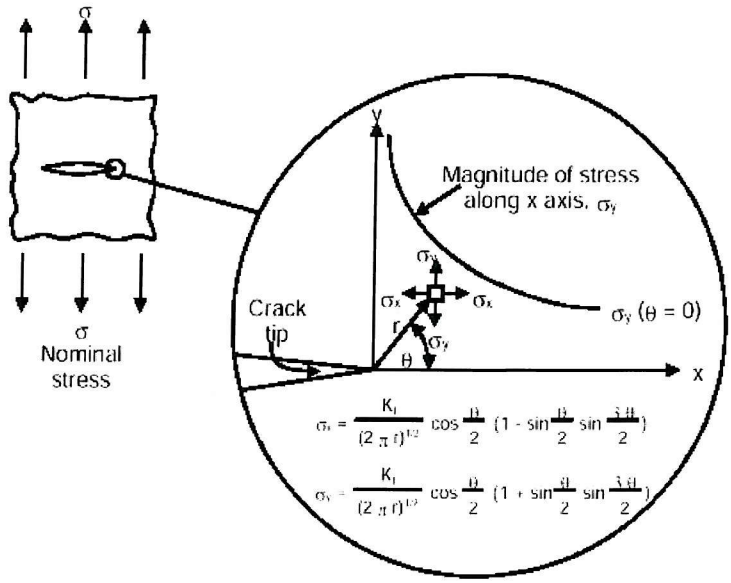

fig.2.19

Elastic Stress Field Distribution Near a Crack

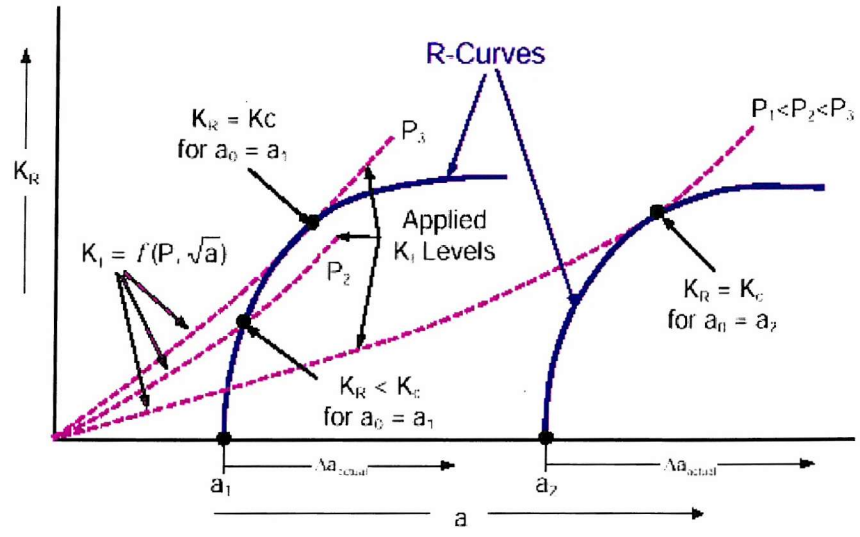

fig.2.20

Typical R Curves

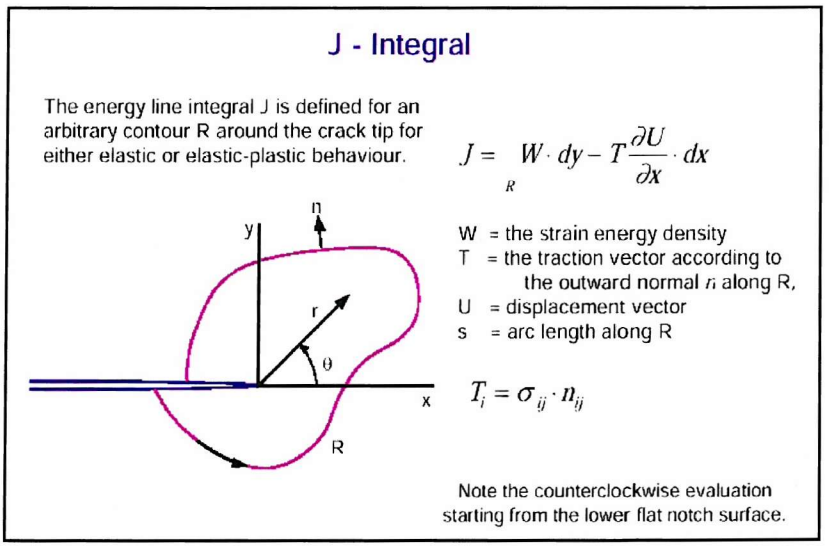

fig.2.21

J-Integral Coordinate System

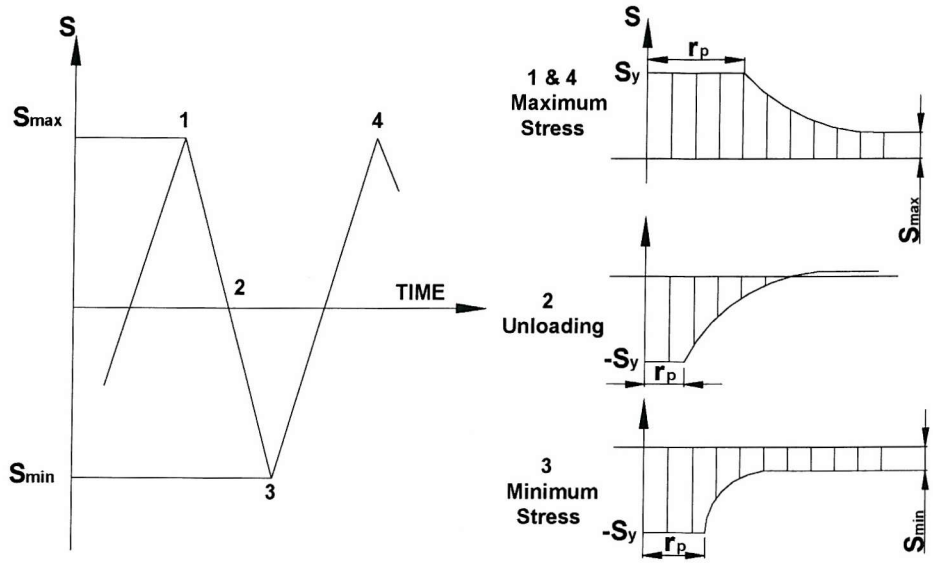

fig.2.22

Elastic-Plastic Stresses at a Crack Tip

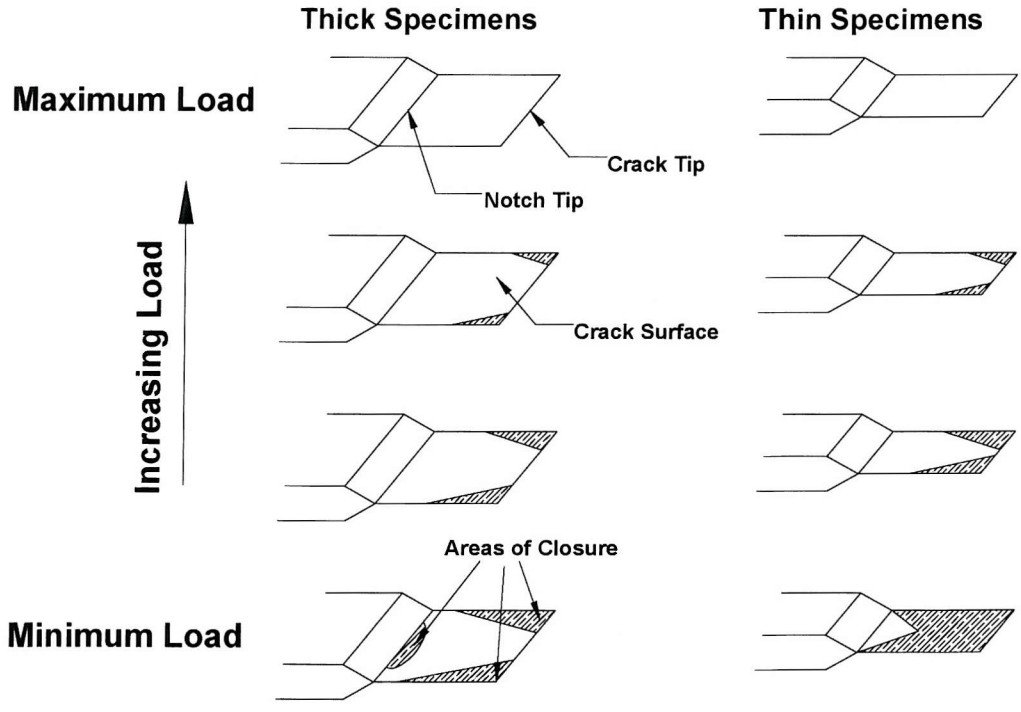

fig.2.23

Crack Closure Behaviour

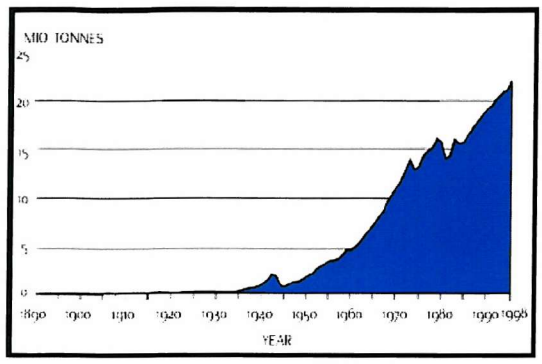

fig.3.1

World Annual Aluminium Production

fig.3.2

Typical Aluminium High Speed Ferry

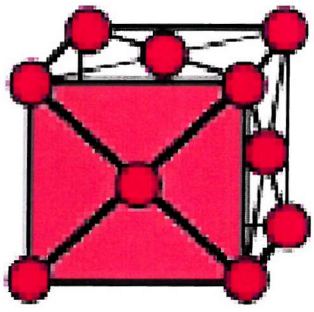

fig.3.3

FCC Atomic structure of Aluminium

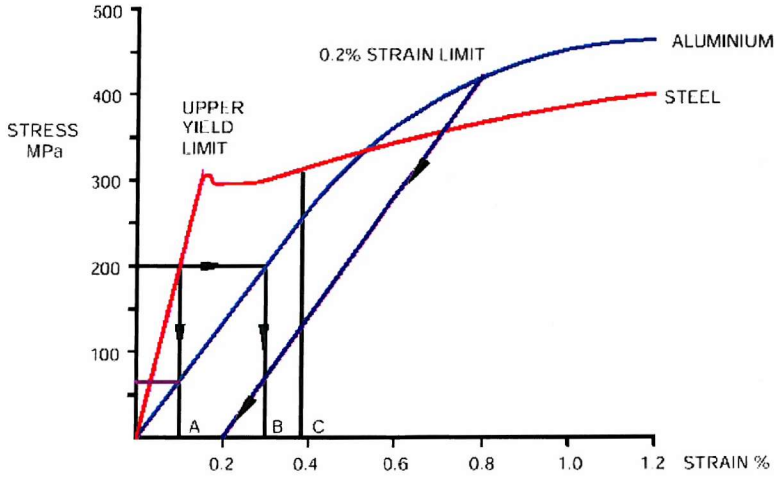

fig.3.4

Stress-Strain Curve of Aluminium & Steel

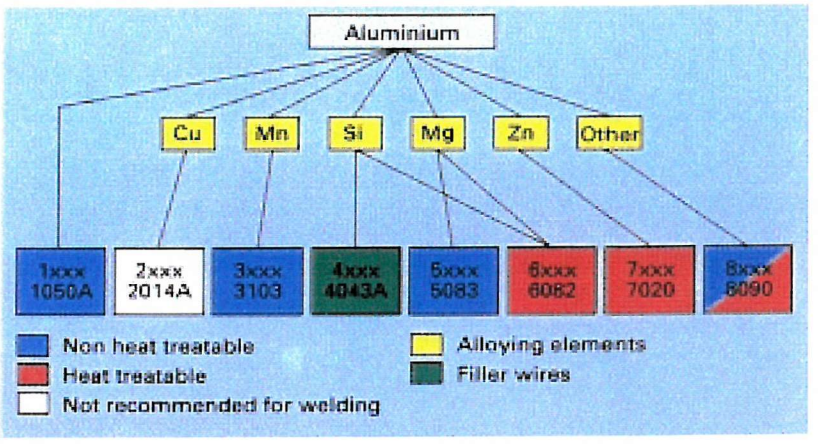

fig.3.5

Aluminium and Its Alloys

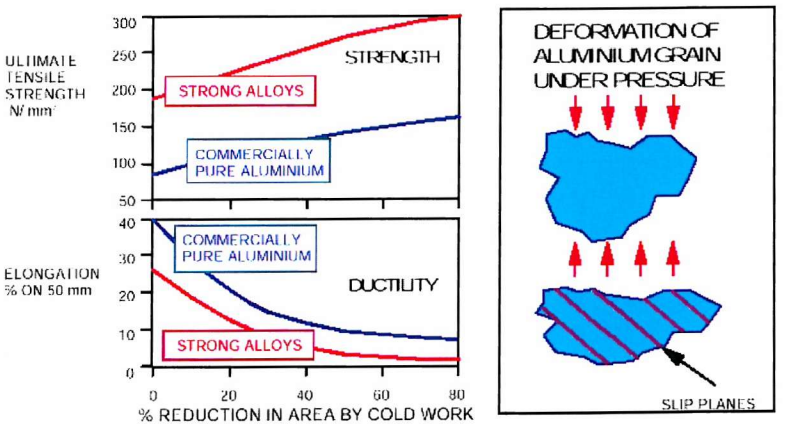

fig.3.6

Strain Hardening Using Slip Planes

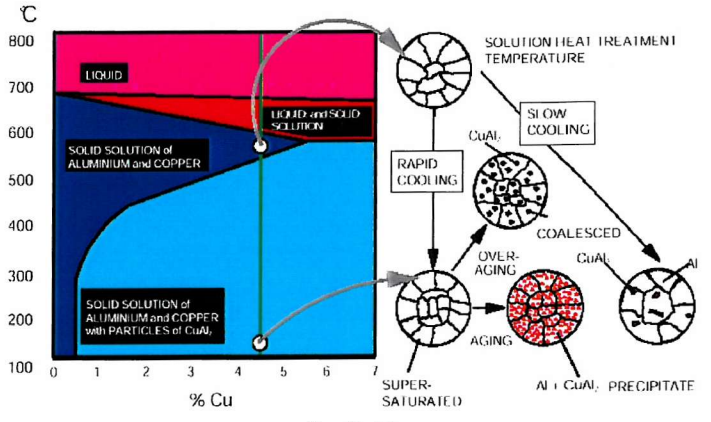

fig.3.7

Solution or Heat Treatment Process of 6000 Aluminium

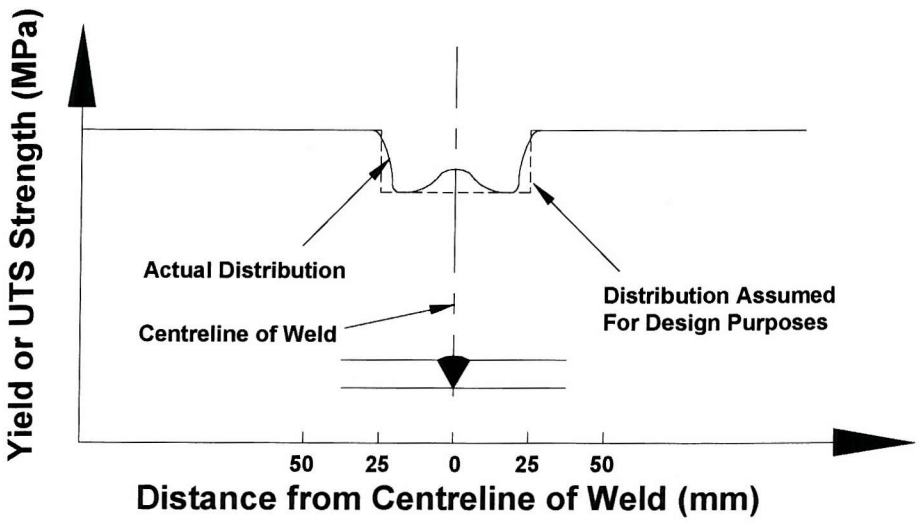

fig.3.8

Distribution of Mechanical Properties in the Vicinity

Of an Aluminium Alloy Weld

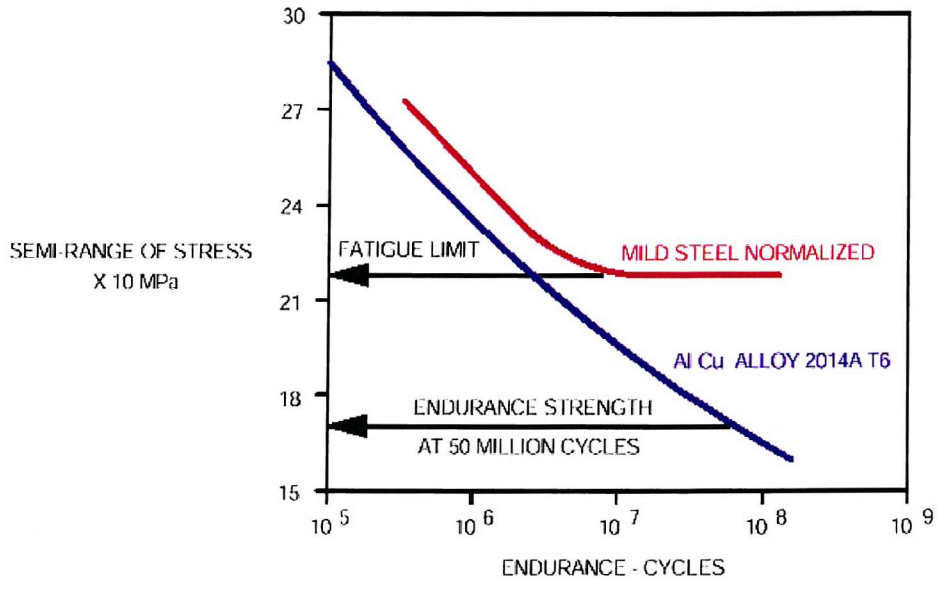

fig.3.9

Typical S-N Curve of Aluminium & Steel

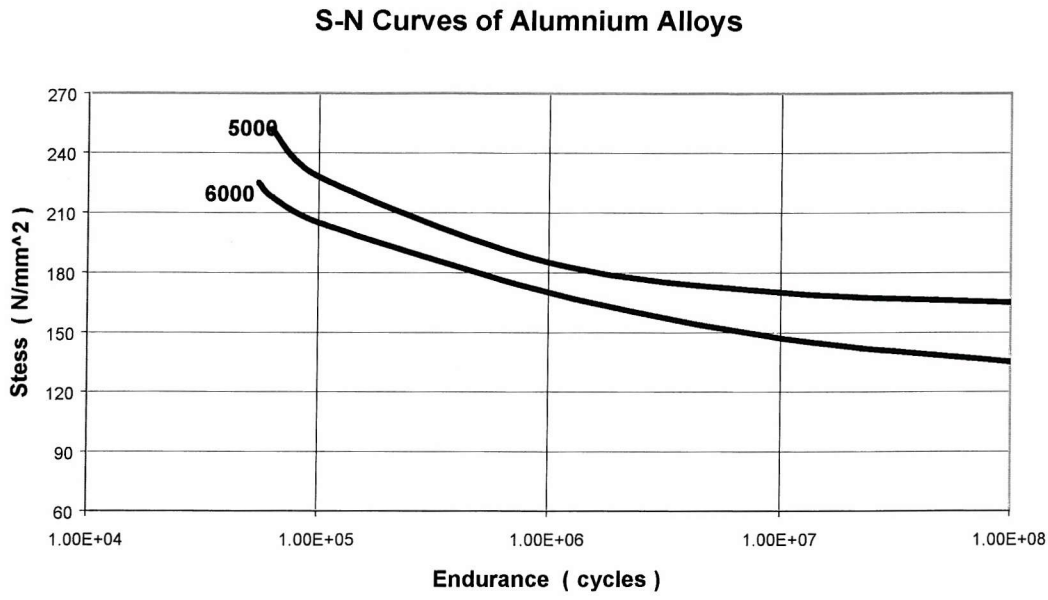

fig.3.10

S-N Curves of 5000 and 6000 Series Alloy

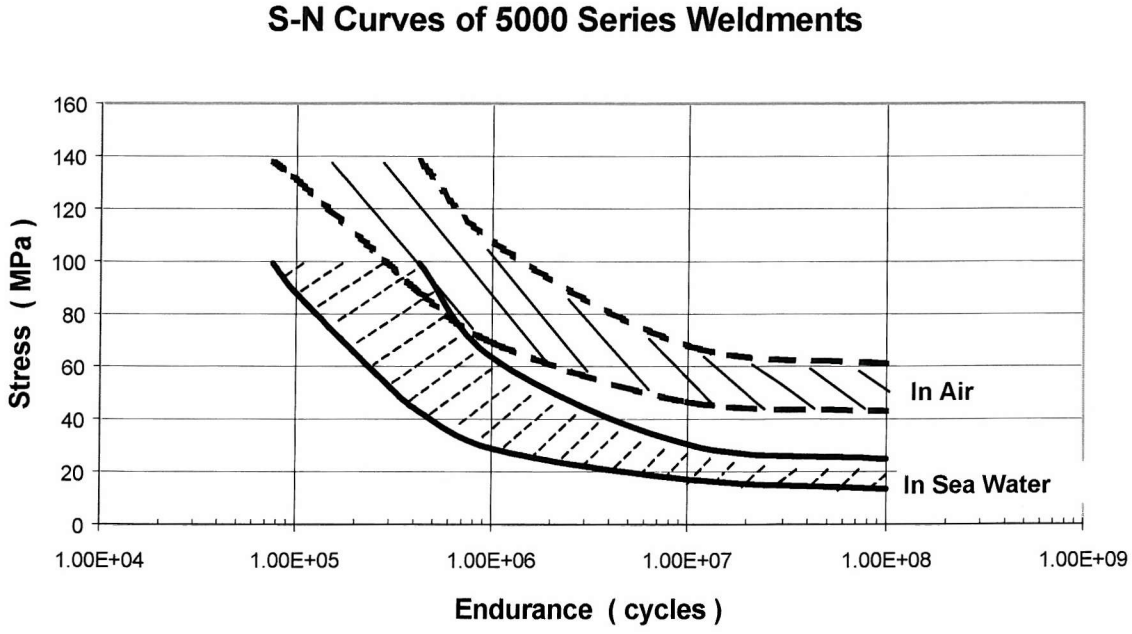

fig.3.11

S-N Curves of Welded and Unwelded Aluminium

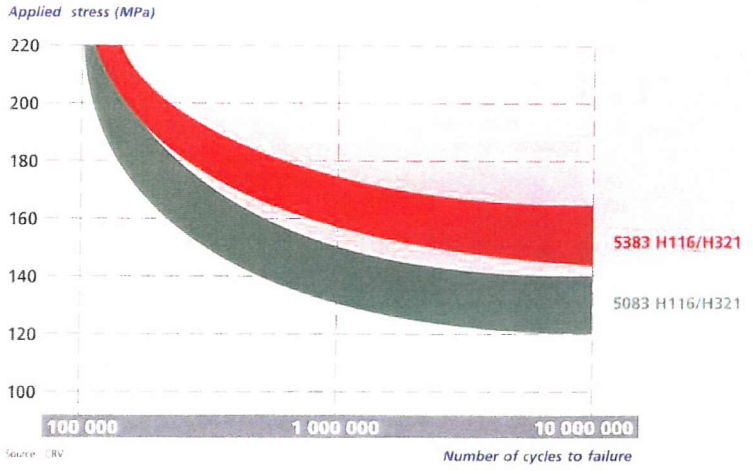

fig.3.12

Improved fatigue characteristics of 5383 Compared to 5083

fig.4.1

Fatigue Crack in Plate

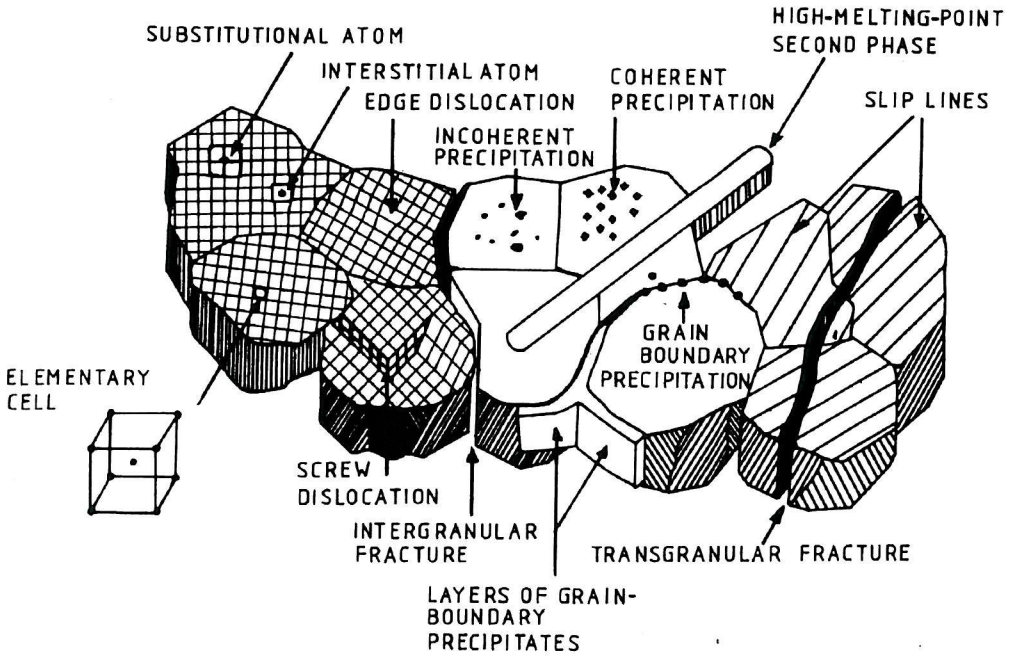

fig.4.2

Microstructural Features in Metallic Structures

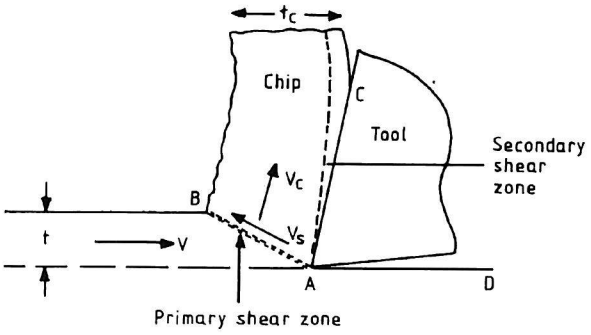

fig.4.3

Orthogonal Cutting Diagram

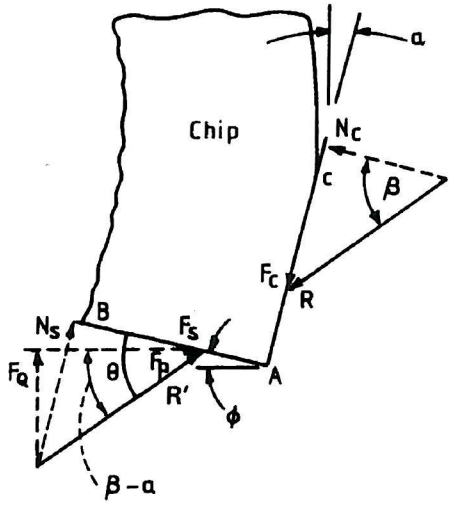

fig.4.4

Free-Body Diagram of Cutting Operation

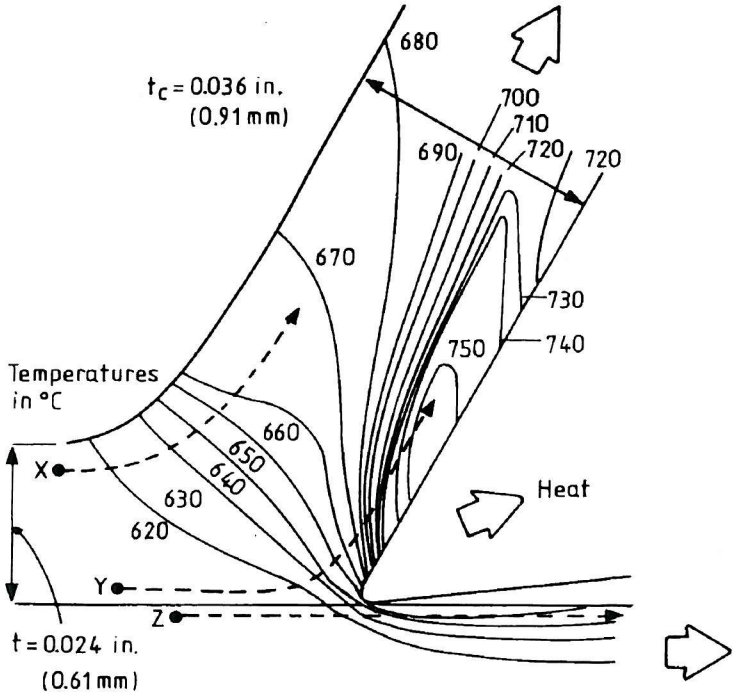

fig.4.5

Temperature Distribution in Chip and Work Piece

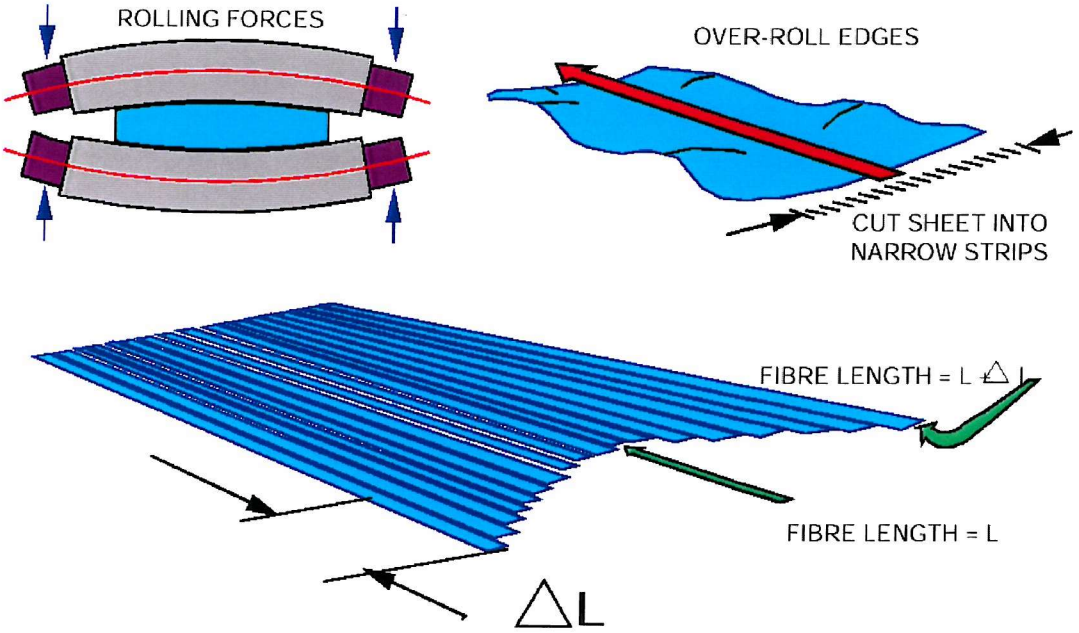

fig.4.6

How The Rolling Process Creates Lines

fig.4.7

Cracked Spacer Bracket

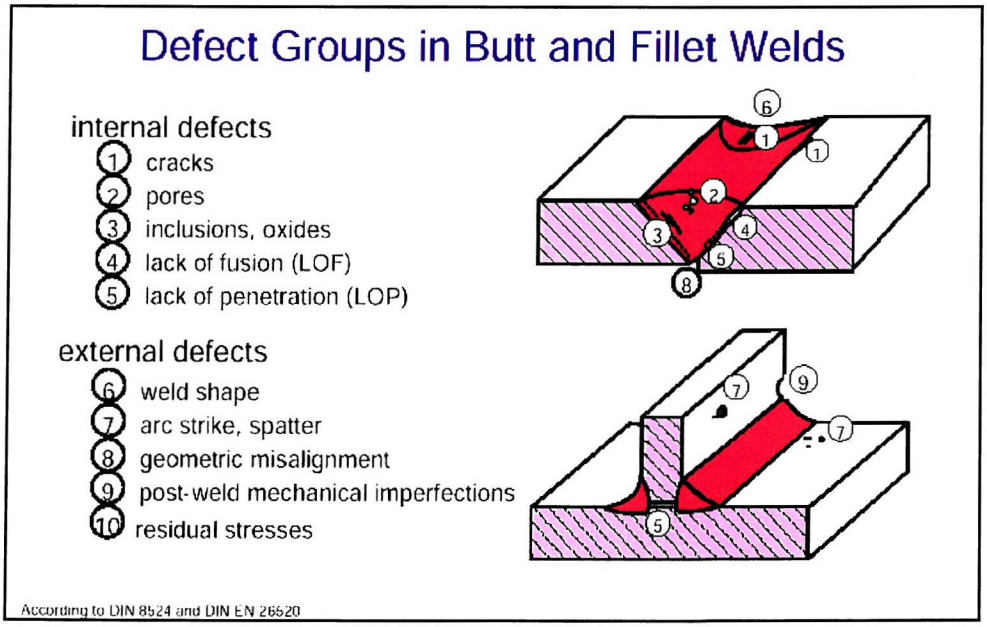

fig.4.8

Typical Weld Imperfections

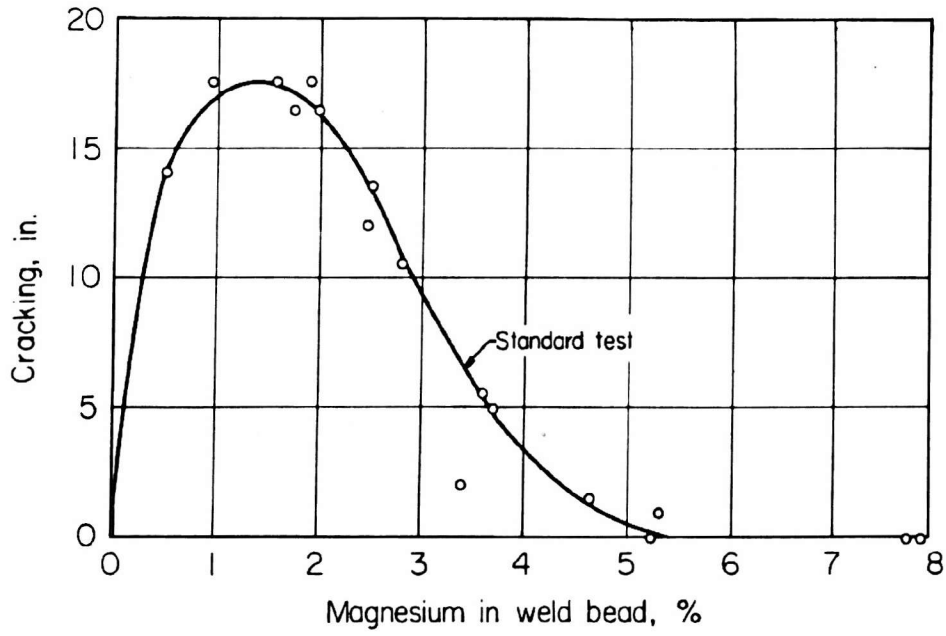

fig.4.9

Effect of magnesium Content on Weld Cracking

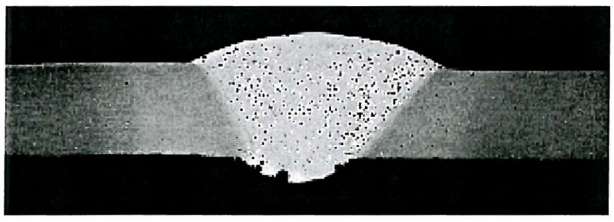

fig.4.10

Typical Weld Porosity

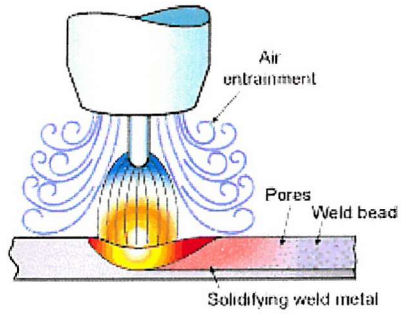

fig.4.11

Anatomy of MIG Welding

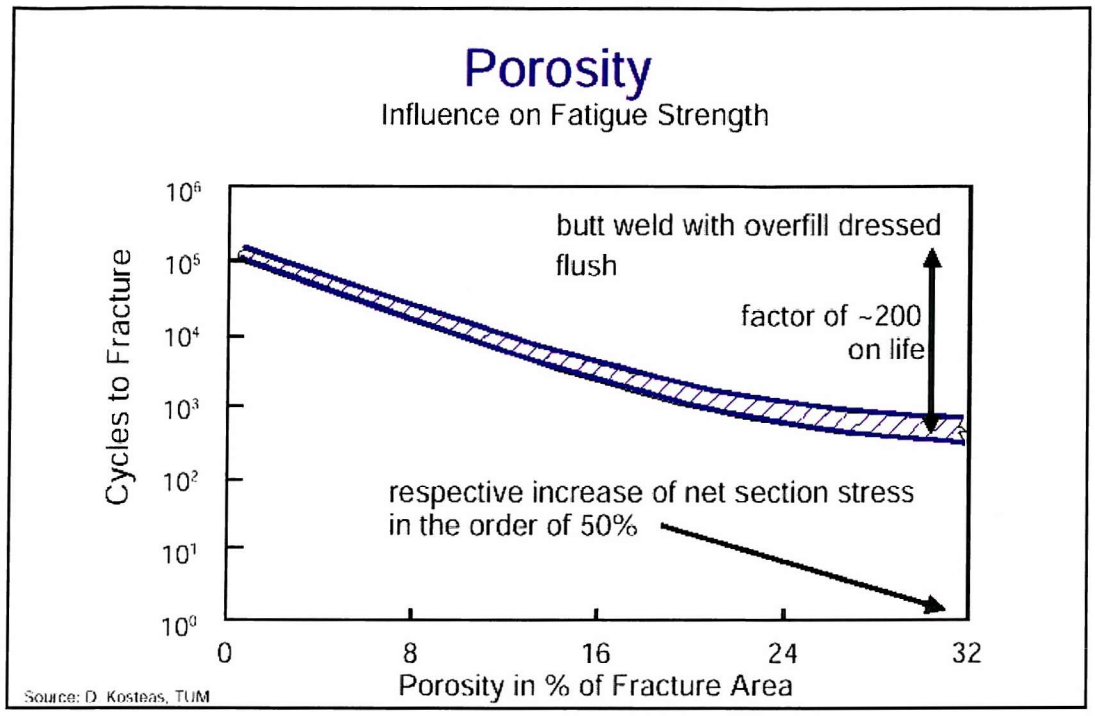

fig.4.12

Effects of Porosity in Welds

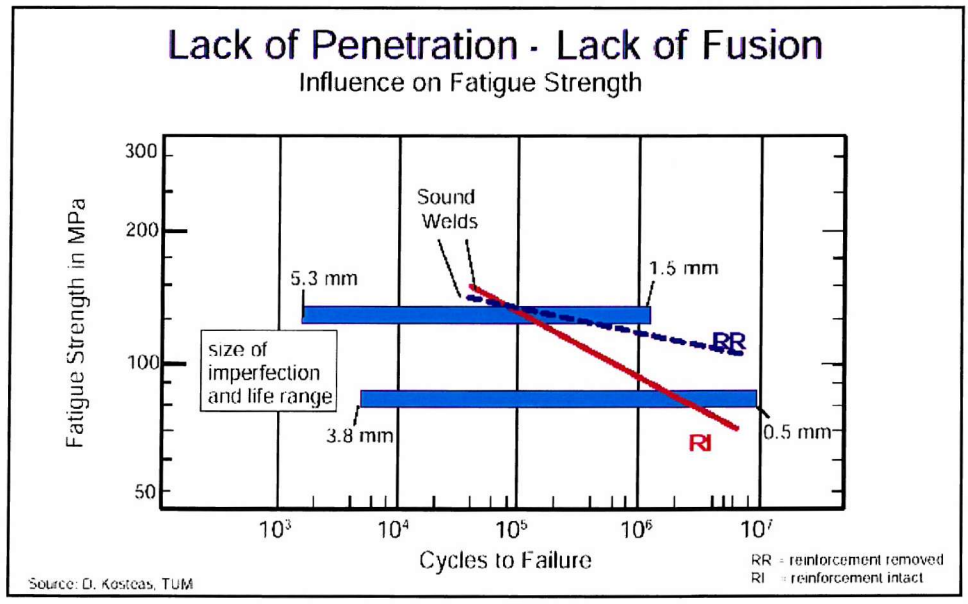

fig.4.13

Effects on fatigue Strength Caused by LOP

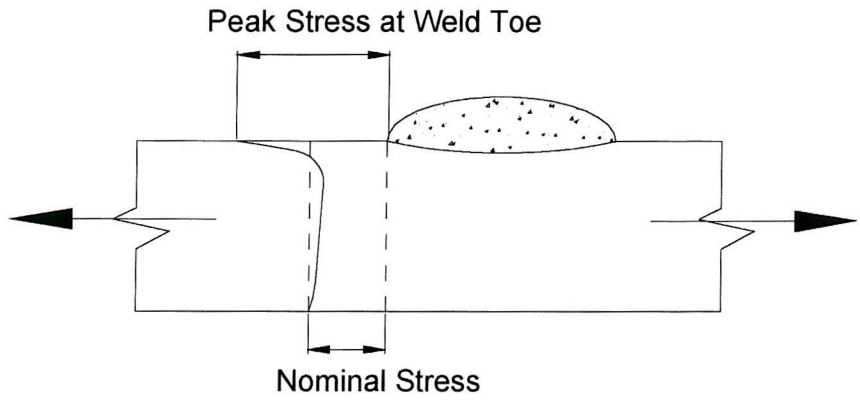

fig.4.14

Stress Concentration at Weld Toe

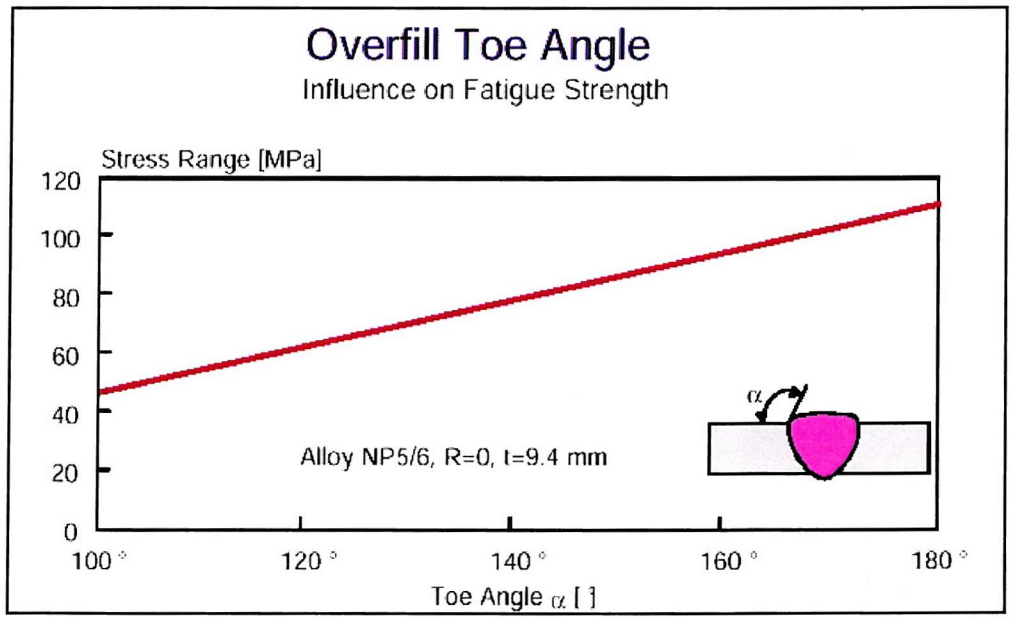

fig.4.15

Effects of Weld Size & Shape on Fatigue

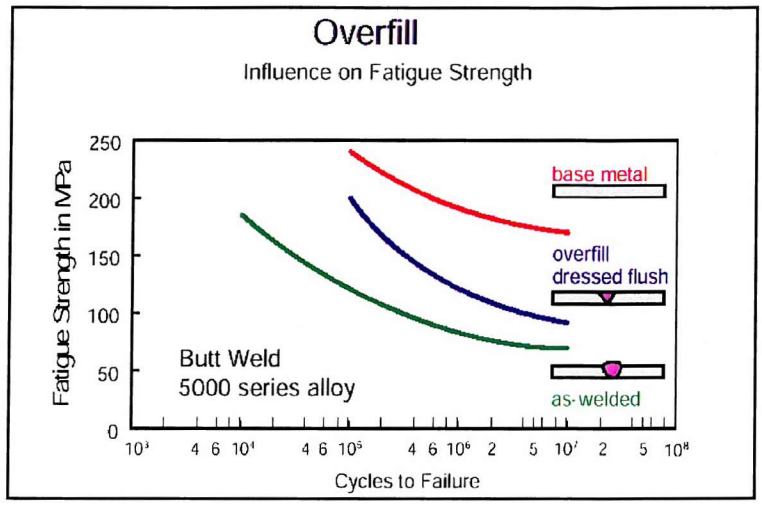

fig.4.16

Effects of Weld Dressing on Fatigue

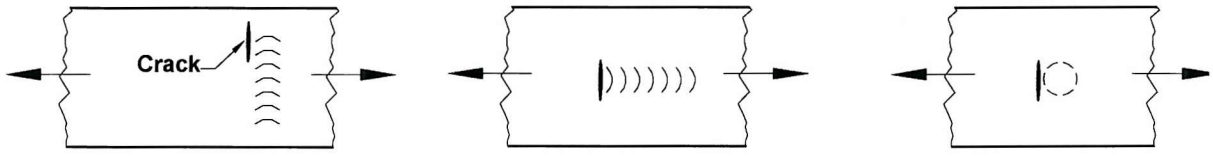

fig.4.17

Arc Strikes & Splatter

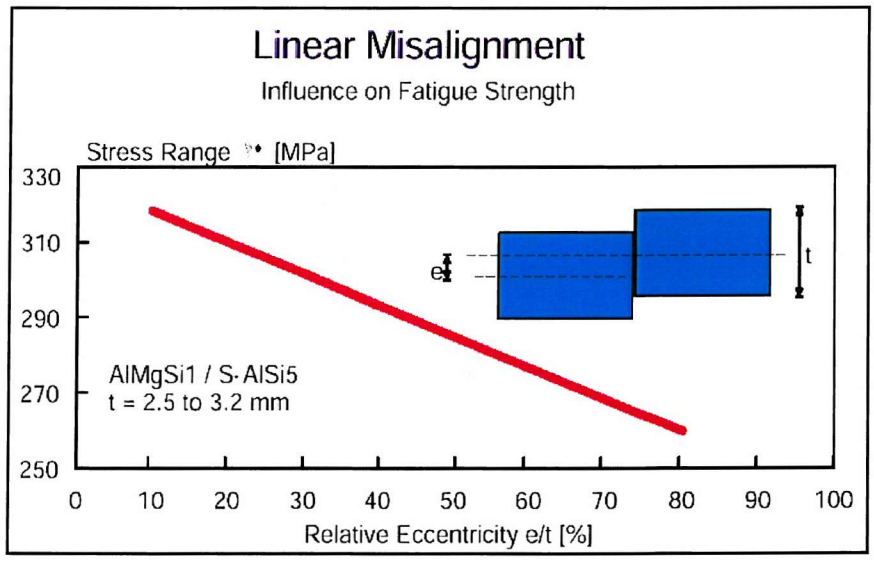

fig.4.18

Linear Misalignment of Plates

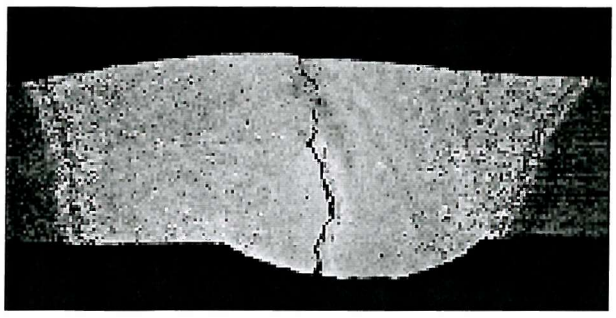

Fig.4.19
Solidification Cracking

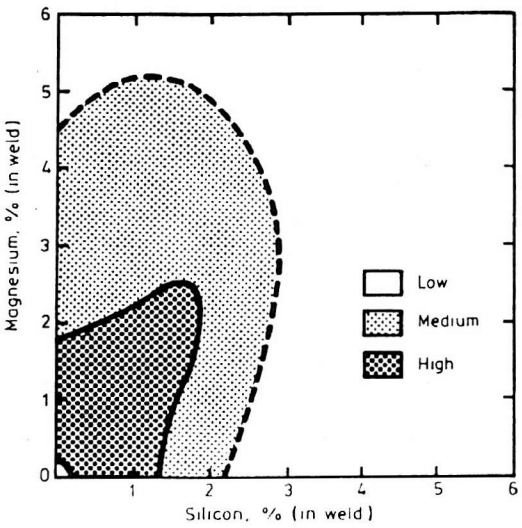

fig.4.20
Susceptibility to Cracking in The Al-Mg-Si Alloys

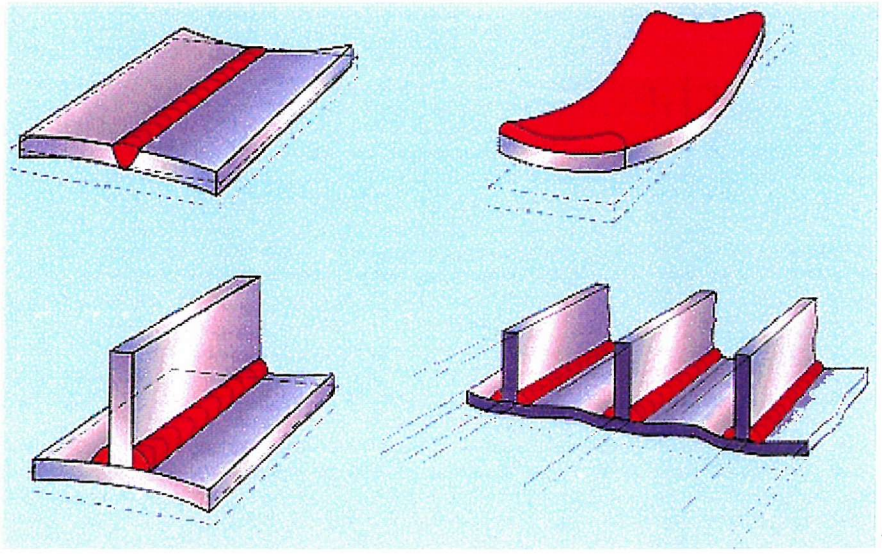

fig.4.21
Typical Modes of Distortion

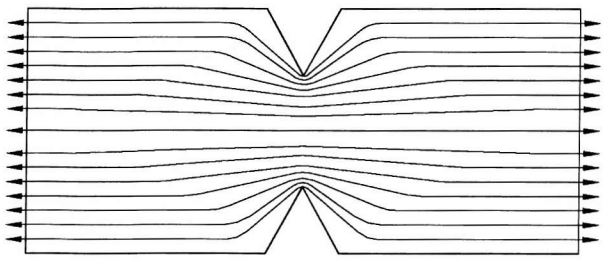

fig.5.1

Tensile Stress Flow lines

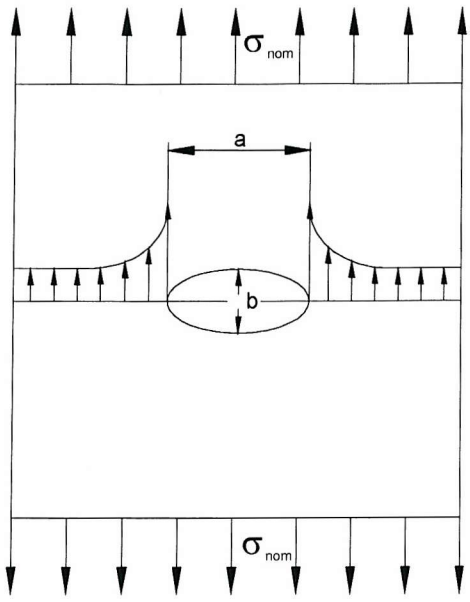

fig.5.2

Elliptical hole in Tension

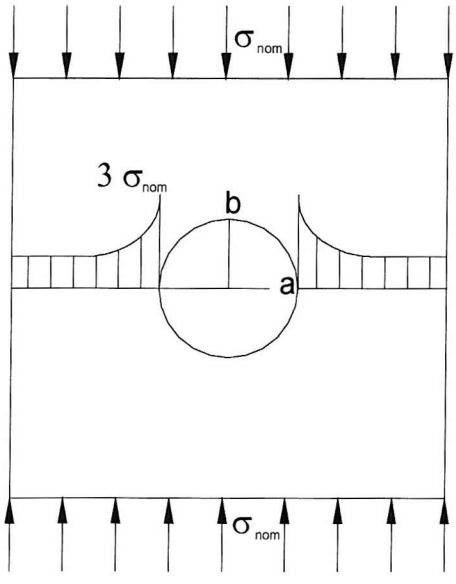

fig.5.3

Circular Hole in Compression

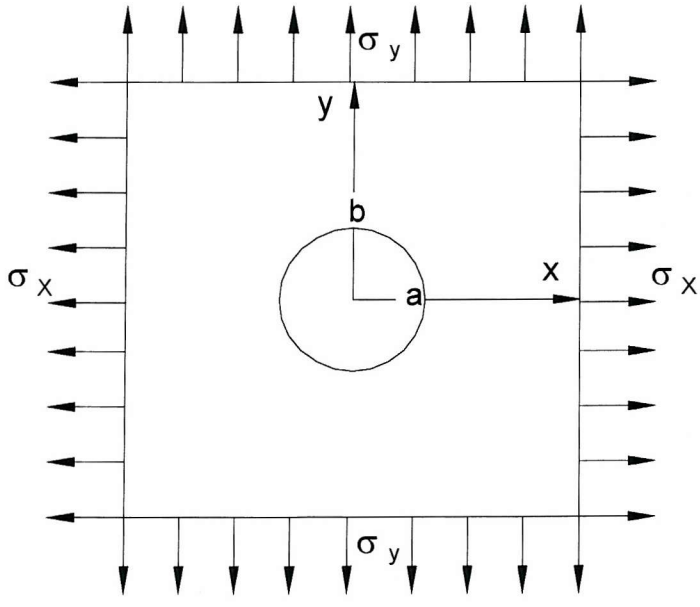

fig.5.4

Combined Tension & Compression

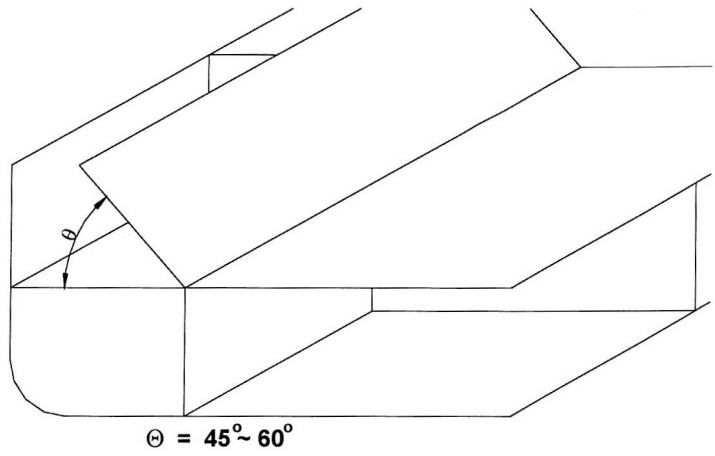

fig.5.5

Double Bottom Bilge Corner Joint

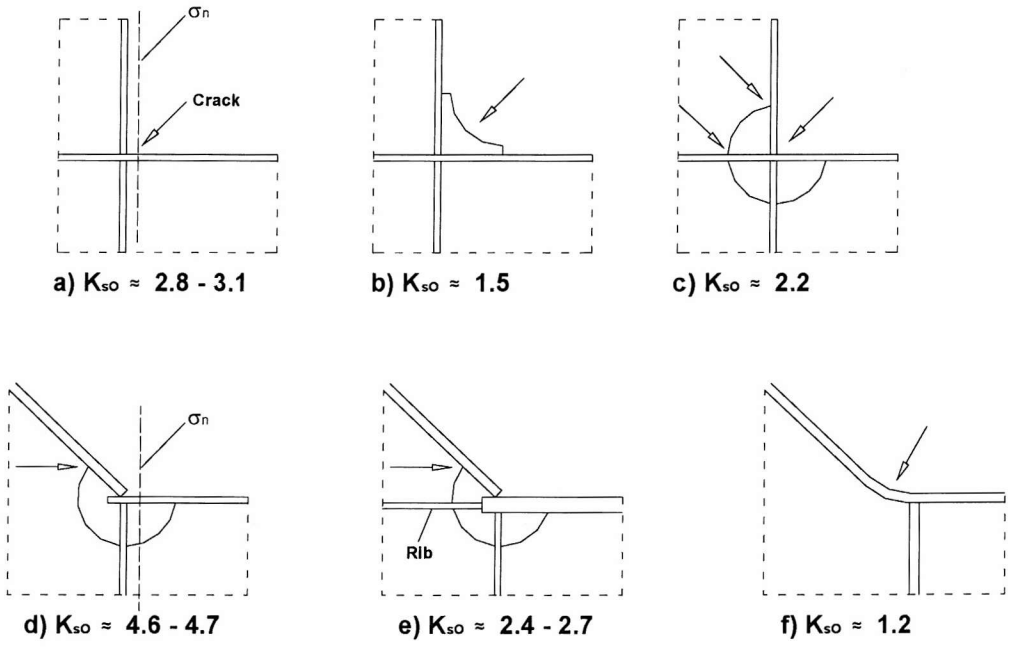

fig.5.6

Typical Double Bottom Corner Joints

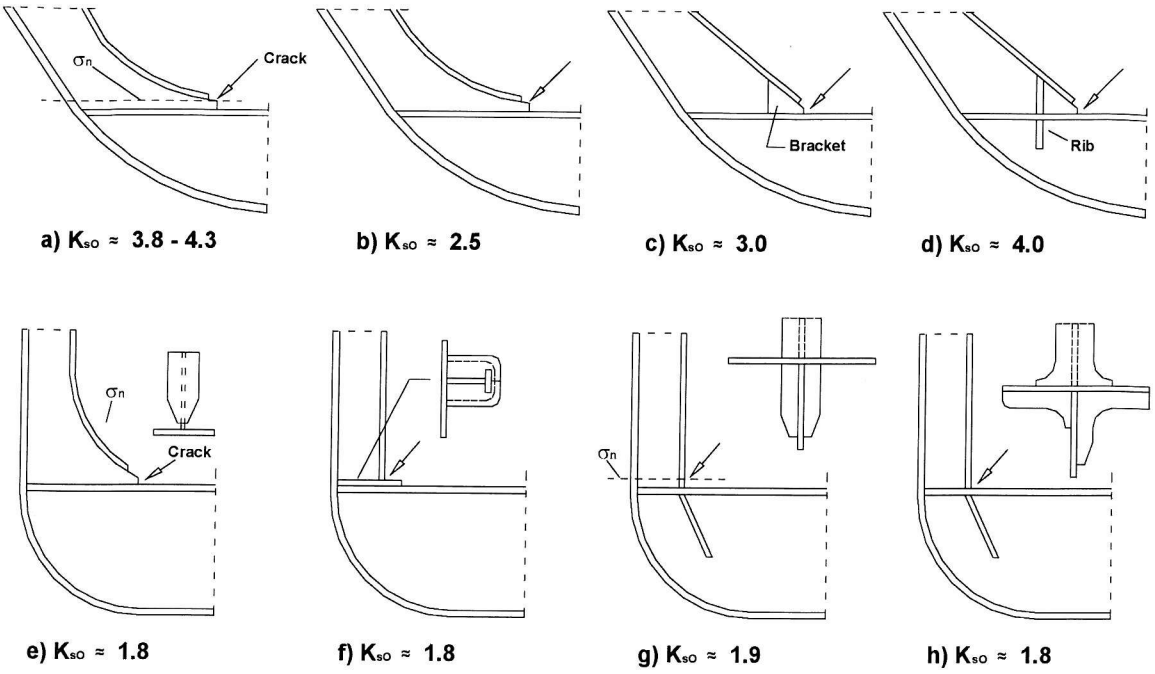

fig.5.7

Typical Corner Side Frame Joints

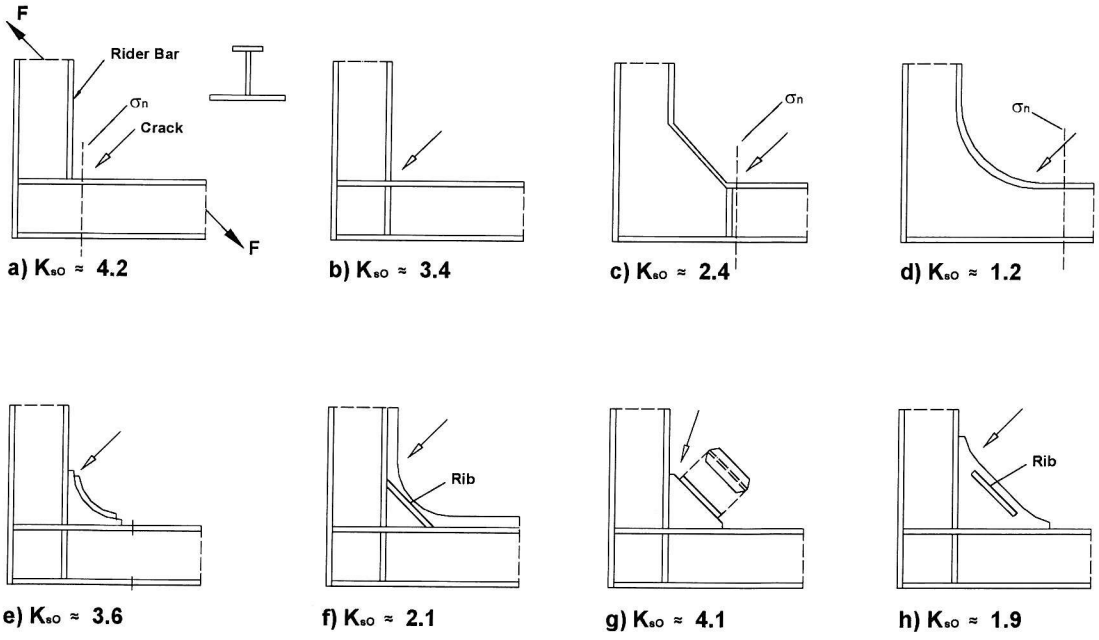

fig.5.8

Typical Transverse Frame Joints

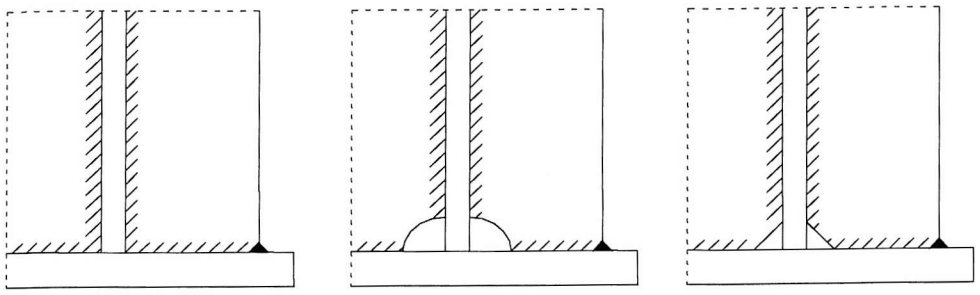

fig.5.9

Frames Webs With & Without Cutout at Inner Corner

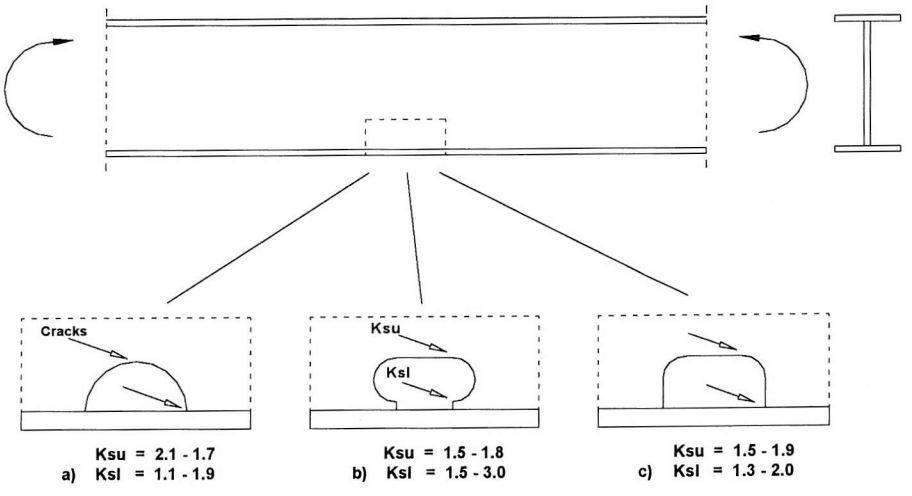

fig.5.10

Weld Ends and Scallops

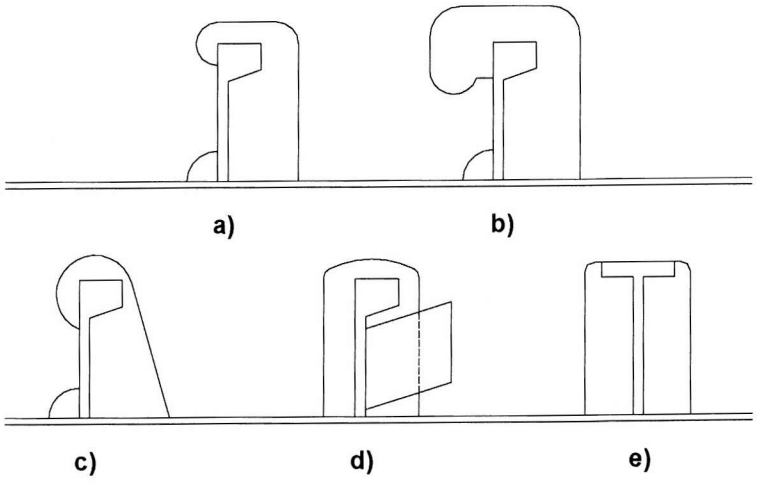

fig.5.11

Typical Ship Yard Longitudinal Cutouts

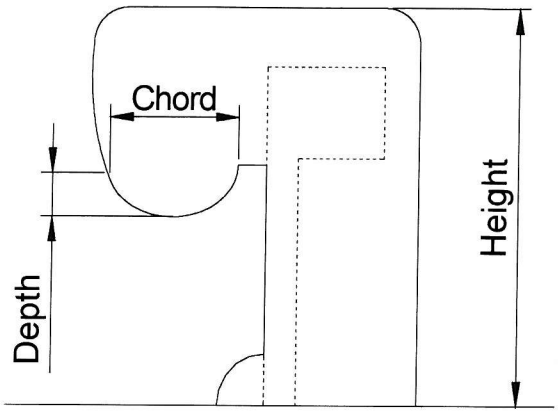

fig.5.12

Cutout Definitions

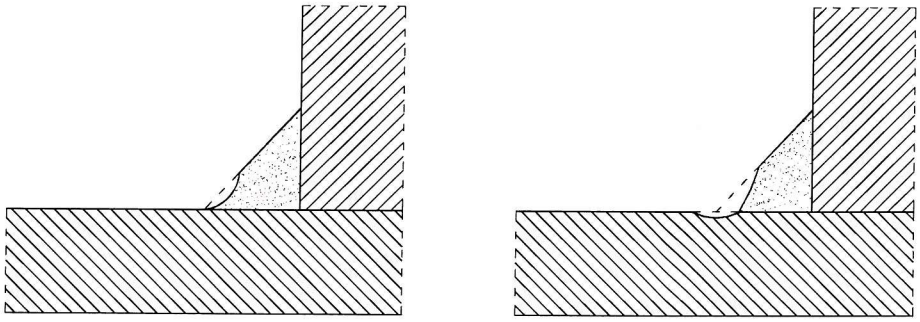

fig.5.13

Post Welding Treatment of Welds

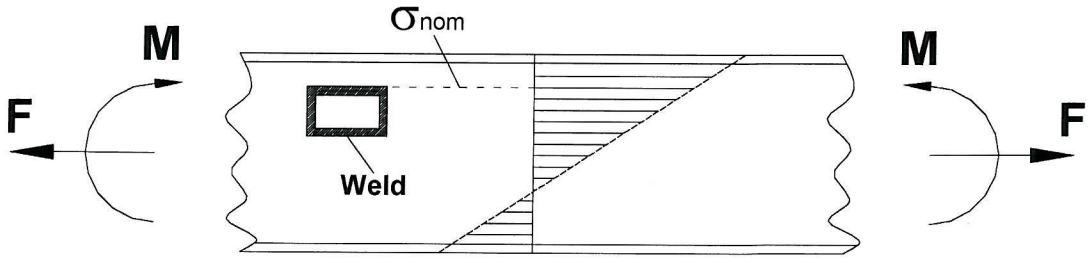

fig.6.1

Nominal Bending Stress in a Beam

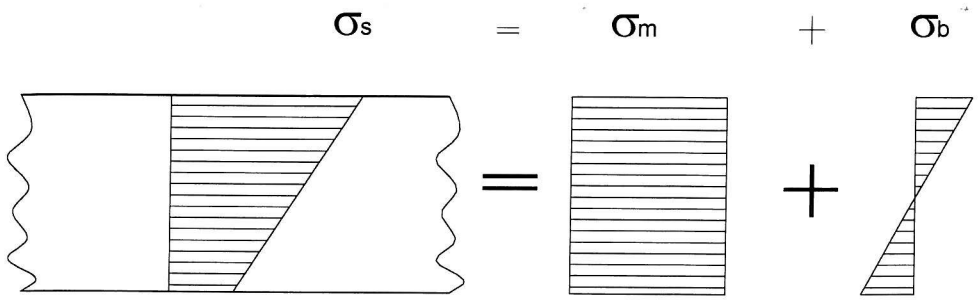

fig.6.2

Bending & Membrane Stress Distribution in a Beam

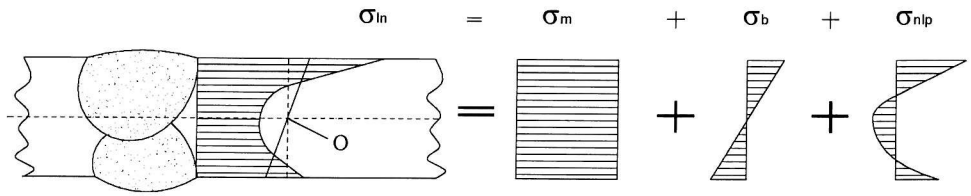

fig.6.3

Notch Stress at a Weld Toe

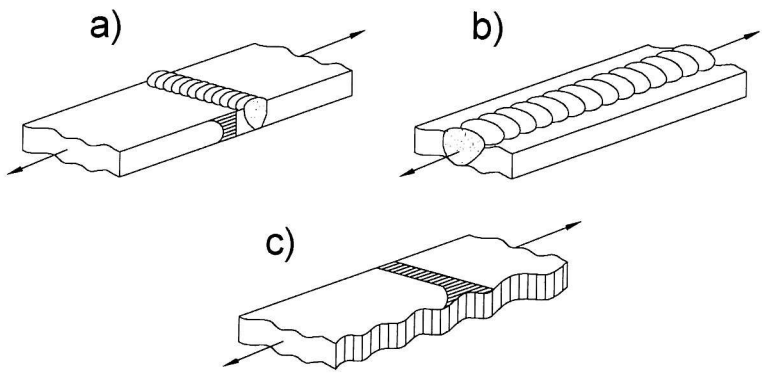

fig.6.4

Typical Notch Stress in Welds

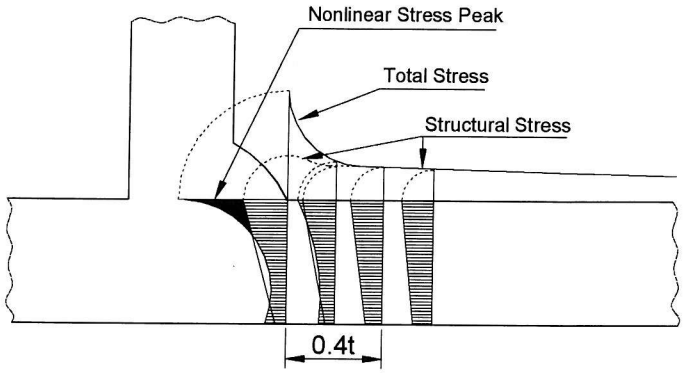

fig.6.5

Non-Linear Notch Stress Distribution

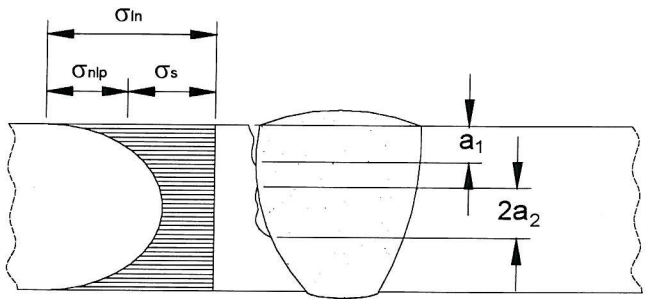

fig.6.6

Effect of Weld Defect on Notch Stress

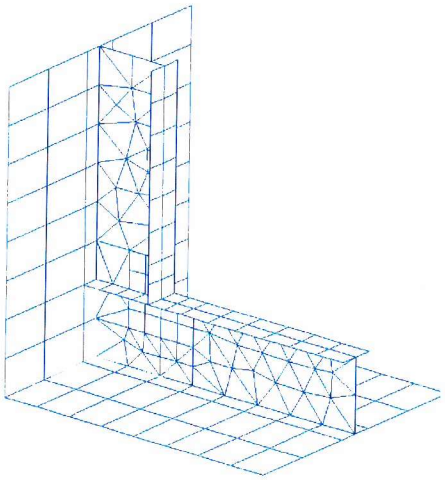

fig.6.7

The Coarse Model

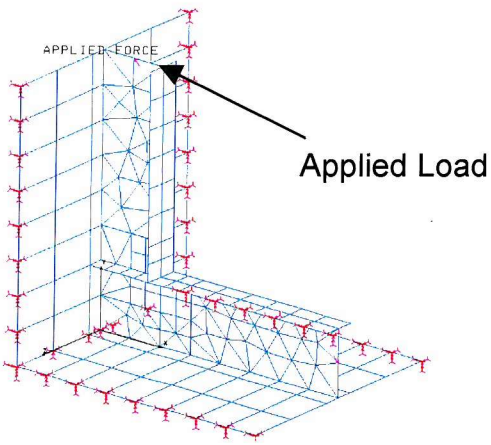

fig.6.8

Applied Loads & Boundary Conditions

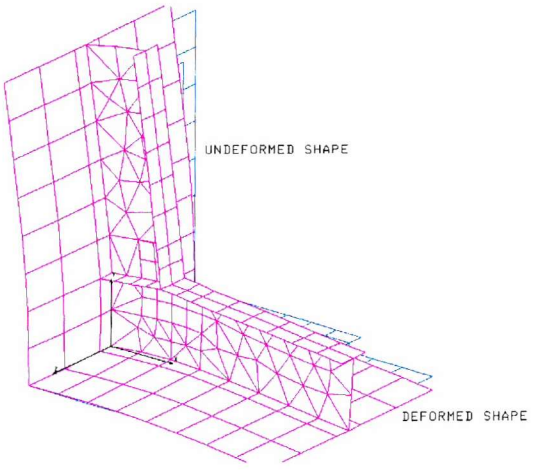

fig.6.9

Deformed FEM Plot

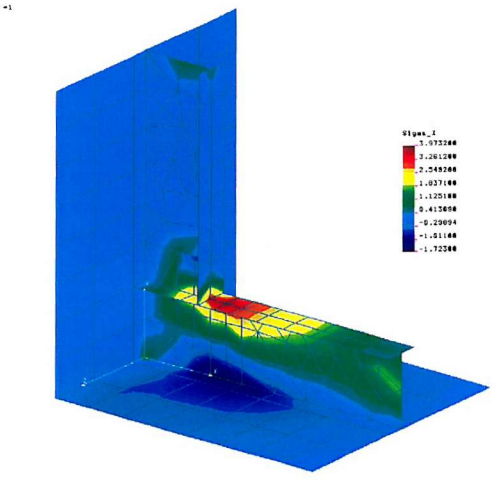

fig.6.10

Stress Plot of Frame

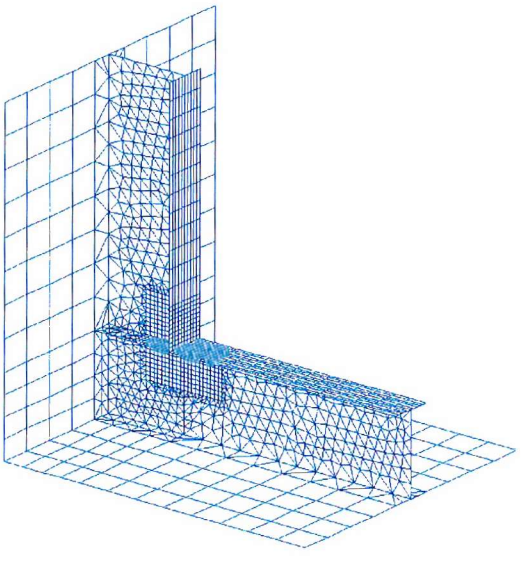

fig.6.11

Fine mesh Model

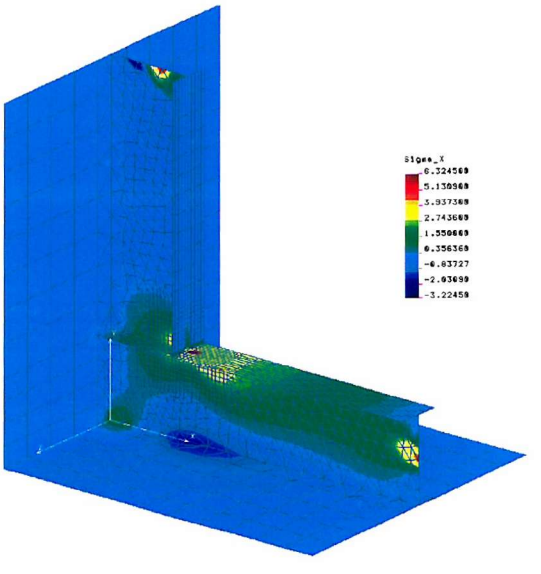

fig.6.12

Stress Plot of Fine Mesh

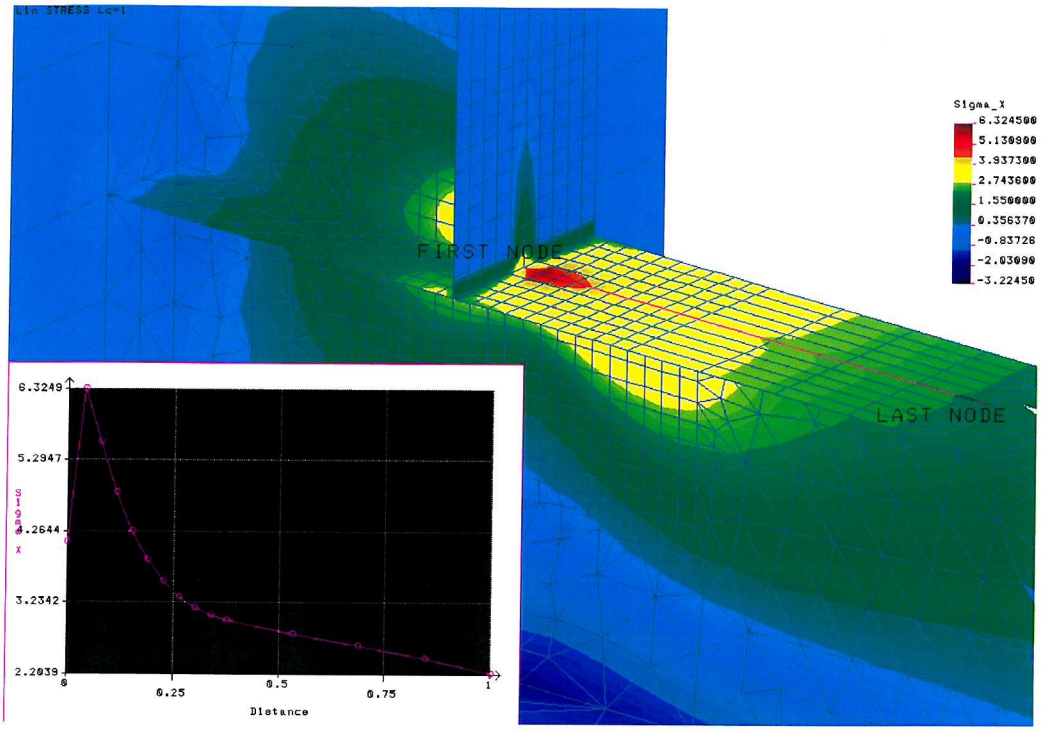

fig.6.13

Close up Membrane Stress Plot

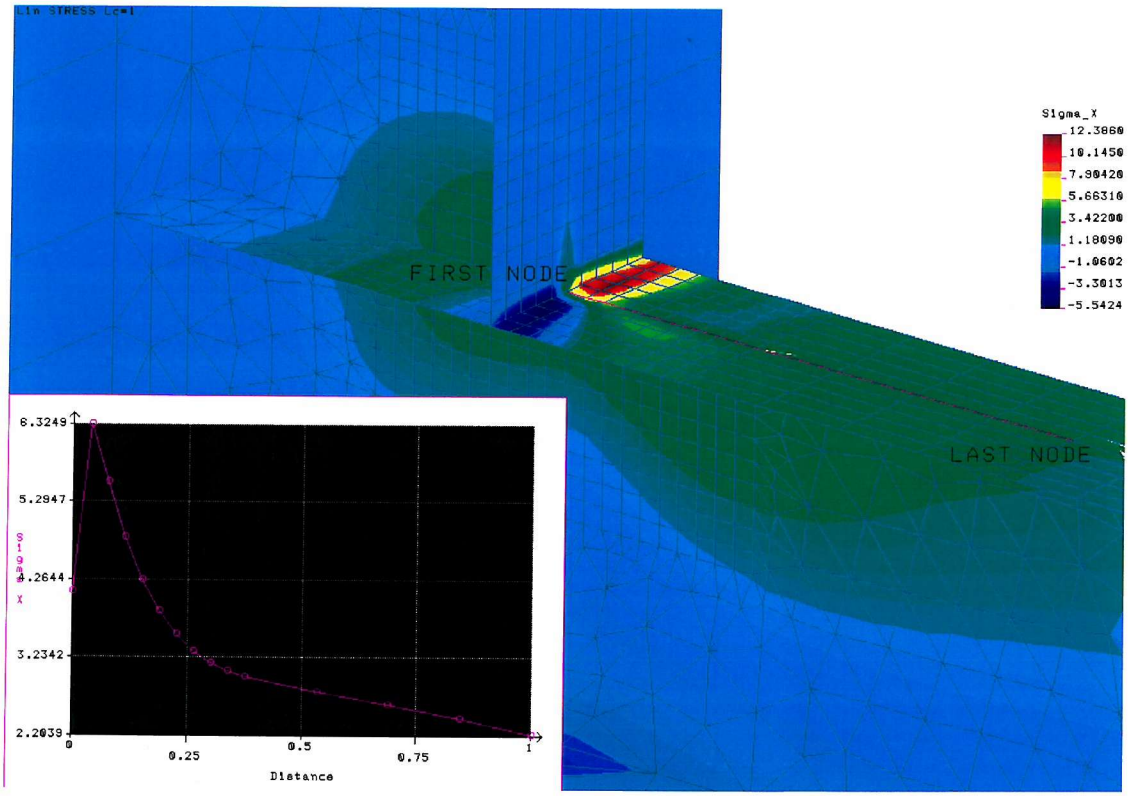

fig.6.14

Top Skin Stress Plot

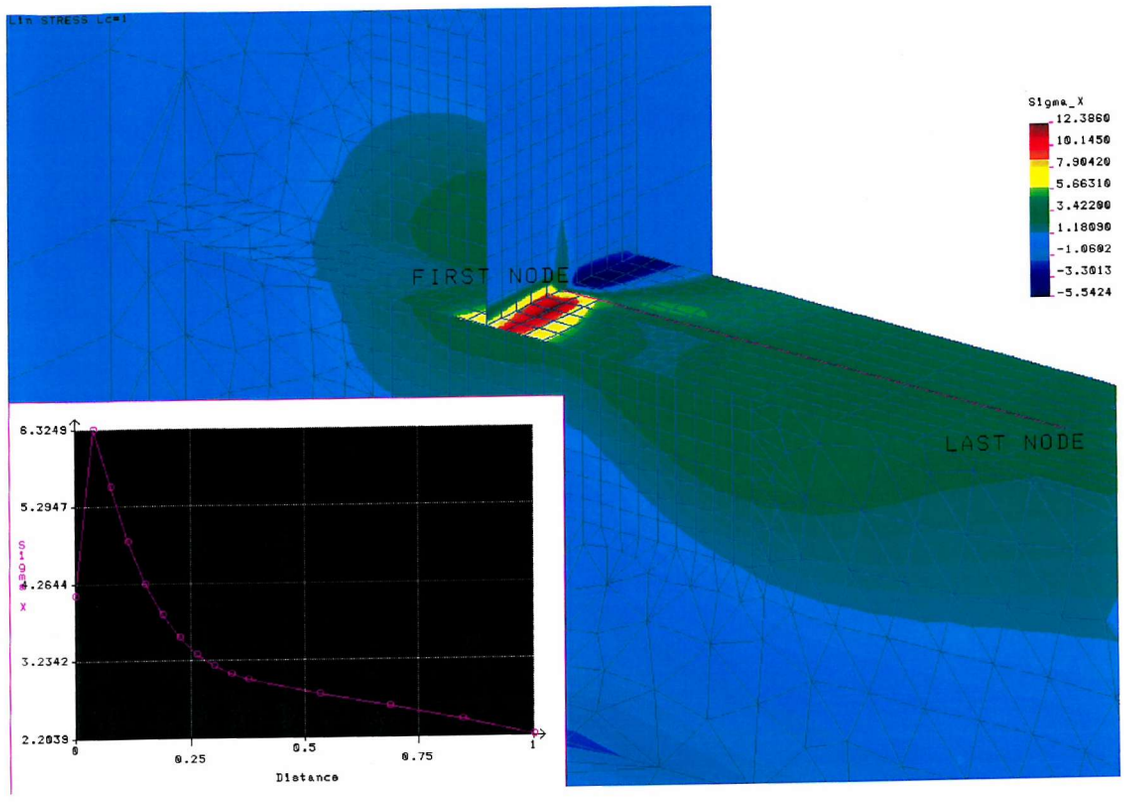

fig.6.15

Bottom Skin Stress Plot

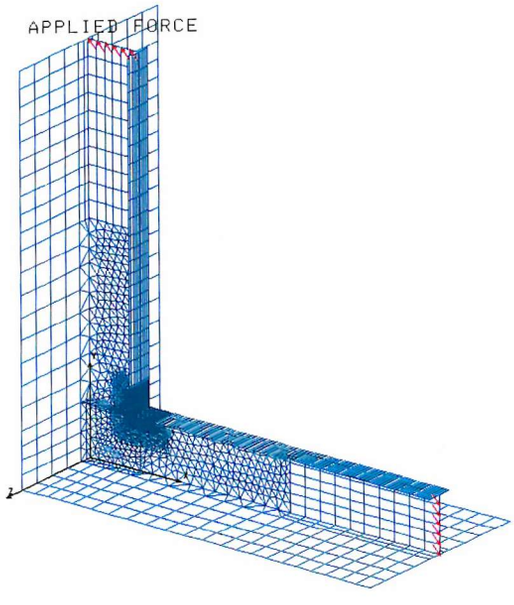

fig.6.16

Evenly Applied Loads

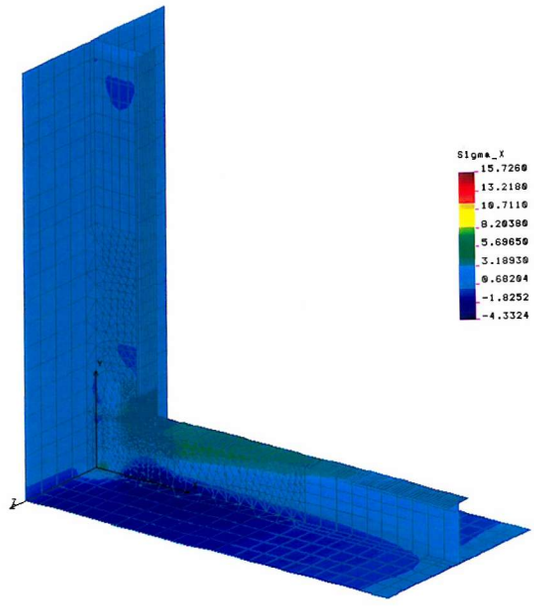

fig.6.17

Stress Plot of Evenly Applied Load Loads

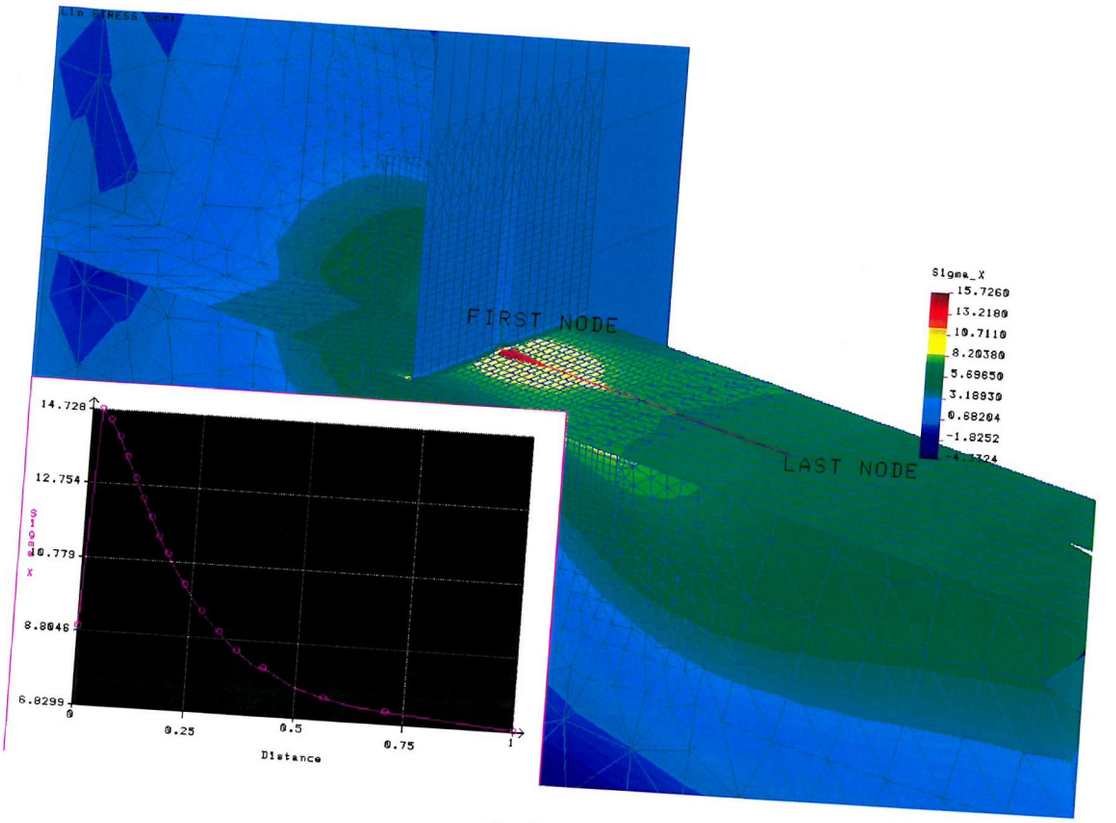

fig.6.18

Close up Stress Plot of Fine Mesh Model

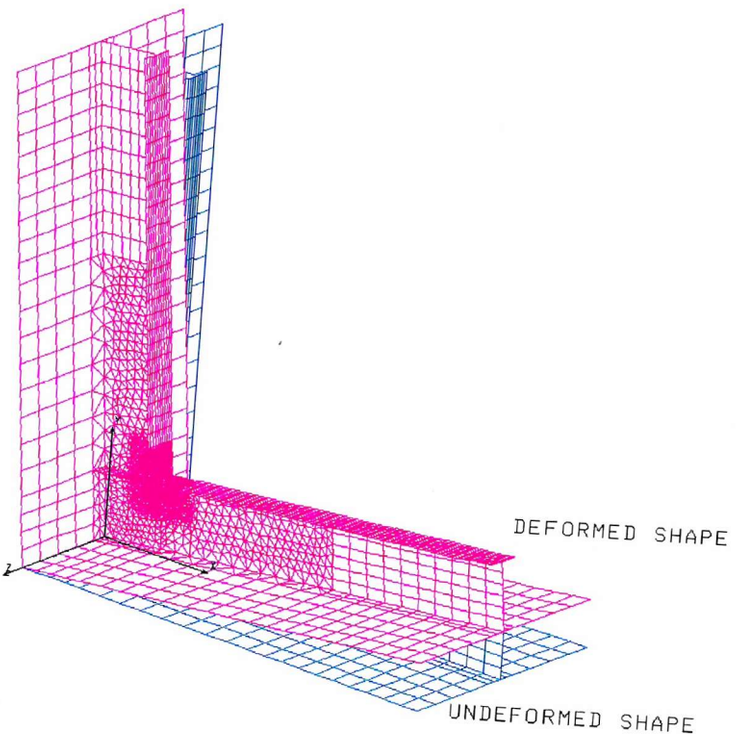

fig.6.19

Deformed Plot of Finer Mesh Model.

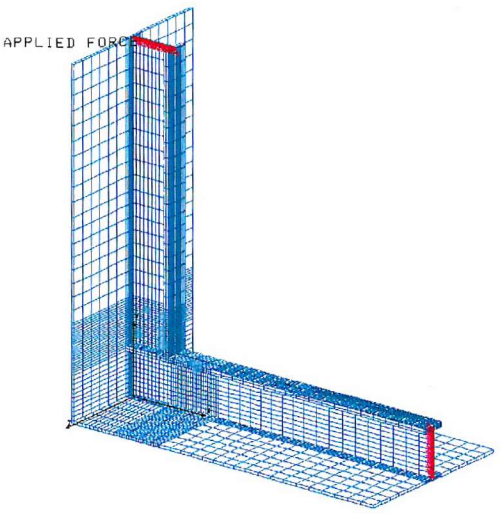

fig.6.20

Basic Solid Model

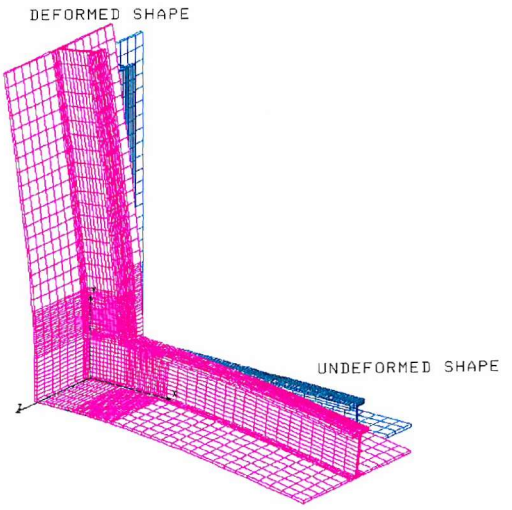

fig.6.21

Deformed Plot of Solid Model

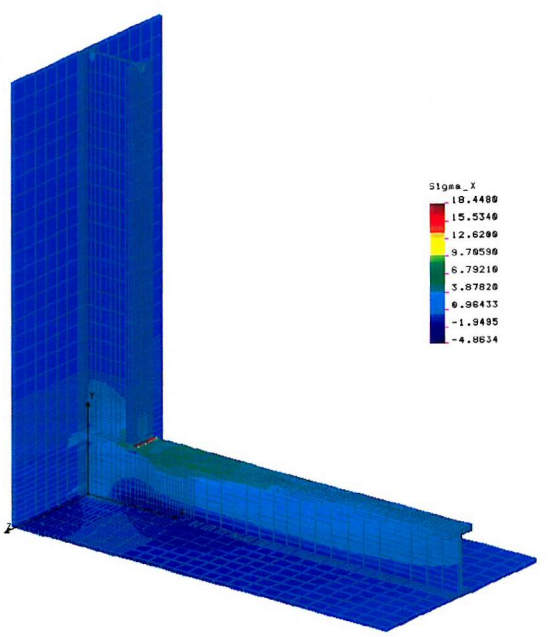

fig.6.22

Stress Plot of Solid Model

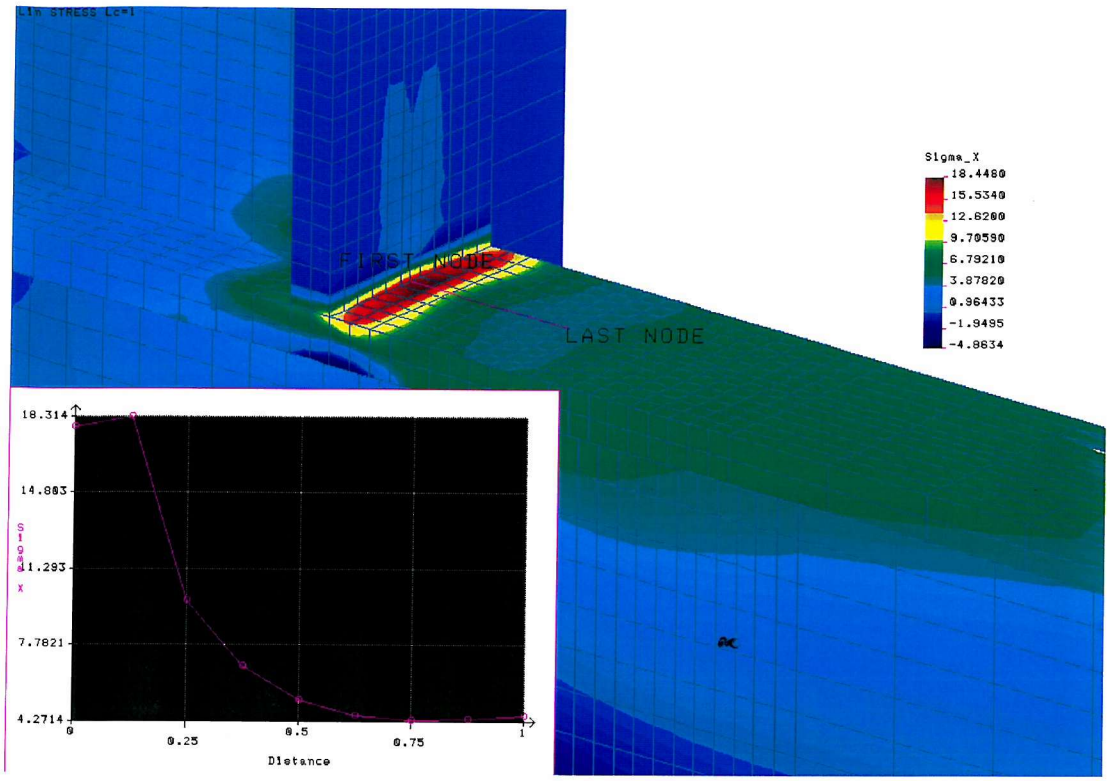

fig.6.23

Close up Stress Plot of the Solid Model

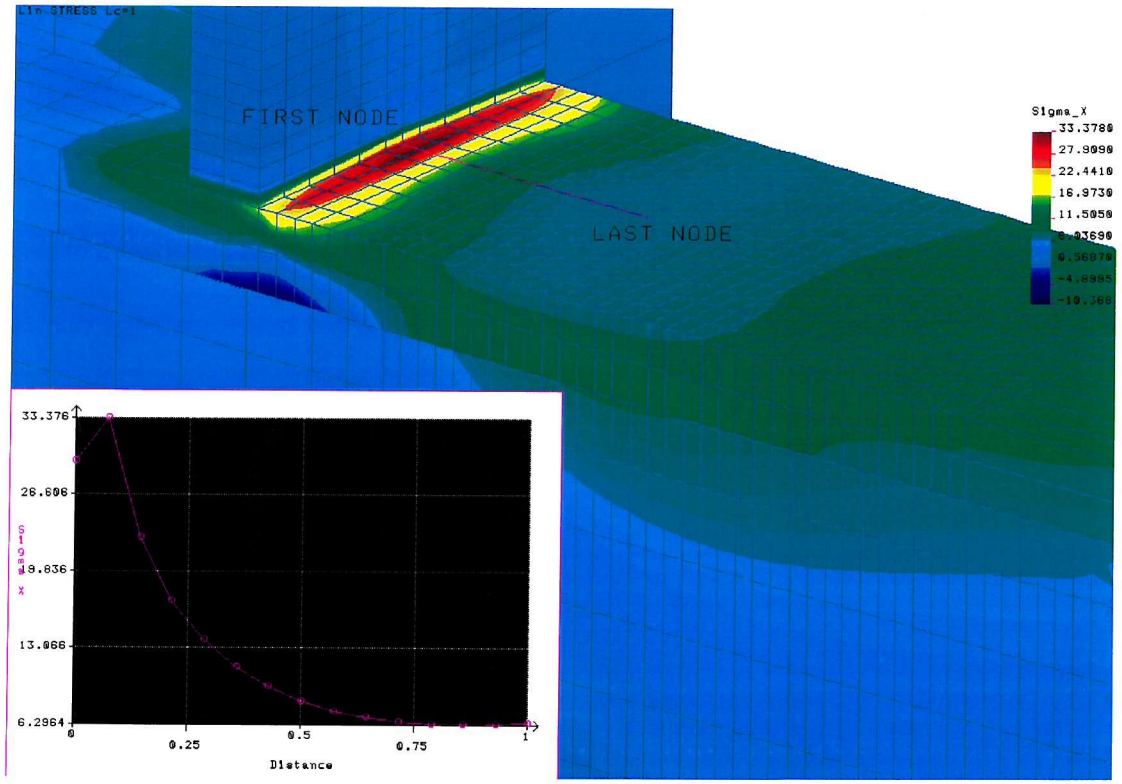

fig.6.24

Stress Plot of Fine Mesh Solid Model

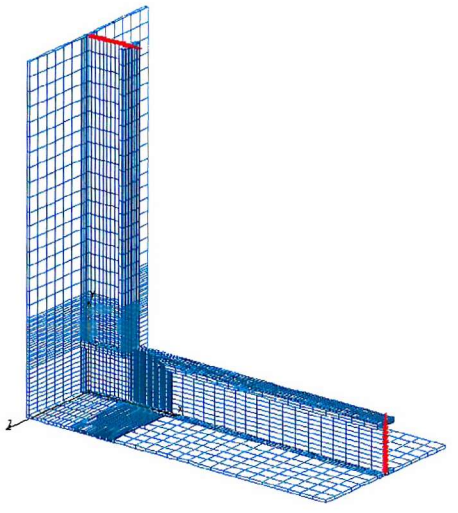

fig.6.25

Welded Joint Model

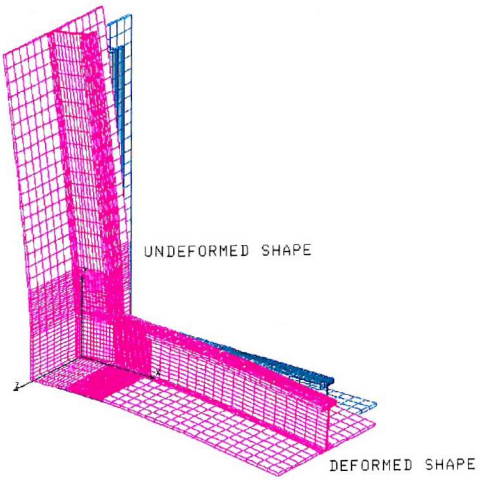

fig.6.26

Deformed Plot Model

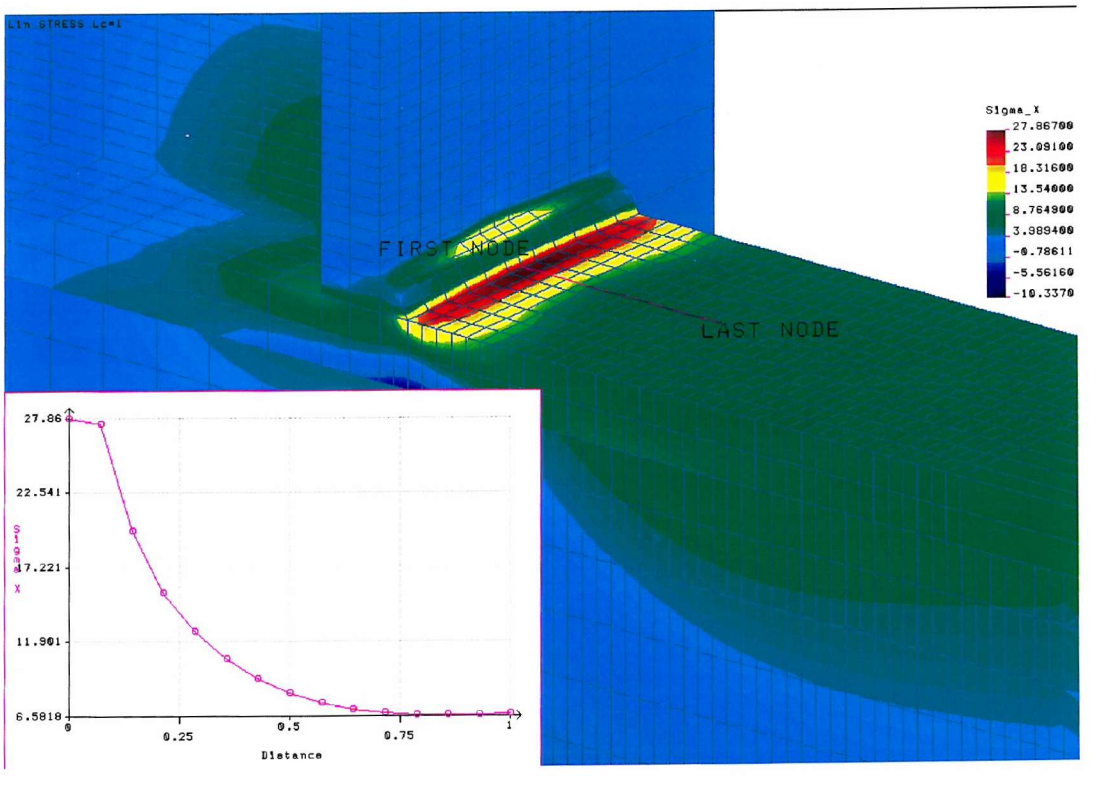

fig.6.27

Stress Plot of Welded Joint

fig 7.1

FBM Tricat

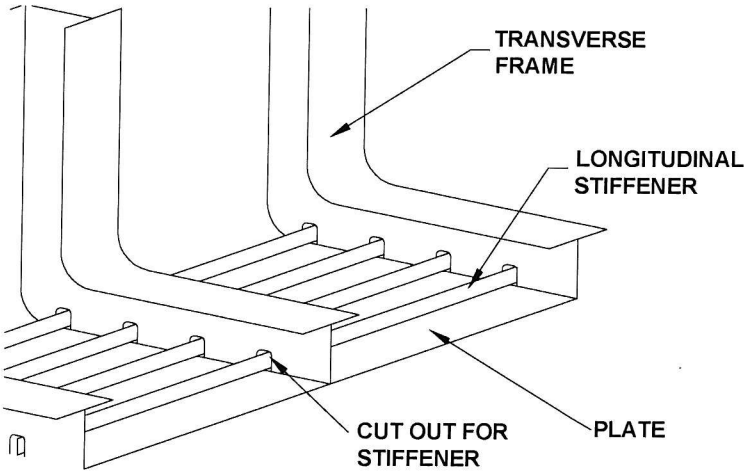

fig.7.2

Typical Longitudinally Framed Vessel

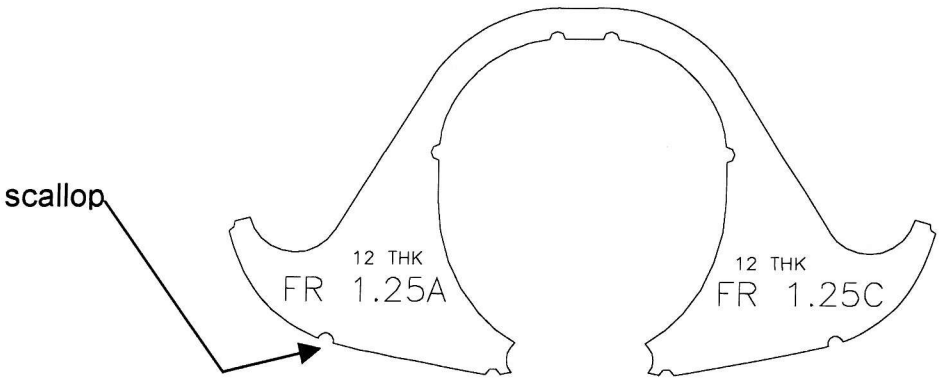

fig. 7.3

A Typical Transverse Web Frame for Waterjet

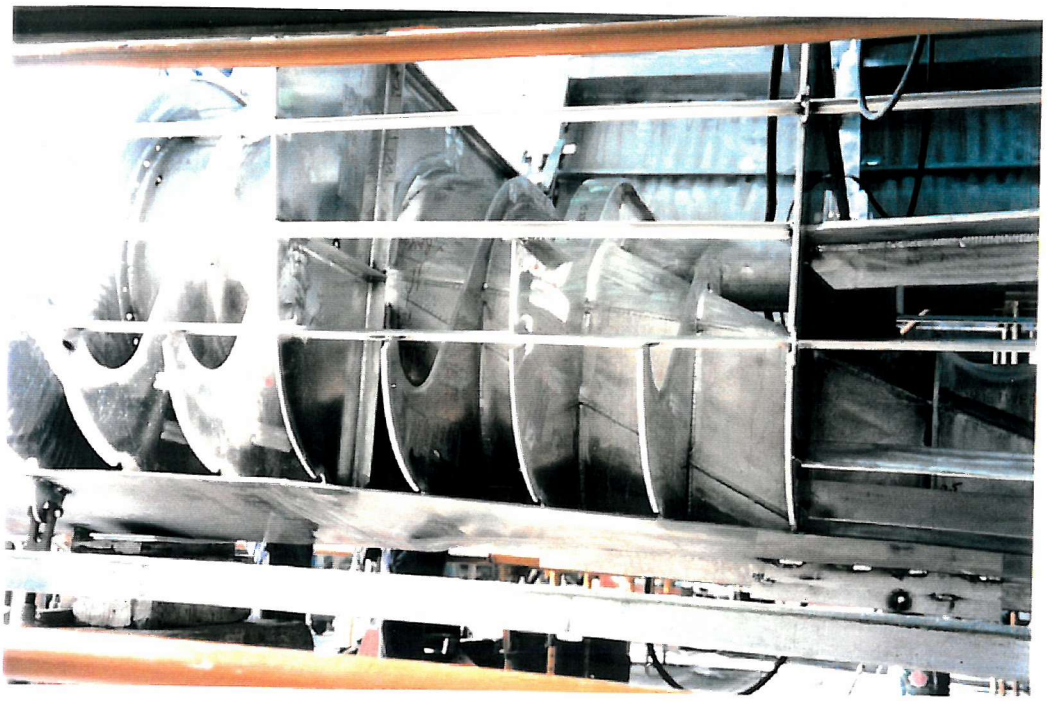

fig.7.4

View of Transverse Framing

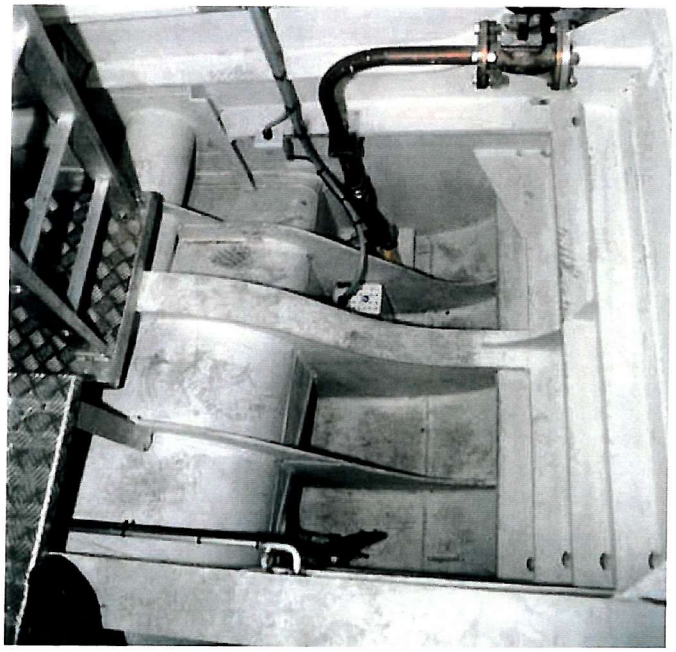

fig.7.5

Painted Bilges with Epoxy Primer

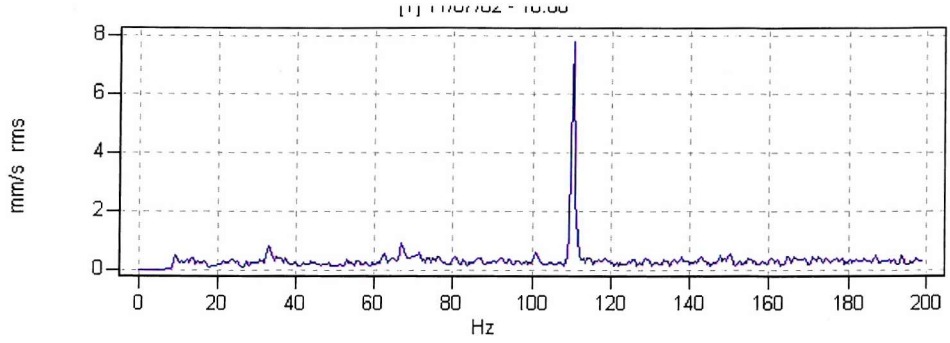

Fig.7.6

Frequency Analysis of Jet Duct Frame

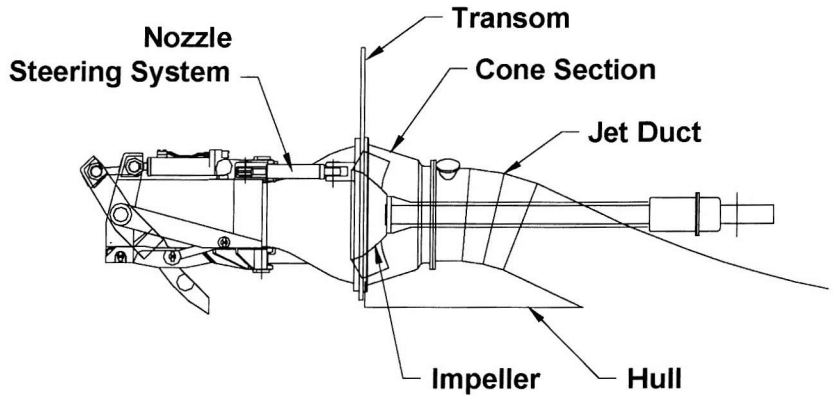

fig.7.7

The Anatomy of a Waterjet

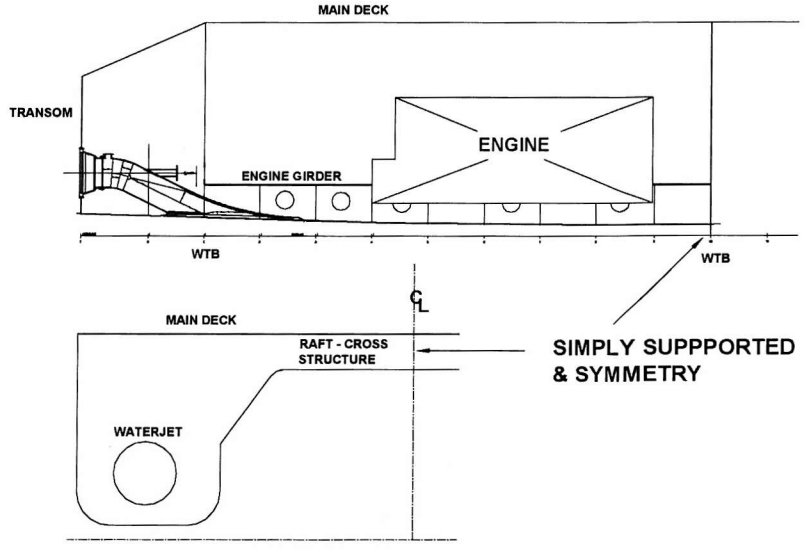

fig.7.8

The Extent of Structure That is Modelled For Analysis

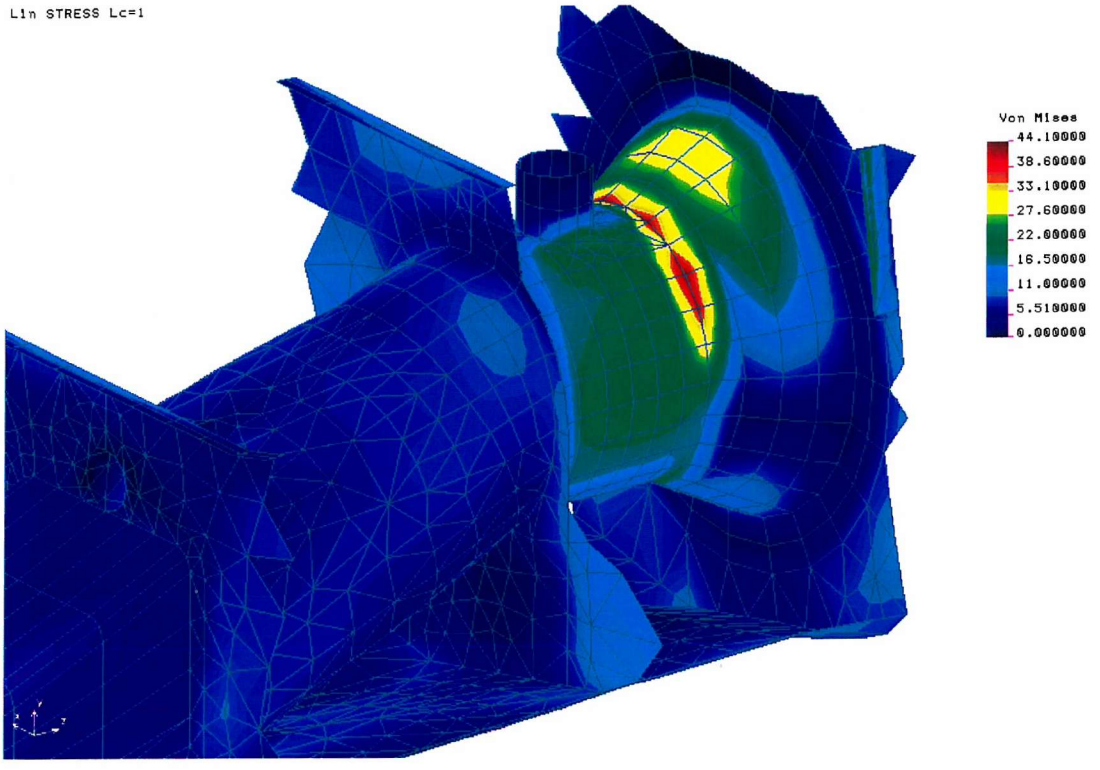

fig.7.9

Coarse Mesh FE model of Jet Duct

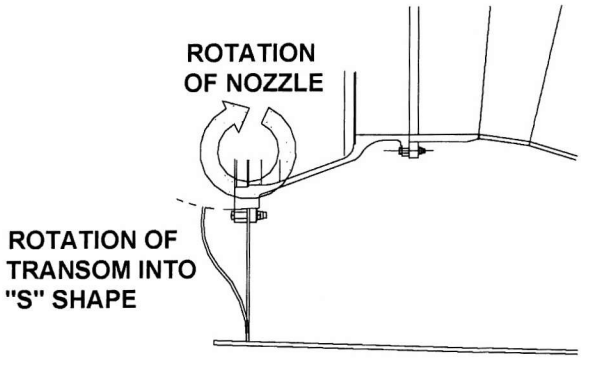

fig.7.10

S Shape Deformation of Transom Plating

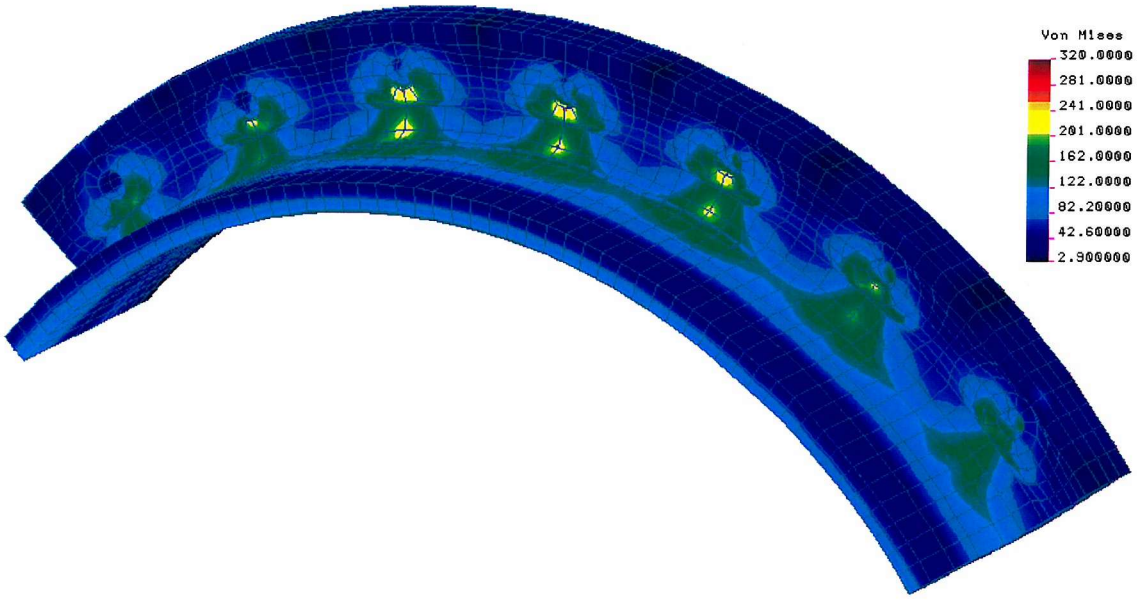

fig.7.11

Fine Mesh Von Mises Stress Plot of the flange

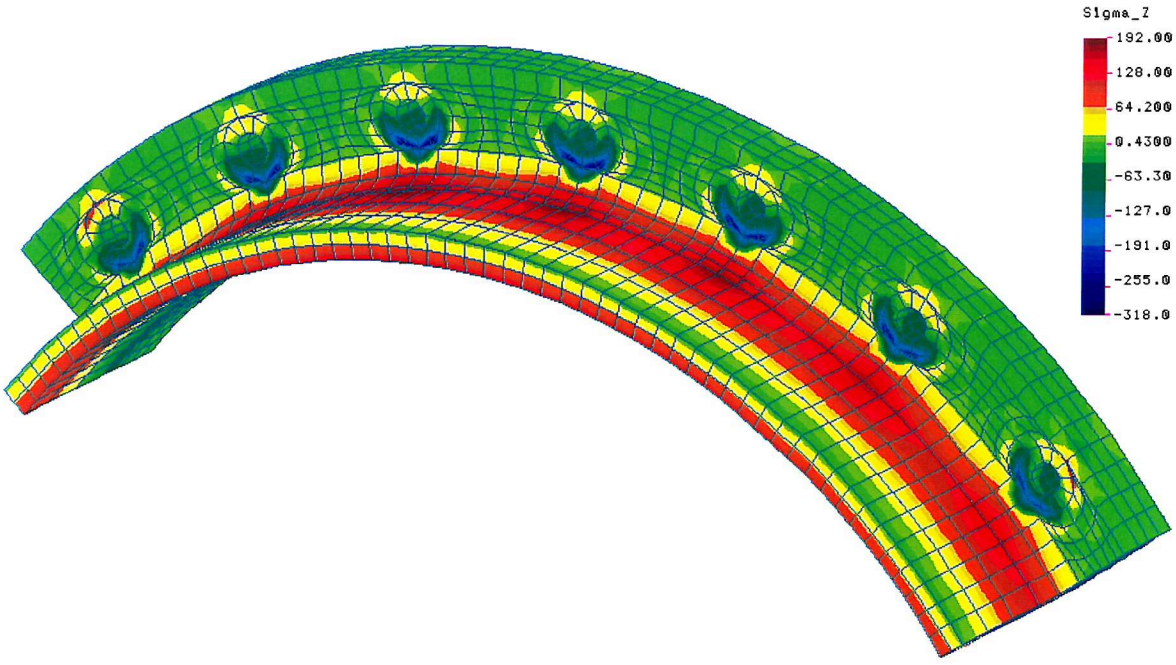

fig.7.12

Stress Plot In plane along the Jet Duct

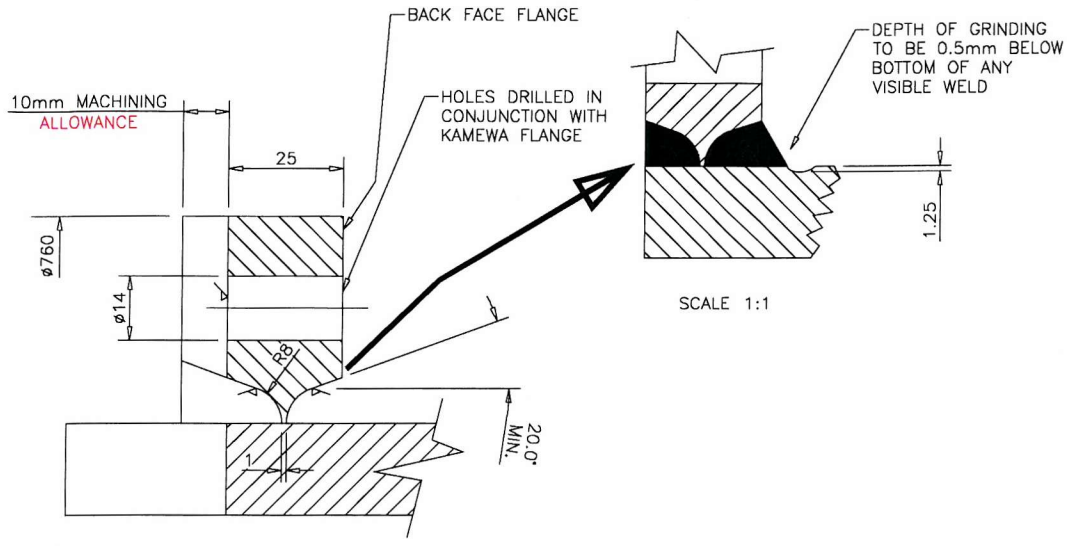

fig.7.13

Post Weld Treatment of Flange

11. List of Tables

Material	Tensile Strength (MNm^{-2})	m
Mild Steel	325	3.3
Low Alloy Steel	680	3.3
Stainless Steel	665	3.1
Pure Aluminium	125	2.9
5000 alloy	310	2.7
6000 alloy	310	4.1

Table 2.1

Fatigue Crack Growth Data for Various Metals

Series	Main Alloy	Effect of Alloying Elements
1000	99% minimum purity	Highly corrosion resistant, low strength, workable and conductive.
2000	Copper alloys	Strength, hardness, machinability
3000	Manganese alloys	Moderate strength, good workability
4000	Silicon alloys	Lowers melting point, moderate strength, corrosion resistant
5000	Magnesium alloys	Moderate to high strength, corrosion resistant.
6000	Magnesium - Silicon alloys	Higher strength, formability, corrosion resistant
7000	Zinc - Magnesium alloy	Highest strength.
8000	Miscellaneous alloys	Miscellaneous.

Table 3.1

The Alloys of Aluminium

Temper		Mechanical or Heat-Treatment Process
- F		As Fabricated
- O		Annealed, recrystallised
- H		Strain Hardened. This applies to products that have their strength increased by cold working only. The " H " is always followed by two or more digits
	- H1	Strain Hardened Only
	- H2	Strain Hardened and then Partially Annealed
	- H3	Strain Hardened and then Stabilised
- W		Solution Heat Treated (wrought products): Unstable, for alloys that spontaneously age at room temperature
- T		Solution Heat Treated to Produce Stable Tempers
	- T2	Annealed to improve ductility and to increase dimensional stability
	- T3	Solution heat treated and then cold worked
	- T4	Solution heat treated and naturally aged to a stable condition
	- T5	Artificially aged after cooling, from elevated temperature
	- T6	Solution heat treated and then artificially aged
	- T7	Solution heat treated and then stabilised
	- T8	Solution heat treated, cold worked and then artificially aged
	- T9	Solution heat treated, artificially aged and then cold worked
	- T10	Artificially aged and then cold worked.

Table 3.2

Aluminium Temper Designations

Work Hardened Tempers			
Condition	Annealed	Work-Hardened	Restored
As-Rolled		F	
Annealed	O, H111		
¼ Hard		H12	H22, H32, H116
½ Hard		H14	

Table 3.3

Most Commonly Used Tempers in Shipbuilding

5083 Alloy Temper Designation	0.2% Proof (MPa) Unwelded	UTS (MPa)	% Elongation	Welded (MPa)
O	125	275	14	125
F	130	280	12	125
H116 / H321	215	300	5	125

Table 3.4

Properties of 5083 When Strain Hardened

Heat-Affected Zone in Welded Aluminium Joints

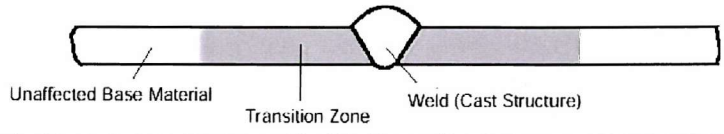

	Material	Starting State	HAZ Strength	Possibility of Increasing HAZ Strength
Non-Heat-Treatable	Al 99,5 AlMn AlMgMn AlMg 3 AlMg 4,5 Mn	Annealed (Recrystallised Structure)	No Change	None
		Half Hard, Hard (Cold-Worked Structure)	Softening Due to Recrystallisation	None
Heat-Treatable	AlMgSi	Cold-Worked, Artificially Aged (Aged Structure)	Softening Due to Coarsening of Precipitates	Repeating Solution Treatment and Aging
	AlZnMg	Naturally Aged, Artificially Aged (Aged Structure)	Softening Due to the Repeated Solution Treatment	a) Natural Aging, 90 Days b) Artificial Aging

Table 3.5

Heat Affect Zone in Welded Aluminium Joints

Aluminium Alloy	0.2% Proof (MPa) Unwelded	UTS (MPa)	Welded (MPa)
6005A – T5	215	260	115
6082 – T6	240	280	115
6061 – T6	240	280	115

Table 3.6

Mechanical Properties of 6000 Series Welded and Unwelded

IMPORTANT KINDS OF TRANSGRANULAR FRACTURE		
Fracture	Typical Occurrence	Characteristics
Microvoid coalescence (ductile fracture)	Stable and unstable fracture. High-stress-intensity fatigue.	Irregular blunt crack fronts. Considerable local plasticity
Cleavage in Steels	Unstable fracture Intermediate and high-stress-intensity fatigue Hydrogen embrittlement	Sharp kinked cracks Brittle fracture
Continuum fatigue (striations)	Intermediate- and high-stress-intensity fatigue	Uniform crack fronts: Limited blunting. Mode I favoured considerable local (cyclic) plasticity
Slip-plane cracking (faceted fracture	Fatigue crack initiation and growth at low stress intensities, especially under torsional loading	Branched, kinked and irregular crack fronts, limited blunting. Mode II favoured Limited local (cyclic) plasticity
Cleavage-like faceted fracture	Low-stress-intensity fatigue Stress corrosion	Branched, kinked and irregular crack fronts, limited blunting. Limited local plasticity

Classification of Intergranular Fracture		
Fracture	Typical Occurrence	Characteristics
Microvoid coalescence along grain boundaries	Stable and unstable fracture and high-stress-intensity fatigue in high-strength steels and aluminium alloys	Limited local plasticity
Low-ductility grain-boundary separation	Sustained load fracture (including creep)	Little evidence of plasticity
Brittle grain-boundary separation	Unstable fracture in temper-embrittled steels and refractory metals	Brittle low-energy fracture

Table 4.1

Microstructure Features in Metallic Materials

Appendix A

Stress Intensity Factor K, for Various Geometric Flaws

Single-Edge Crack

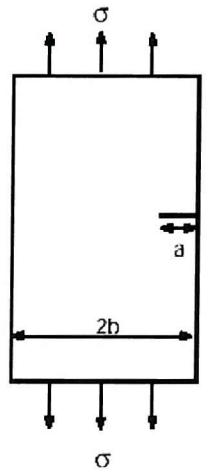

For a semi-finite edge-cracked specimen:

$$K_I = 1.12\,\sigma(\pi a)^{1/2}$$

For a finite width edge-cracked specimen:

$$K_I = \sigma(\pi a)^{1/2}\, f(a/b)$$

Correction factor for a single-edge crack in a finite width plate

a/b	f(a/b)
0.10	1.15
0.20	1.20
0.30	1.29
0.40	1.37
0.50	1.51
0.60	1.68
0.70	1.89
0.80	2.14
0.90	2.46
1.00	2.86

K_I values for various crack geometries

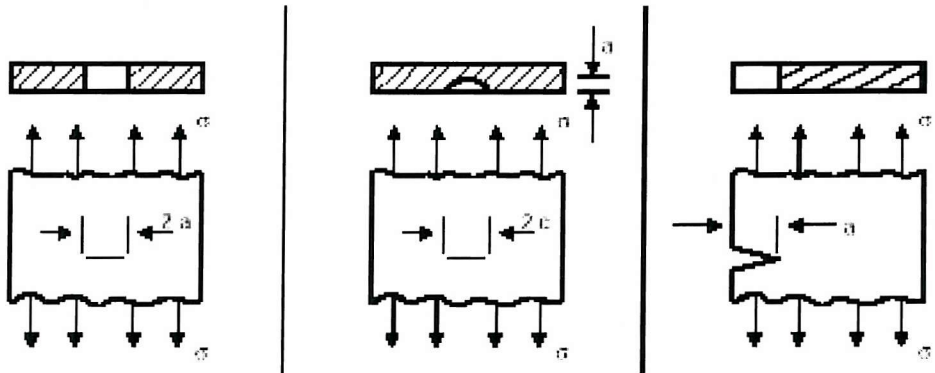

Through thickness crack

$K_I = \sigma\sqrt{\pi a}$

Surface crack

$K_I = 1.12 \cdot \sigma \cdot \sqrt{\pi \frac{a}{Q}}$

where $Q = f(a/2c, \ldots)$

Edge crack

$K_I = 1.12 \cdot \sigma \cdot \sqrt{\pi a}$

Relation between material toughness, flaw size and stress

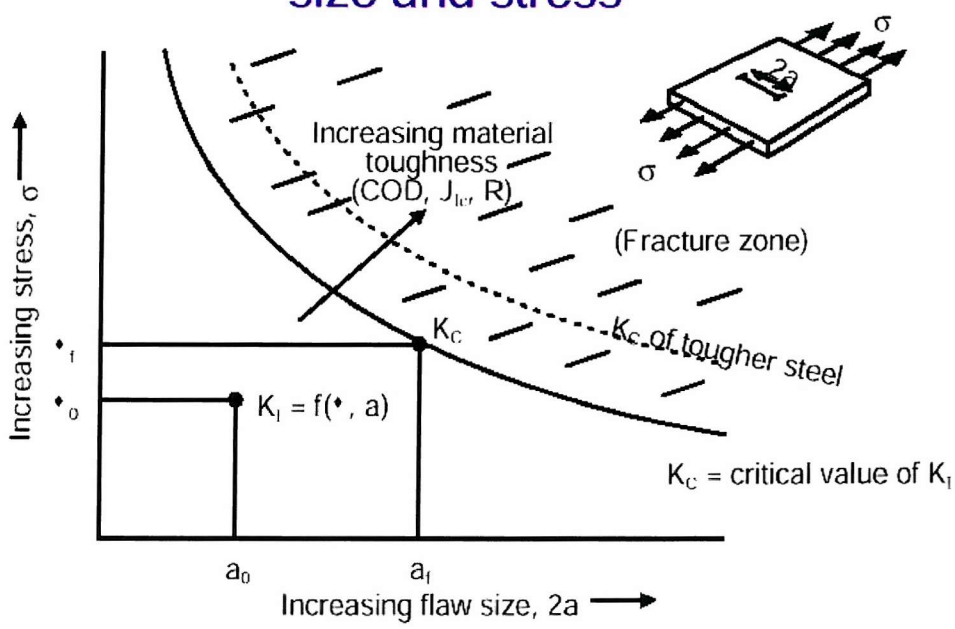

Through-Thickness Crack

Finite Width Plate

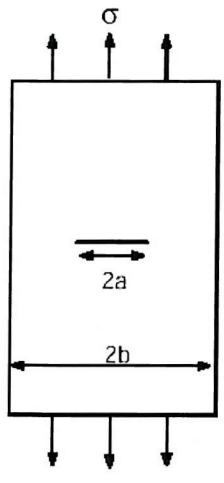

Tangent correction for finite width

a/b	$\left[\sec((\pi \cdot a)/(2 \cdot b))\right]^{1/2}$
0.074	1.00
0.207	1.03
0.275	1.05
0.337	1.08
0.410	1.12
0.466	1.16
0.535	1.22
0.592	1.29

$$K_I = \sigma\sqrt{\pi \cdot a} \cdot \left[\sec((\pi \cdot a)/(2 \cdot b))\right]^{1/2}$$

Infinite Width Plate

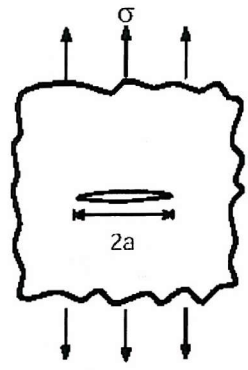

Nominal Stress

$$K = \sigma\sqrt{\pi \cdot a}$$

Double-Edge Crack

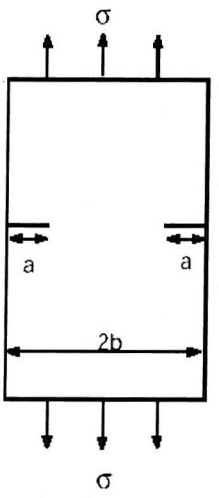

Tangent correction for finite width

a/b	$\left[\sec((\pi \cdot a)/(2 \cdot b))\right]^{1/2}$
0.074	1.00
0.207	1.03
0.275	1.05
0.337	1.08
0.410	1.12
0.466	1.16
0.535	1.22
0.592	1.29

$$K_I = 1.12\sigma\sqrt{\pi \cdot a} \cdot \left[\sec((\pi \cdot a)/(2 \cdot b))\right]^{1/2}$$

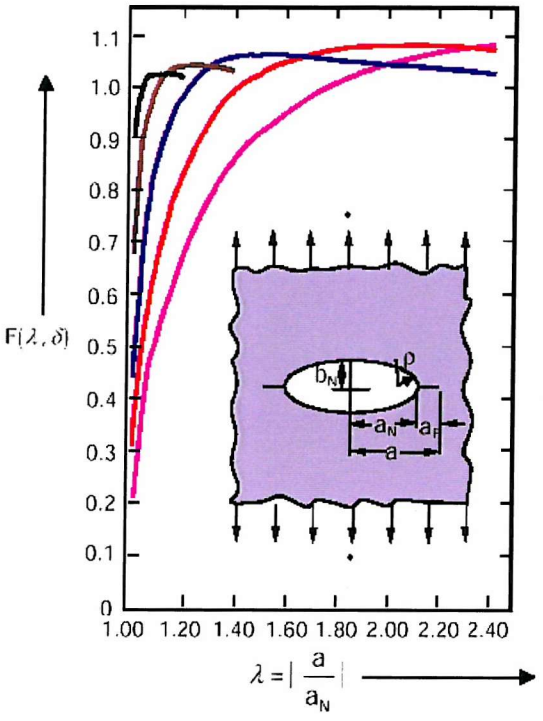

Cracks Emanating from Circular or Elliptical Holes

The stress intensity factor in the case of a finite plate is

$$K_I = F(\lambda, \delta) \cdot \sigma \sqrt{\pi \cdot a}$$

where $\lambda = \left| \frac{a}{a_N} \right|$ and $\delta = \left(\frac{b_N}{a_N} \right|$

For a circular hole $\delta = 1.0$

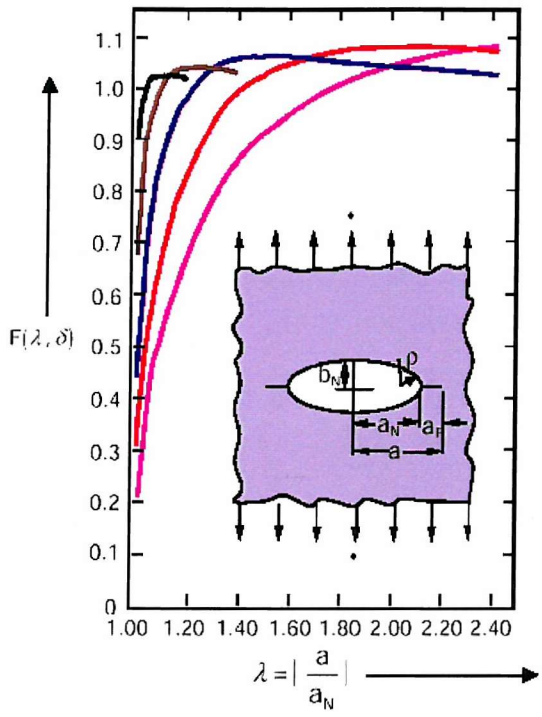

Cracks Emanating from Circular or Elliptical Holes

The stress intensity factor in the case of a finite plate is

$$K_I = F(\lambda, \delta) \cdot \sigma \sqrt{\pi \cdot a}$$

where $\lambda = \left| \frac{a}{a_N} \right|$ and $\delta = \left| \frac{b_N}{a_N} \right|$

For a circular hole $\delta = 1.0$

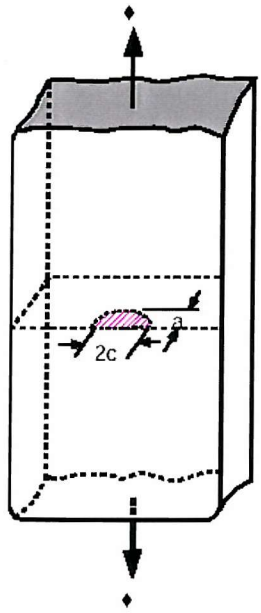

Surface Crack

"Thumbnail Crack"

The stress intensity factor can be calculated from the equations of elliptical crack using a free surface correction factor of 1.12 and for the position ß=π/2

$$K_I = 1.12 \cdot \sigma \left| \frac{\pi \cdot a}{Q} \right|^{\frac{1}{2}}$$

with $Q = \theta_0^{\,2}$ and the elliptic integral

$$\theta_0 = \int_0^{\frac{\pi}{2}} \left| 1 - \frac{c^2 - a^2}{c^2} \sin^2 \theta \right|^{\frac{3}{2}} \cdot d\theta$$

Q is regarded as a shape factor because its values depend on a and c.
For values of Q see Figure 2402.03.15.

Flaw Shape Parameter, Q

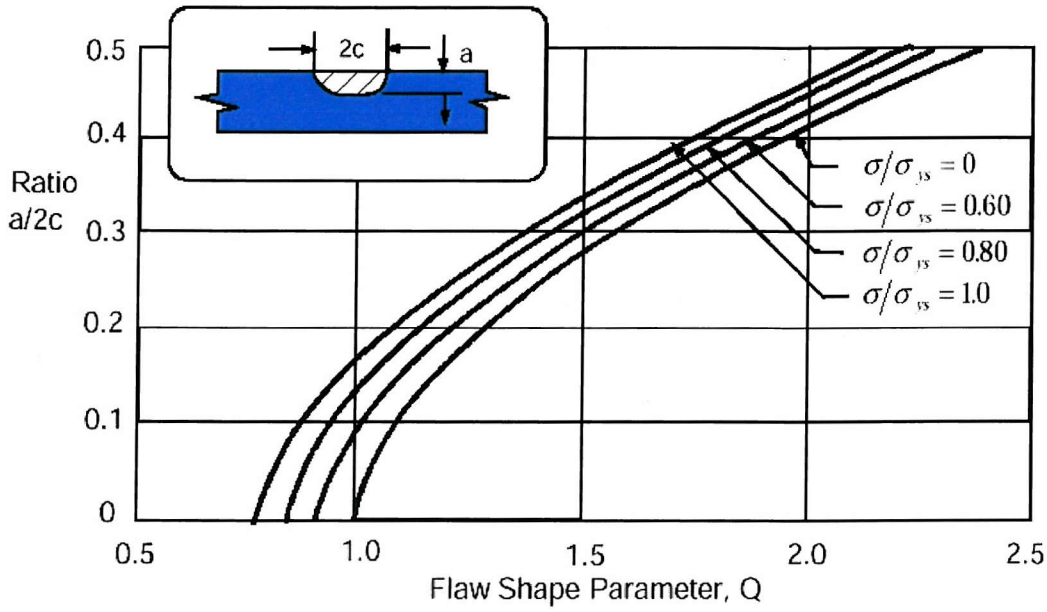

Stress Field Equations in the Vicinity of Crack Tips

Mode I	Mode II	Mode III
$\sigma_x = \frac{K_I}{\sqrt{2\pi \cdot r}} \cos\frac{\theta}{2}\left[1 - \sin\frac{\theta}{2}\sin\frac{3\theta}{2}\right]$	$\sigma_x = -\frac{K_{II}}{\sqrt{2\pi \cdot r}} \sin\frac{\theta}{2}\left[2 + \cos\frac{\theta}{2}\cos\frac{3\theta}{2}\right]$	$\tau_{xz} = -\frac{K_{III}}{\sqrt{2\pi \cdot r}} \sin\frac{\theta}{2}$
$\sigma_y = \frac{K_I}{\sqrt{2\pi \cdot r}} \cos\frac{\theta}{2}\left[1 + \sin\frac{\theta}{2}\sin\frac{3\theta}{2}\right]$	$\sigma_y = \frac{K_{II}}{\sqrt{2\pi \cdot r}} \sin\frac{\theta}{2}\cos\frac{\theta}{2}\cos\frac{3\theta}{2}$	$\tau_{yz} = \frac{K_{III}}{\sqrt{2\pi \cdot r}} \cos\frac{\theta}{2}$
$\tau_{xy} = \frac{K_I}{\sqrt{2\pi \cdot r}} \sin\frac{\theta}{2}\cos\frac{\theta}{2}\cos\frac{3\theta}{2}$	$\tau_{xy} = \frac{K_{II}}{\sqrt{2\pi \cdot r}} \cos\frac{\theta}{2}\left[1 - \sin\frac{\theta}{2}\sin\frac{3\theta}{2}\right]$	
$\sigma_z = \nu(\sigma_x + \sigma_y)$	$\sigma_z = \nu(\sigma_x + \sigma_y)$	$\sigma_x = \sigma_y = \sigma_z = \tau_{xy} = 0$
$\tau_{xz} = \tau_{yz} = 0$	$\tau_{xz} = \tau_{yz} = 0$	
$u = \frac{K_I}{G}\left[\frac{r}{2\pi}\right]^{1/2} \cos\frac{\theta}{2}\left(1 - 2\nu + \sin^2\frac{\theta}{2}\right)$	$u = \frac{K_{II}}{G}\left[\frac{r}{2\pi}\right]^{1/2} \sin\frac{\theta}{2}\left(2 - 2\nu + \cos^2\frac{\theta}{2}\right)$	$w = \frac{K_{III}}{G}\left[\frac{r}{2\pi}\right]^{1/2} \sin\frac{\theta}{2}$
$v = \frac{K_I}{G}\left[\frac{r}{2\pi}\right]^{1/2} \sin\frac{\theta}{2}\left(2 - 2\nu - \cos^2\frac{\theta}{2}\right)$	$v = \frac{K_{II}}{G}\left[\frac{r}{2\pi}\right]^{1/2} \cos\frac{\theta}{2}\left(-1 + 2\nu - \sin^2\frac{\theta}{2}\right)$	
$w = 0$	$w = 0$	$u = v = 0$

Appendix B

Stress Concentration Factors for Various Shapes

Stress Concentrations for Plate with Fillet

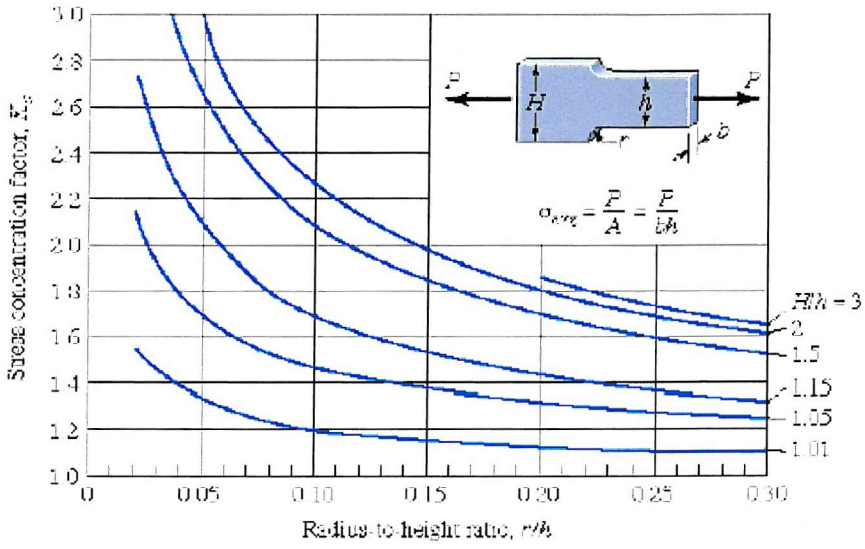

Stress Concentrations for Plate with Fillet (cont.)

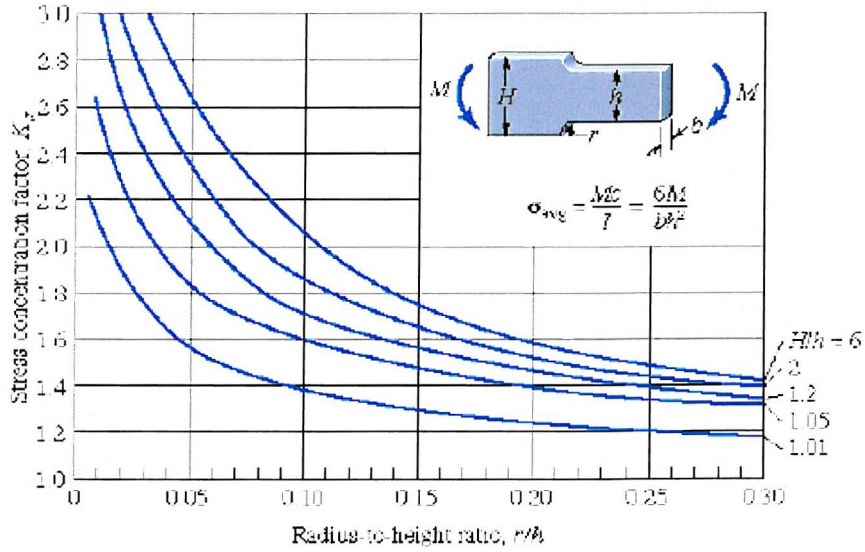

Stress Concentrations for Plate with Hole

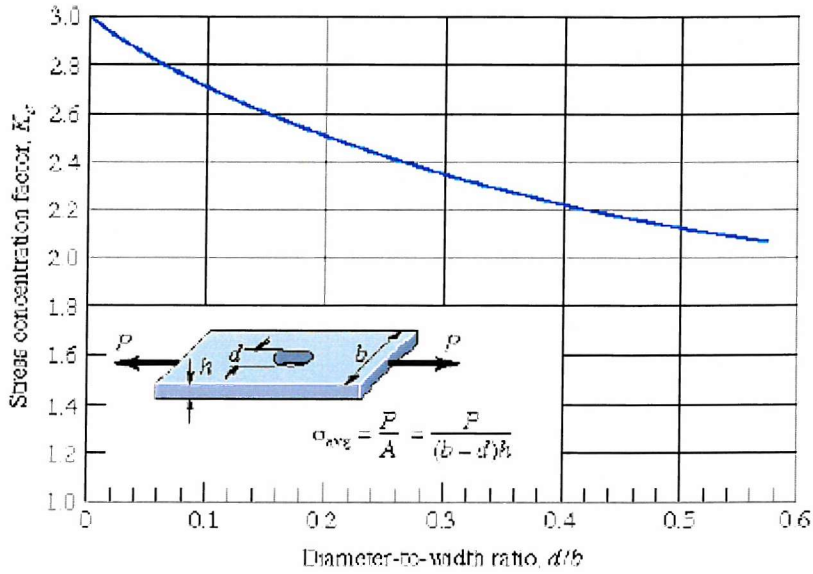

Stress Concentrations for Plate with Hole (cont.)

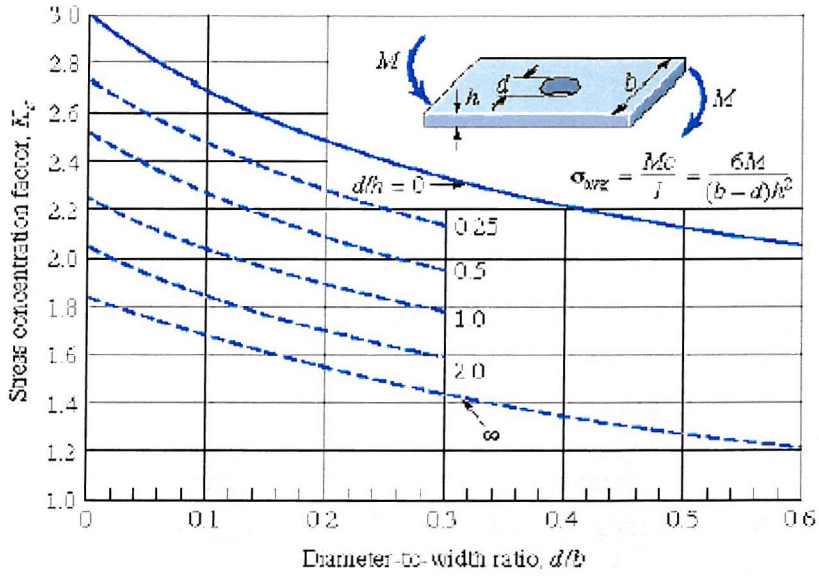

Stress Concentrations for Bar with Fillet (cont.)

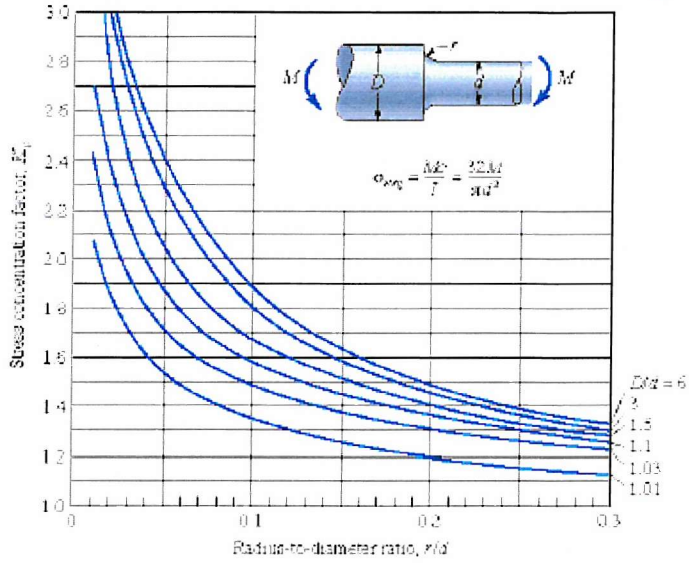

Stress Concentrations for Bar with Fillet (cont.)

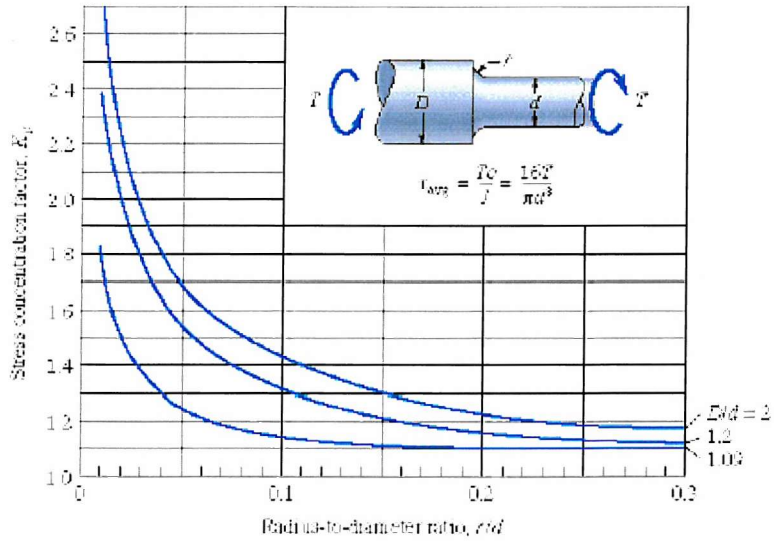

Stress Concentrations for Bar with Groove (cont.)

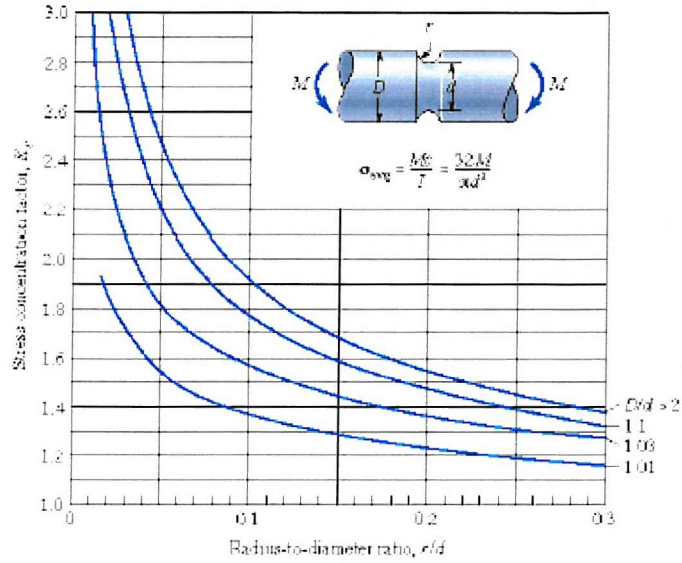

Stress Concentrations for Bar with Groove (cont.)

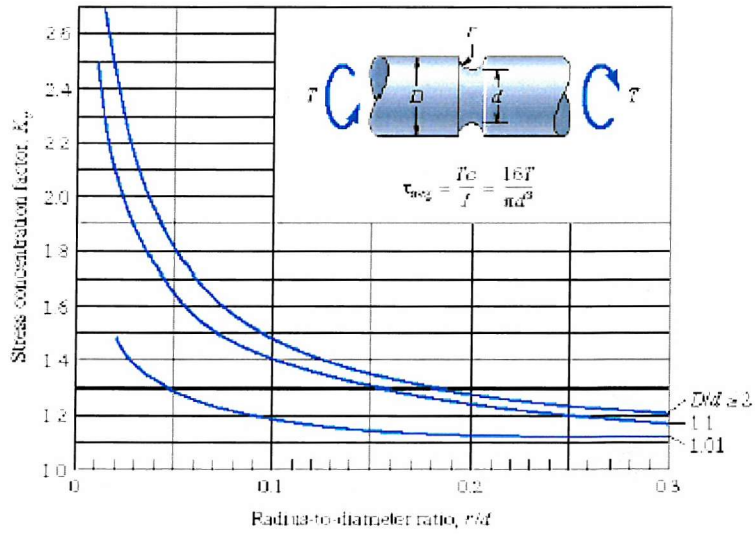

Appendix C

Element types used during the FEA of the transom on the Tricat.

SHELL ELEMENT

The shear deformation effect is neglected for this element. Six degrees of freedom per node (three translations and three rotations) are considered for structural analysis. The element is assumed to be isotropic with constant thickness for structural problems and orthotropic for thermal problems. Special Features include, Buckling and in-plane loading. Stress components including von Mises stress are available in the element coordinate system at the centroid of the element for top and bottom fibres. Principal stresses may optionally be requested. In addition, nodal force per unit length and stress components can also be calculated and printed. The directions of force and moment components per unit length for this element are illustrated in fig.7.8.

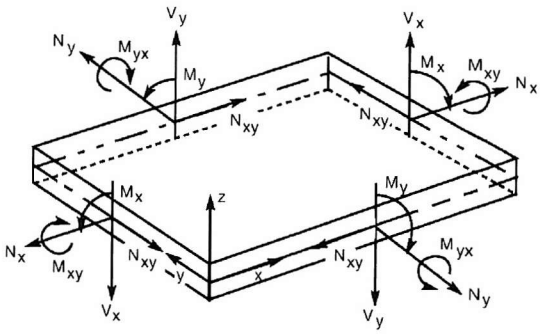

Shell Element Notation System

Beam Element Type

For structural analysis, six (6) degrees of freedom (three translations and three rotations) are considered per node, fig.7.9. One (1) degree of freedom per node, representing the temperature, is used for the thermal module. A third node, or an orientation angle, is also required. This element permits using unsymmetric cross-section, when the shear centre is not coincident with the centre of gravity. For the element, two nodes (1 and 2) an offset is allowed from the centroidal axis. Special Features include: Buckling, Inplane loading, nodes offset, unsymmetric cross-sections, ASME code check.

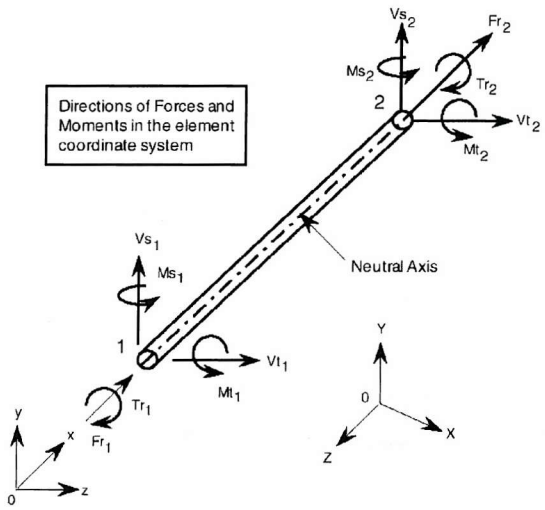

3D Beam Element Notation System

Solid Element Type

This Solid [6.15] is an 8- to 20-node three-dimensional element for the analysis of structural and thermal problems, fig.7.10. Three translational degrees of freedom per node are considered for structural analysis. Only one degree of freedom per node, representing the temperature, is used for the thermal module. Prism and tetrahedron-shaped elements may be considered only with the 8-node element option. Special features include: Buckling, Geometric Stiffness consideration, in plane loading flag.

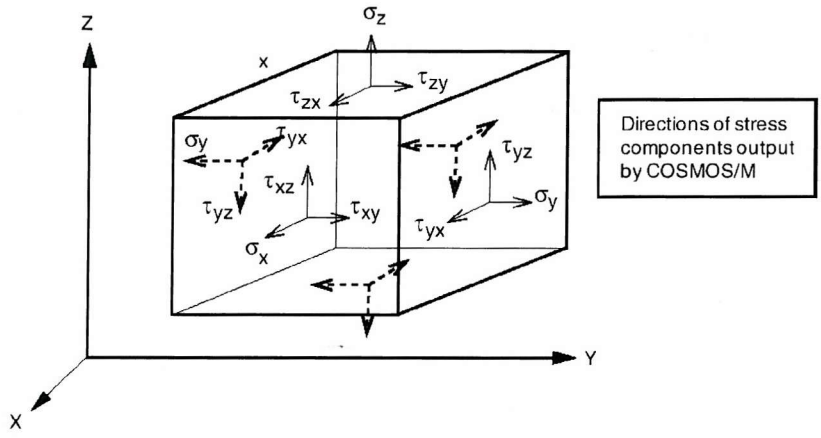

Solid Element Notation System